Master's thesis

NTNU
Norwegian University of Science and Technology
Faculty of Natural Sciences
Department of Chemical Engineering

Kevin Golden

Monitoring Techniques for C. glutamicum GABA Producers in Fed-Batch Fermentations

Master's thesis in Chemical Engineering
Supervisor: Nadav Bar
June 2020

NTNU
Kunnskap for en bedre verden

Kevin Golden

Monitoring Techniques for *C. glutamicum* GABA Producers in Fed-Batch Fermentations

Masters thesis
for the degree of Chemical Engineering

Trondheim, June 2020

Norwegian University of Science and Technology
Faculty of Natural Sciences
Department of Chemical Engineering

NTNU
Innovation and Creativity

NTNU

Norwegian University of Science and Technology

Masters thesis
for the degree of Chemical Engineering

Faculty of Natural Sciences
Department of Chemical Engineering

Masters thesis at NTNU

Printed by NTNU-trykk

Abstract

Industrial fermentation produces a wide variety of products during this day and age. Typical products include fuels, industrial chemicals, food and beverage additives, healthcare products, and microbial enzymes to name just a few. Efficiently fermenting these products with optimal substrates will allow profitable and cheaper bio-alternatives. A specific substrate of interest in this study is spent sulfite liquor or SSL. Along with the bacteria and substrate selection, optimally controlling and monitoring the fermentation process is essential. Investigating further into new bacteria strains, carbon media combinations, and fermentation models will aid the progress in the microbial process research field.

Microbial bio-catalytic processes are non-linear systems with some unknown dynamics and are highly dependent on the specific conditions of the process. However, models which contain knowledge about the process and the application of estimators to acquire information of the states is beneficial for bio-process development. The use of the information carried by the carbon dioxide measurements seems to have yet to be investigated for online measurements of other states. This work applies an Unscented Kalman Filter for biomass estimations and compares the performances with an Extended Kalman Filter. The aim of this work is to obtain reliable values of on-line signals with in-situ near-infrared spectroscopy and infrared measurements for the carbon dioxide. Simultaneously, GABA amongst other results have also been acquired from a new *Corynebacterium glutamicum* strain during the fermentation experimentation.

The results of this work shows successful implementation of a non-linear unstructured kinetic model used alongside both an Unscented and an Extended Kalman filter for state estimation. The results from the model and Kalman filter combination have been found to have a low amount of error when following the *C. glutamicum* raw sensor data. The Unscented Kalman filter performed better than the Extended Kalman filter, due to the non-linear nature of the fermentation. The state estimators have been applied to a fermentation with *C. glutamicum* wild type strain for biomass and substrate estimation. To extend the model and estimated state with a product, a *C. glutamicum* strain for GABA production on SSL was acquired. The HPLC measurements of GABA were not entirely correct due to the signal saturation in the measurements, therefore the need to improve the HPLC method is required. This complication made the experiments not available for parameter estimation. The original plan was to have an available model for the GABA producer strain and to then test the estimators. However, due to the spread of the COVID-19 pandemic and its resultant time limitations, only preliminary non-GABA producing results have been collected.

Sammendrag

Fermenteringsindustrien i dag produserer et bredt utvalg av produkter. Typiske produkter inkluderer brensel, industrielle kjemikalier, tilsetningsstoffer til mat og drikke, helseprodukter og mikrobielle enzymer for å nevne noen få. Effektiv fermentering av disse produktene med optimale substrater vil tillate billigere og mer lønnsomme bioalternativer. Et spesifikt underlag av interesse blir Spent Sulfite Liquor, eller SSL, i denne studien. Sammen med valg av bakterier og substrat er det viktig å kontrollere og overvåke gjæringsprosessen optimalt. Videre undersøkelser i nye bakteriestammer, kombinasjoner av karbonmedier og gjæringsmodeller vil hjelpe fremdriften innen mikrobiell prosessforskningsfelt.

Mikrobielle biokatalytiske prosesser er ikke-lineære systemer med noe ukjent dynamikk og er svært avhengige av de spesifikke forholdene i prosessen. Imidlertid er modeller som inneholder kunnskap om prosessen og anvendelsen av estimatorer for å skaffe informasjon om delstatene gunstig for bioprosessutvikling. Bruken av informasjonen fra karbondioksydmålingene ser ut til å være ennå ikke undersøkt for målinger av andre stater på nettet. Dette arbeidet bruker et usentrert Kalman-filter for estimering av biomasse og sammenligner forestillingene med et utvidet Kalman-filter. Målet med dette arbeidet er å oppnå pålitelige verdier av online signaler med in-situ nær-infrarød spektroskopi og infrarød måling for karbondioksid. Samtidig er GABA blant andre resultater også ervervet fra en ny *Corynebacterium glutamicum* stamme under gjæringseksperimenteringen.

Resultatene av dette arbeidet viser vellykket implementering av en ikke-lineær, ustrukturert kinetisk modell brukt sammen med både et usentrert og et utvidet Kalman-filter for tilstandsestimering. Resultatene fra modellen og Kalman-filterkombinasjonen har vist seg å ha en lav mengde feil når du følger *C. glutamicum* rå sensordata. Det usentrerte Kalman-filteret presterte bedre enn det utvidede Kalman-filteret, på grunn av den ikke-lineære karakteren av gjæringen. Staten estimatorer har blitt brukt til en gjæring med *C. glutamicum* villtype stamme for estimering av biomasse og underlag. For å utvide modellen og estimert tilstand med et produkt, a *C. glutamicum* -stamme for GABA-produksjon på SSL ble anskaffet. HPLC-målingene av GABA var ikke helt riktige på grunn av signalmetningen i målingene, derfor er behovet for å forbedre HPLC-metoden nødvendig. Denne komplikasjonen gjorde at eksperimentene ikke var tilgjengelige for parameterestimering. Den opprinnelige planen var å ha en tilgjengelig modell for GABA-produsentstammen og deretter teste estimatorene. På grunn av spredningen av pandemien og tidsbegrensningene har imidlertid bare foreløpige ikke-GABA-produserende resultater blitt samlet.

Preface

This master's thesis is the final work of the two year International Master's program in Chemical Engineering at the Norwegian University of Science and Technology. This was written at the Department of Chemical Engineering in the Process Systems Engineering Research Group.

Foremost, I would like to express my gratitude to my supervisor, Professor Nadav Bar. Firstly, for enabling me to work on such a project and secondly, for his expertise, guidance, and patience throughout the process of writing my thesis. I would like to thank my co-supervisor, PhD candidate Andrea Tuveri. Thank you for mentoring me throughout my thesis work. Without his countless hours of help, this work would not have been completed to the degree that it has. I would like to thank Dr. Fernando Pérez-García for his mentoring of my work in the Cyber Genome lab. I would like to thank PhD candidate Pedro Antonio Lira Parada for the guidance pertaining to fermentation modeling and other Cyber Genome lab related activities. I would like to thank Head Engineer Christopher Sørmo for educating me about the safety procedures related to the Cyber Genome lab and maintaining the lab throughout the numerous experiments. Lastly, I would like to proudly express my gratitude to NTNU for accepting me into the International Masters program. I have grown immensely, both professionally and as an individual, during my studies.

I, Kevin Golden, hereby declare this is an independent work according to the exam regulations of the Norwegian University of Science and Technology.

Kevin Golden

Kevin Golden

Table of Contents

List of Tables

List of Figures

List of Abbreviations

ADP	-	Adenosine diphosphate
ATP	-	Adenosine triphosphate
BBM	-	Black box model
Ca	-	Calcium
CCER	-	Calculated carbon dioxide evolution rate
CDW	-	Cell dry weight
CER	-	Carbon dioxide evolution rate
CTR	-	Carbon dioxide transfer rate
CoA	-	Co-enzyme A
CU	-	Concentration units
DNA	-	Deoxyribonucleic acid
DSP	-	Downstream process
EKF	-	Extended Kalman filter
GABA	-	Gamma aminobutyric acid
GAD	-	Glutamic acid, or glutamate, decarboxylase
GBM	-	Gray box model
GMO	-	Genetically modified organism
GYP	-	Glucose-Yeast Extract-Peptone agar medium
HMF	-	Hydroxymethylfurfural
HPLC	-	High performance liquid chromatography
IPTG	-	Isopropyl β-d-1-thiogalactopyranoside
IR	-	Infrared spectroscopy
LAB	-	Lactic acid bacteria
Mg	-	Magnesium
MPC	-	Model predictive control
MRS	-	De Man, Rogosa and Sharpe agar medium
MRSS	-	Sodium glutamate modified MRS medium

MSG	-	Monosodium glutamate
NADH	-	Nicotinamide adenine dinucleotide
NIR	-	Near-infrared spectroscopy
OCER	-	Observed carbon dioxide evolution rate
OD	-	Optical density
OD600	-	Optical density at 600 nanometer wavelength
ODE	-	Ordinary differential equation
PA4	-	Polyamide 4
PFD	-	Process flow diagram
pH	-	Potential of hydrogen
RPM	-	Revolutions per minute
RPS	-	Revolutions per second
SKM	-	Structured kinetic model
SPKF	-	Sigma-Point Kalman filter
SSL	-	Spent sulfite liquor
STD	-	Standard deviation
TBD	-	To be determined
UKF	-	Unscented Kalman filter
UKM	-	Unstructured kinetic model
USP	-	Upstream process
WBM	-	White box model

List of Symbols

A	-	Cross-sectional area of bioreactor [m^2]
A_f	-	Air volumetric flow rate [$\frac{L}{min}$]
CER	-	Carbon evolution rate [$\frac{g}{L \cdot hr}$]
CO_2^*	-	Carbon dioxide saturation concentration [$\frac{mol_{CO_2}}{L}$]
CO_2	-	Carbon dioxide concentration [$\frac{g_{CO_2}}{L}$]
CO_{2_d}	-	Carbon dioxide concentration dissolved into the bulk liquid phase [$\frac{mol_{CO_2}}{L}$]
$CO_{2_{mol}}$	-	Carbon dioxide concentration in moles [$\frac{mol_{CO_2}}{L}$]
ΔC_{moy}	-	Driving force potential [$\frac{mol}{L}$]
D	-	Diameter of impeller [m]
D_B	-	Diameter of bioreactor [m]
F	-	Feed rate [$\frac{L}{hr}$]
H	-	Henry constant [$\frac{atm \cdot m^3}{mol}$]
H_2O	-	Dihydrogen monoxide, or water, concentration [$\frac{mol_{H_2O}}{L}$]
HCO_3^-	-	Bulk phase bicarbonate ion concentration [$\frac{mol_{HCO_3^-}}{L}$]
K_1	-	Equilibrium constant of carbon dioxide hydration with water [$\frac{mol}{L}$]
K_2	-	Equilibrium constant of carbon dioxide hydration with hydroxide ion [$\frac{mol}{L}$]
k_1	-	Forward rate constant for r_1 [$\frac{1}{hr}$]
k_2	-	Forward rate constant for r_2 [$\frac{L}{mol \cdot hr}$]
k_{-1}	-	Backward rate constant for r_1 [$\frac{L}{mol \cdot hr}$]
k_{-2}	-	Backward rate constant for r_2 [$\frac{1}{hr}$]
k_d	-	Cell death coefficient [$\frac{1}{hr}$]
$k_L a_{CO_2}$	-	Volumetric carbon dioxide transfer coefficient [$\frac{1}{hr}$]
k_S	-	Substrate specific constant [$\frac{g}{L}$]
K_W	-	Water dissociation constant [$\frac{mol^2}{L^2}$]
M_{CO_2}	-	Molecular weight of carbon dioxide [$\frac{g}{mol}$]
μ	-	Specific rate of biomass growth [$\frac{1}{hr}$]
μ_{max}	-	Maximum specific growth rate [$\frac{1}{hr}$]

N - Impeller speed $[rps]$

N_{cd} - Minimum impeller speed for complete dispersion of the sparged gas $[rps]$

OH^- - Hydroxide ion concentration $[\frac{mol}{L}]$

P_{CO_2} - Partial pressure of carbon dioxide [atm]

Q_G - Volumetric gas flow rate $[\frac{m^3}{s}]$

R - Ideal gas constant $[\frac{atm \cdot m^3}{K \cdot mol}]$

r_1 - Rate of reaction of carbon dioxide hydration with water $[\frac{mol}{L \cdot s}]$

r_2 - Rate of reaction of carbon dioxide hydration with hydroxide ion $[\frac{mol}{L \cdot s}]$

ρ_{CO_2} - Density of carbon dioxide $[\frac{g}{L}]$

S - Substrate concentration $[\frac{g_{Substrate}}{L}]$

S_{in} - Substrate feed concentration $[\frac{g_{Substrate}}{L}]$

T - Temperature inside the bioreactor $[K]$

t - Time $[hr]$

V - Bioreactor volume $[L]$

V_G - Superficial gas velocity $[\frac{m}{s}]$

X - Biomass concentration $[\frac{g_{Biomass}}{L}]$

$Y_{\frac{X}{S}}$ - Yield coefficient of biomass per substrate consumed $[\frac{g_{biomass}}{g_{Substrate}}]$

$Y_{\frac{CO_2}{X}}$ - Yield coefficient of carbon dioxide per biomass consumed $[\frac{g_{CO_2}}{g_{biomass}}]$

1 Introduction

Understanding the overall intracellular kinetics and formation of products within a cell is a very demanding and complex task [1]. However, doing so allows researchers to take advantage of this knowledge and manipulate microbial cells to produce highly complex molecules at a cost effective rate [2]. Bacteria have been used recently in history to produce numerous pharmacological and food-use molecules [3]. In specific, fermentation currently is utilized to produce fuels, industrial chemicals, food and beverage additives, healthcare products, and microbial enzymes to name just a few [4, 5]. The previous statement is exemplified in Figure 1.1. Therefore, investigating further into this broad research field is very worthwhile for countless industries.

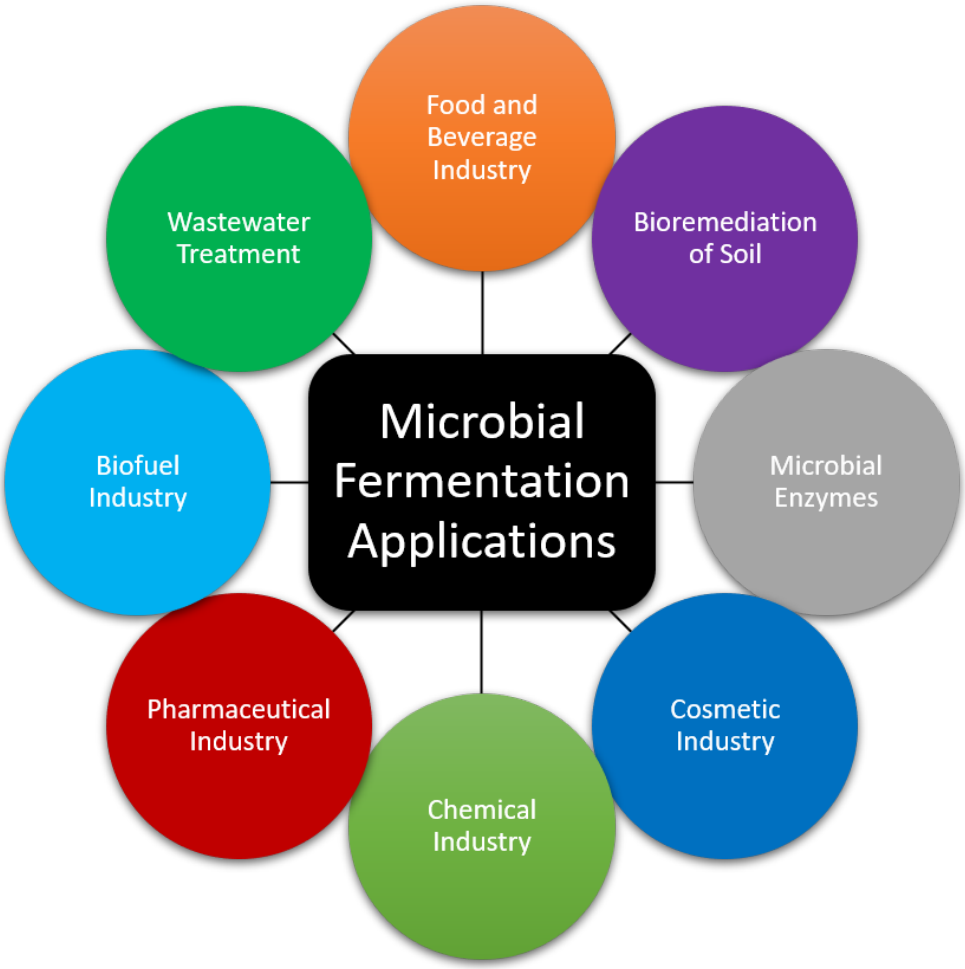

Figure 1.1: Applications of microbial fermentation in various industrial sectors [5]. These sectors include: food and beverage, soil, enzymes, cosmetics, chemicals, pharmaceuticals, biofuels, and wastewater treatment.

High frequency measurements are of great importance in monitoring and control applications however information of all states in a desirable frequency is not possible. In a fermentation system the protocols to quantify *offline* biomass, X, through cell dry weight, CDW, has a main disadvantage of often infrequent and delayed measurements. An alternative is to determine *online* optical density, OD, through specific absorbance wave lengths, in particular *in-situ* near-infrared, NIR, probes for monitoring OD values [6]. The correlation between OD data with the concentration of biomass has challenges of discrepancies in the NIR probes estimations under low concentrations and with different stirring regimes. Noise is generated in the NIR signal at high stirring regimes due to formation of small bubbles.

Previous reports include a model-free Extended Kalman filter, EKF, for parameter and state estimation which use macroscopic and elemental balances with transfer rates of O_2 and CO_2 in the liquid phase as secondary measurements with the use of delayed measurements, model equations and secondary variables, as the carbon dioxide evolution rate, CER [7, 8]. An interesting paper includes the application of a Sigma-Point Kalman filter, or SPKF, with NIR spectroscopy coupled with partial least squares modeling while holding the process noise constant and varying the measurement noise with linear regression from past data [9]. Furthermore, since different measurements contain valuable information about the cell growth and can make the estimator more robust, this combination of NIR and carbon dioxide concentration signals can be fused to obtain more accurate biomass values. The solution this work proposes uses available information from the *online* measurements and combines them by using an Unscented Kalman filter, or UKF, describing the system through an unstructured model with Monod-like kinetics. Within this approach, random effects due to measurement noise are filtered out and the estimators will give more accurate values for states such as biomass and substrate concentrations.

1.1 Motivation

The motivation of this thesis is to develop an estimator and model to monitor the process of a new strain of bacteria in conjunction with a new carbon source. Gamma-Aminobutyric Acid, or GABA, was desired to be produced from this new strain and spent sulfite liquor as a carbon source to aid in formulating the system. Studies of *Corynebacterium glutamicum* for GABA production have only just begun so looking into new strains and carbon sources is paramount for success in this endeavor [10–14]. This includes conducting fermentation experiments to investigate the stability of the strain in a bioreactor. As of now, this strain has only been fermented in flasks, so the behavior in a bioreactor is still unknown. The stability of the strain will be judged in the presence of multiple differing carbon sources, as the goal is to see how the strain performs with spent sulfite liquor as the source of sugars. Along with determining the stability it is unknown whether the consumption of the sugars is parallel or consecutive. Lastly, the performance regarding the production of the product in question will also be evaluated. Once data is obtained for the variables in question a model and an estimator can then be implemented with the pertinent states and parameters. The estimator will help to reduce the amount of necessary measurements as these measurements of the product and sugars have a long delay. The only way to overcome the measurement limitations is to have an estimator, or observer, in conjunction with the model. Once the model and observer are properly working this system should closely follow the raw data of the multiple unique experiments. Ultimately, this system can be used to control various bio-processes accordingly.

1.2 Objective

In order to better understand any circumstance which can occur with this highly volatile fermentation process, a mathematical model should be developed. This model should include the differential state equations of volume, biomass, product, substrate, and carbon dioxide. These states are the main factors of the fermentation characteristics and can be measured scientifically and accurately [15]. Most importantly this model should be able to use fast, reliable data, such as the carbon dioxide concentration, to determine the product and biomass production. In conjunction with this model an estimator will also be developed. This estimator, or observer, will be of the Kalman filter variety. In conclusion, the objective of this thesis is to analyze a simple, robust model and estimator which can be efficiently implemented to monitor fermentation and allow further control applications.

1.3 Outline

The thesis is divided into eight sections which are described briefly in this outline [16]:

1. Introduction - This section introduces the context of the thesis, motivation of the work, describes methodological objectives to solving the problem of interest, and outlines the structure of the thesis for the reader.

2. Background - This section provides background information for fermentation, *Corynebacterium glutamicum*, GABA, SSL, and model theory including observers. This section gives the foundation of knowledge required to understand the results and conclusions.

3. Materials and Methods - This section details the chemicals, bacteria, equipment, documented methods, and the different types of experimentation done which allows for reproduction of any experiments of interest.

4. Modeling - This section delves into the state ordinary differential equations which ultimately model the behavior of a specific fermentation process when given the initial conditions. The section also describes the usage of parameter estimation in conjunction with the model, which is vital for accurate control.

5. Kalman Filters - This section derives both the Unscented and Extended Kalman filter for use in fermentation applications.

6. Results and Discussion - This section presents the results of the model, Kalman filters, GABA production, and poses a careful analysis of said results.

7. Conclusion - This section serves to provide an overview of the thesis work while giving special attention to concisely summarize the results and discussion.

8. Further Work - This section offers insight of what the future of this research area might bring, specifically relating to this thesis. This section also involves doing more experiments to verify that the results are indeed correct.

2 Background

2.1 Fermentation

Industrial fermentation consists of upstream and downstream processes. The upstream process, known as USP, always involves the production microorganism (bacteria or fungi), the carbon source (sugars used by the microorganism), and broth medium (which can be aerated, inoculated, stirred, and monitored) [17, 18]. The important production microorganism parameters involve the robustness, the productivity, the yield, and the economic efficiency. The important aspect of carbon and medium optimization involves maximizing profit margin as well as product yield as a function of the carbon source and nutrients provided. In many cases the medium of choice are byproducts of other industrial processes, often involving sugar or lignocellulosic products. These three main constituents are then combined to begin the fermentation process [19]. Optimizing industrial fermentation involves rigorous control of environmental conditions in order to obtain high growth of biomass and yield of product. It is also important for the fermentation equipment to be inert and sterilized adequately. The operation and type of fermentation equipment also directly influences the fermentation kinetics. The downstream process, or DSP, involves any process after the fermentation in the process flow diagram as seen in Figure 2.1. For example, this involves any isolation, purification, filtration, harvesting, and storage [20]. During these processes the inefficiencies accumulate and turn into various wastes. For example, if the microorganism were to produce an undesired product then said product would need to be separated creating waste, or if the microorganisms are ingesting an inefficient substrate generating waste [21].

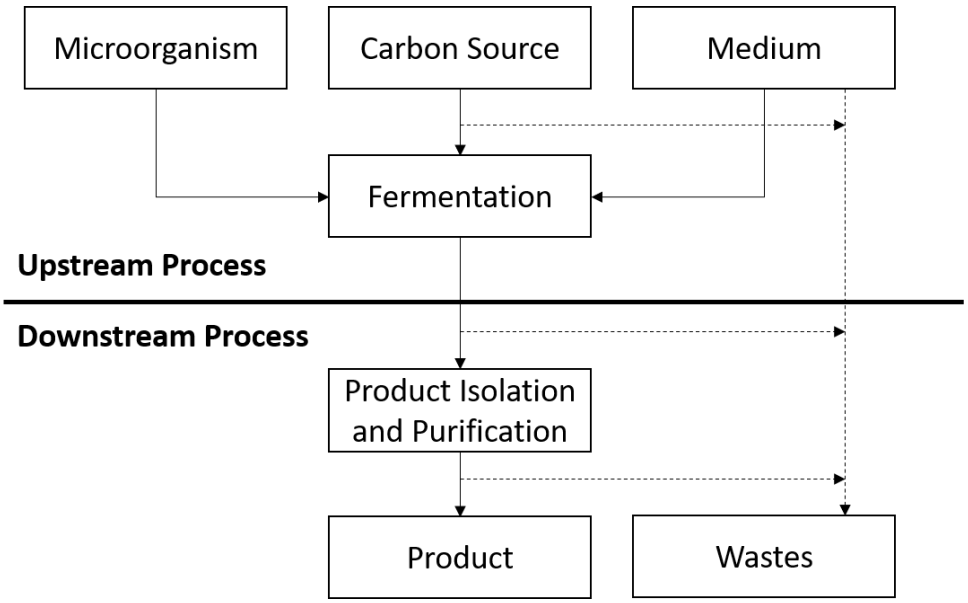

Figure 2.1: Simplified fermentation process flow diagram [19]. A medium, carbon source, and microorganism are required to start the upstream fermentation process successfully. Once product is being made the downstream process can then isolate and purify the desired product. During the upstream and downstream processes wastes are created, as the process is not completely efficient.

2.1.1 Fermentation Conditions

Fermentation can be divided into two main categories: aerobic and anaerobic. Aerobic fermentation is the process in which cells utilize sugars for metabolism in the presence of oxygen [22]. The aerobic condition often is faster but needs more energy input through agitation which aerates the culture. However, the aerobic condition also produces much more cellular energy. The aerobic condition produces 38 ATP per glucose molecule to be exact [23]. The anaerobic condition is fermentation in the absence of oxygen. This requires less energy input though it is much slower compared to aerobic fermentation [24]. The slower anaerobic process also only produces 2 ATP per glucose molecule [25]. Seen in Figure 2.2, the pathways for each condition are shown. In the anaerobic condition, lactate (which can be turned into ATP), alcohols/other products, and carbon dioxide are produced. In the aerobic condition, oxygen allows for respiration of the cell creating ATP, carbon dioxide, and water. Most industrial fermentations use the aerobic condition as time is very valuable compared to the cost of utilities [17].

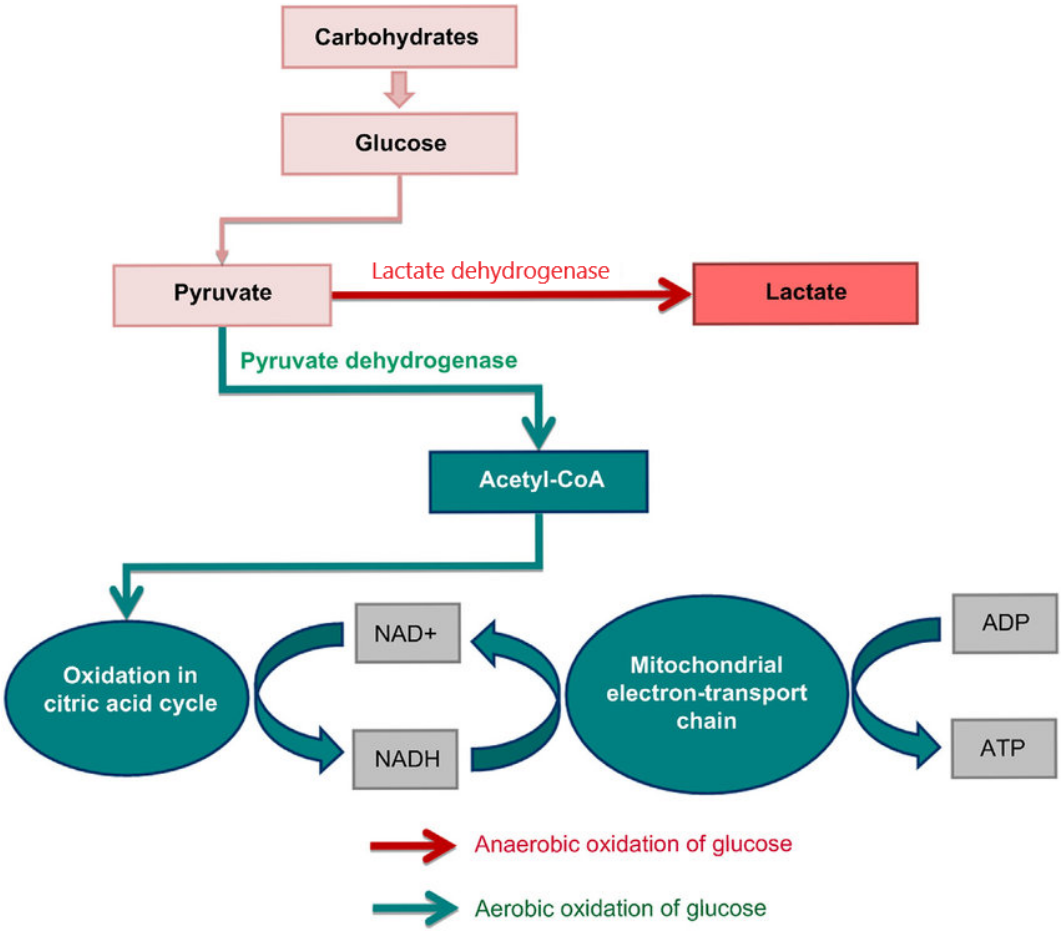

Figure 2.2: Depiction of anaerobic and aerobic fermentation pathways [26]. The substrate carbohydrates are first converted to pyruvate. Depending on the aerobic conditions, the pyruvate will go through either the lactate or pyruvate dehydrogenase. Depending on the enzyme used, the product will either be lactate along with carbon dioxide and other products or acetyl-CoA which provides ATP to the cell for use and produces carbon dioxide and water.

2.2 *Corynebacterium Glutamicum*

Corynebacterium glutamicum, or *C. glutamicum* has a long history of utilization as an industrial organism. *C. glutamicum* is a gram-positive, non-pathogenetic bacteria which was engineered to serve industrial purposes since 1970 [27, 28]. *C. glutamicum* can be found in soil, sewage, vegetables, and fruits [29]. *C. glutamicum* has also been found to be capable of using multiple sugars and organic acids for respiration [30]. Corynebacteria have been found to be nutritionally fastidious, meaning the need for vitamins and other amino acids in the carbon medium to survive and replicate. In particular, *C. glutamicum* has the ability to metabolize glucose, xylose, sucrose, fructose, and mannose [31, 32]. The main product of industrial applications are various amino acids [33, 34]. The largest section, being the l-glutamate amino acid, produces around 1.5 million tons per year [27]! New product segments such as biofuels, xylitol, putrescine, and gamma-aminobutyric acid are now being turned to for *C. glutamicum* production [35–38].

This study primarily delves into the fermentation using different strains of *C. glutamicum* with differing carbon sources to either produce GABA or no products as a control. The two strains being studied are the wild type strain, used in the first experiment for a baseline, and the GMO strain. This GMO strain in question is known as *C. glutamicum* ATCC13032 (pVWx1-galBmut-manA)(pEKEx3-xylAB). This strain is the wild type strain modified with three vectors, or plasmids, incorporated into the bacteria. These vectors enable the bacteria to use galactose, mannose, and xylose as a carbon source. This specific strain also enables the bacteria to produce GABA, as the wild type strain cannot produce GABA without modifications. Without the respective vectors, researchers typically use solely glucose as it is very reliable in a bioreactor setting for research.

It has been shown that the growth rate of the wild type strain is approximately 0.54 $\frac{1}{hr}$, which is considerably higher than the 0.40 $\frac{1}{hr}$ growth rate of the infamous *E. coli* [39]. When the bacteria is in the stationary phase it plateaus in the number of living cells where the division and death are in equilibrium. This, along with many favorable traits, is a big factor in why a GMO *C. Glutamicum* strain is an attractive option [40].

Figure 2.3 shows the inner workings of a typical bacteria cell. It can be seen that there is no nucleus, therefore inserting new DNA as a plasmid is relatively easy for GMO bacteria strains. Important bacteria structures include flagella, pili or fimbriae, and cell wall [41]. Bacteria are fairly robust especially if the population can move with their flagellum. Chemotaxis using flagellum has been found to be very important in survivability of bacteria cultures [42].

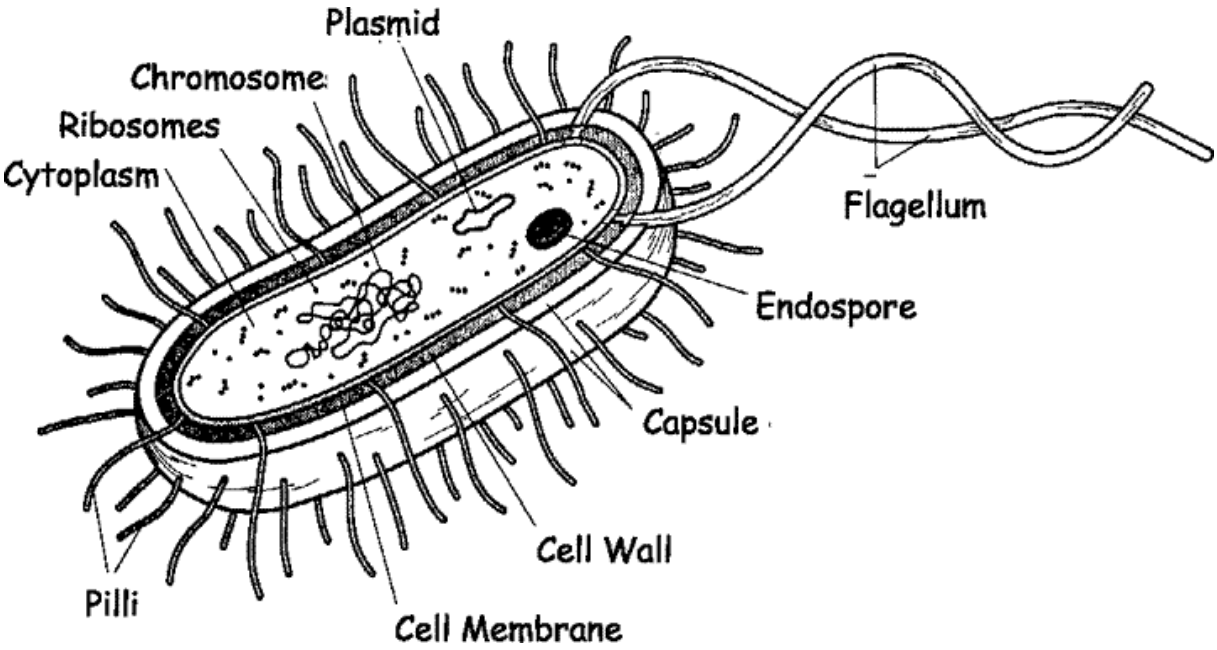

Figure 2.3: The schematic diagram of bacterial cell structure [43]. In order to not destroy the bacteria, the cell membrane and wall must stay intact. Plasmids are inserted into the bacteria in order to introduce new genetic material which the bacteria can use.

2.3 Gamma-Aminobutyric Acid

Gamma-aminobutyric acid, also known as GABA, is a four carbon non-protein amino acid which is produced by the decarboxylation of glutamate found widely in organisms [44]. Glutamate is the most common industrial product for the wild type *C. glutamicum*. GABA has been found to have neurological affects which many scientists contend have been central in neural control theory since 1950 [45]. Apparently it is the primary neurotransmitter inhibitor for 20 to 40% of the cortical neurons [46]. An example of a significant breakthrough has been the finding of significant reductions of GABA concentrations in varying epileptic syndromes [47]. Another massive potential use for GABA is as a bio-plastic polyamide 4 or PA4 [48, 49]. PA4 is biodegradable in the soil compared to the commonly used polyamide 6 which has poor biodegradability [50, 51]. Therefore, satisfying this huge demand of GABA economically can only be met by using microorganisms for its production [52]. GABA, produced from glutamate, can be seen along with its pathways in Figure 2.4. The most important pathway being the glutamate decarboxylase, or GAD, which is a pyridoxal 5′-phosphate-dependent enzyme that catalyzes the α-decarboxylation of glutamate to GABA [14, 53].

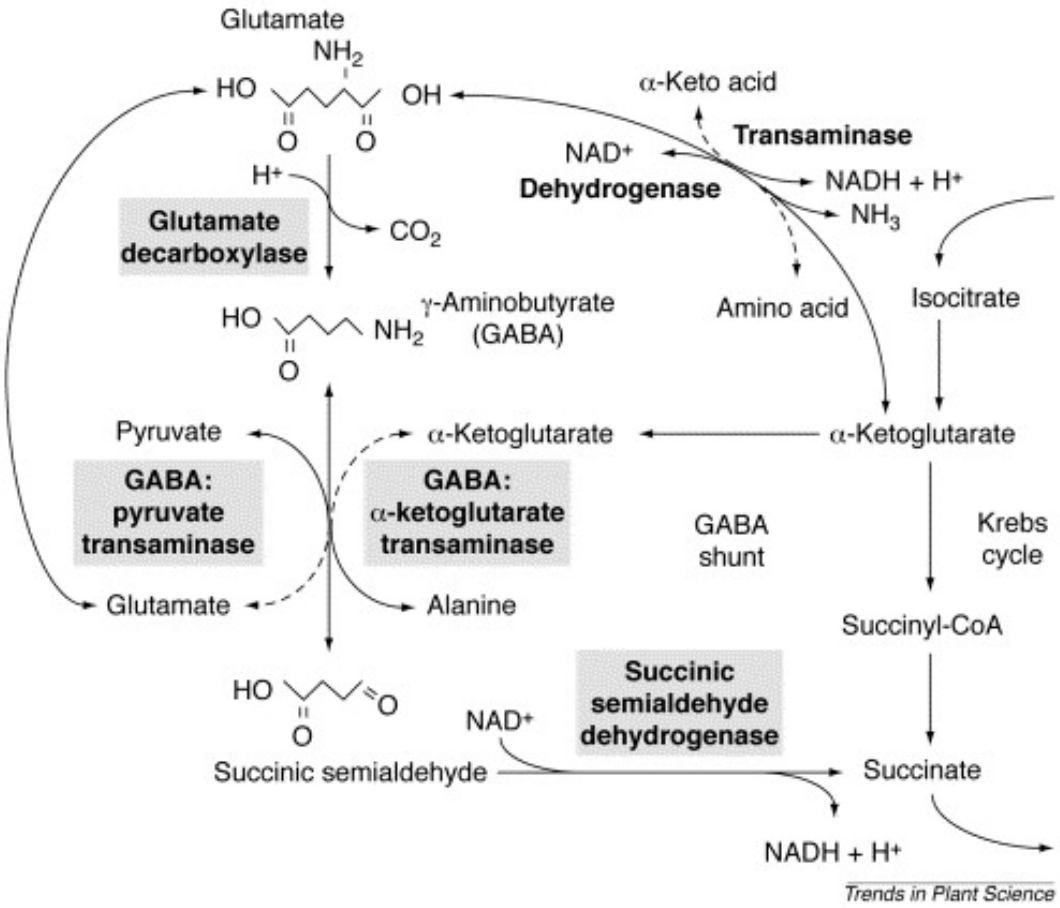

Figure 2.4: The gamma-aminobutyric acid (GABA) metabolic pathways in the new strain [54]. Enzymes are indicated in bold while those specifically associated with the GABA are in bold and highlighted in grey. It can be seen that glutamate can easily be converted into GABA.

Table 2.1 shows the current state of GABA fermentation research. It can be seen that fed-batch fermentation experiments can help limit high substrate concentration inhibition [55, 56]. It has also been determined that cell and GAD production is very dependent on the medium composition and fermentation conditions [57, 58]. The study which produced the highest concentration of GABA, 204.5 $\frac{g}{L}$, was with *E. coli* with sodium glutamate in a fed-batch fermentation [59]. However the highest productivity, 34.3 $g/L/hr$, was also with *E. coli* with glutamic acid in a fed-batch fermentation [60].

When looking at the results of strictly *Corynebacterium glutamicum* only, the highest concentration of GABA produced was 61 $\frac{g}{L}$ using glucose [61]. The highest productivity for strictly *C. glutamicum* was 0.904 $g/L/hr$ using glucose from the same study [61]. These maximums were achieved with a glucose medium under fed-batch fermentation conditions.

Table 2.1: The current progress in GABA production indicating the different bacteria strains, substrates, fermentation conditions, and productivity [38, 62].

Strains	**Substrates**	**Fermentation conditions**	**GABA**		**Ref.**
			Titer (g/L)	**Productivity** (g/L/hr)	
Bifidobacterium dentium NFBC2243	MRS and MSG medium	One-step, batch	12.32	0.171	[63]
Corynebacterium glutamicum GAD	Glucose medium	One-step, batch	12.37	0.172	[14]
C. glutamicum GAD pknG	Glucose medium	One-step, batch	31.1	0.259	[11]
C. glutamicum	Glucose	One-step, fed-batch	38.6	0.536	[10]
C. glutamicum	Glucose	One-step, batch	31.1	0.259	[64]
C. glutamicum	Glucose	One-step, fed-batch	26.32	0.439	[65]
C. glutamicum	Glucose	One-step, fed-batch	61	0.904	[61]

Continued on next page

Table 2.1 – *Continued from previous page*

Strains	Substrates	Fermentation conditions	GABA		Ref.
			Titer (g/L)	Productivity (g/L/hr)	
C. glutamicum G01 and *L. plantarum* GB01-21	Cassava powder	Two-step, fed-batch	80.5	2.68	[62]
Escherichia coli	Glutamic acid	IPTG induction, one-step, fed-batch	38.6	34.3	[60]
E. coli	Sodium glutamate	IPTG induction, one-step, fed-batch	204.5	8.52	[59]
Lactobacillus brevis	Sodium glutamate	Two-step, fed-batch	103.1	0.536	[66]
L. brevis IFO12005	Komeshochukusu and GYP	One-step, batch	1.05	0.022	[67]
L. brevis GABA 057	GYP medium	One-step, batch	23.38	0.487	[68]
L. brevis	GYP medium	One-step, batch	4.6	0.19	[69]
L. brevis	MRSS medium	One-step, batch	15.37	0.32	[70]
L. brevis GABA 100	Black raspberry with MSG medium	One-step, batch	13.0	0.0451	[71]
L. brevis NCL912	Glucose medium	One-step, batch	35.66	0.743	[72]
L. brevis BJ20	Kimchi	One-step, batch	2.465	0.0037	[73]
L. brevis DPC6108	MRS and MSG medium	One-step, batch	20.47	0.284	[63]
Lactobacillus buchneri MS	MRS broth	One-step, batch	25.88	0.54	[74]

Continued on next page

Table 2.1 – *Continued from previous page*

Strains	Substrates	Fermentation conditions	GABA		Ref.
			Titer (g/L)	Productivity (g/L/hr)	
Lactoccoccus lactis subsp. *lactis*	Brown rice juice, germinated soybean juice, and skim milk with MSG medium	One-step, batch	7.2	0.05	[75]
L. lactis subsp. *lactis* 017	Skim milk	One-step, batch	2.7	0.056	[76]
L. lactis subsp. *lactis* B	Brown rice juice, germinated soybean juice, and skim milk	One-step, batch	6.41	0.321	[77]
Lactobacillus paracasei NFRI 7415	MRS broth	One-step, batch	31.15	0.325	[57]
Lactobacillus plantarum DSM19463	MRS medium	One-step, batch	0.4981	0.062	[78]
Streptococcus salivarius subsp. *thermophilus* Y2	MSG medium	One-step, batch	7.985	0.321	[79]

2.4 Spent Sulfite Liquor

C. glutamicum efforts have recently shifted to finding alternative carbon sources. Currently, the carbon feed within the industry still heavily relies on only glucose and fructose [80]. Alternative carbon sources such as galactose, arabinose, glycerol, and xylose have been recently been established for utilization [81–84]. Taking bio-byproducts of popular processes, which have little to no direct use, can be a popular option for the carbon source in fermentation. For instance, SSL or spent sulfite liquor, is a common bio-byproduct in the pulp and paper industry using sulfite cooking [85]. A common flow diagram for sulfite processes can be seen in Figure 2.5. This process flow diagram, or PFD, shows how wood chips and white liquor combine in digesters which form unbleached pulp and black liquor which is also known as spent sulfite liquor. This concentrated liquor is typically used in a boiler for steam generation which recovers some energy in the process. SSL can also be neutralized and then the byproducts taken from the liquor, however it is not very efficient [86]. Consequently, many researchers are working on a better and more efficient use of SSL. Fermentation of SSL is an option being explored for many differing strains of bacterium. Many of these strains can have some success but are usually limited by either inhibitory compounds or not being able to utilize all the available sugars effectively [87].

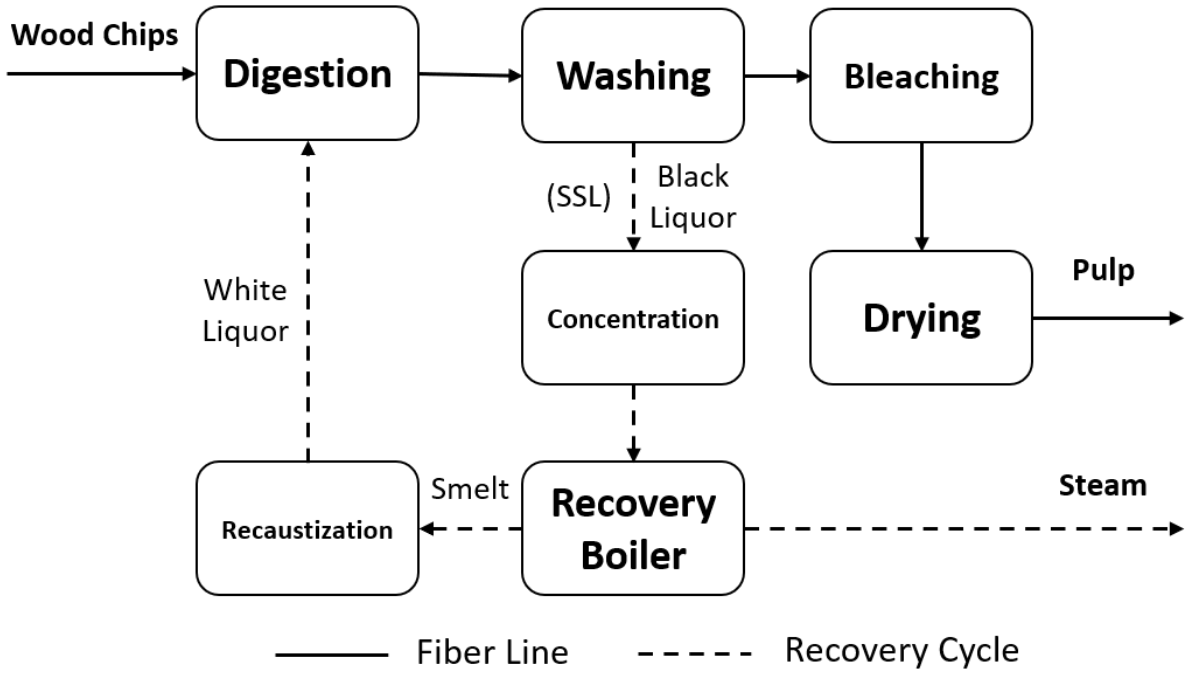

Figure 2.5: Process flow diagram of the sulfite pulp process [88]. The two end products are SSL, or black liquor, and pulp from wood chips and fresh white liquor. The equipment involved in this process are: digesters, bleaching tanks, storage tanks, and washing/drying tanks.

Norway, in particular, has some of the largest bio-refineries in the world and being able to utilize SSL for more varied purposes would be highly beneficial [89, 90]. However, SSL does have some toxins which can potentially inhibit the fermentation process. In order to determine the effects of the potentially harmful toxins, fermentations will be done with three different carbon sources (non-synthetic SSL, synthetic SSL, and glucose). The common SSL solution contains many varying levels of monosaccharides and toxins, seen in Table 2.2.

Table 2.2: Typical industrial spent sulfite liquor for both weak and strong concentrations [91]. SSL has a composition of arabinose, xylose, galatose, glucose, mannose, furfural, HMF, acetic acid, and lignosulfates.

Industrial SSL Components	Weak SSL (g/L)	Strong SSL (g/L)
Arabinose (C5)	1.67	14.44
Xylose (C5)	25.01	138.24
Galactose (C6)	2.44	17.60
Glucose (C6)	2.35	19.21
Mannose (C6)	1.73	7.41
Furfural	0.17	0.12
HMF	0.03	0.04
Acetic Acid	6.92	5.03
Lignosulfonates	47.32	427.05

In the synthetic SSL substrate version for the experiment, the common monosaccharides are reduced to the primary sugars while also excluding the toxins. The toxins which non-synthetic SSL contains are mainly sulfite, furfural, and acetic acid which inhibit product capabilities from monosaccharides with microorganisms [92].

2.5 Model Theory

Having strict control and complete understanding of the key variables in any industrial process is vital to properly fermenting products [93]. When developing a model for industrial use, mathematical models will increase in complexity due to the larger scales. This scaling ultimately influences the environmental conditions which alters the kinetics, the mixing, the homogeneity of the temperature, and the balance of the pH in the mixture [94]. Many mechanistic models are obtained from empirical observations via experimentation. This allows for a deeper understanding and foundation for a model whose formulation requires very specialized knowledge. Fortunately, non-mechanistic models can be a viable alternative system. These models are able to describe the general behavior of fermentation without knowledge of the kinetics of the process. Figure 2.6 details the various types of model structures. Mechanistic models can be formulated as structured, unstructured, segregated, and unsegregated. A mechanistic model is often referred to as a white box model or WBM. These WBMs can accurately describe microorganism processes while understanding the phenomena correlated to these processes. Non-mechanistic models can be formulated using statistics, a neural network, or fuzzy logic. A non-mechanistic model is often referred to as a black box model or BBM. This naming convention is due to the opaque nature of the inner workings of BBMs.

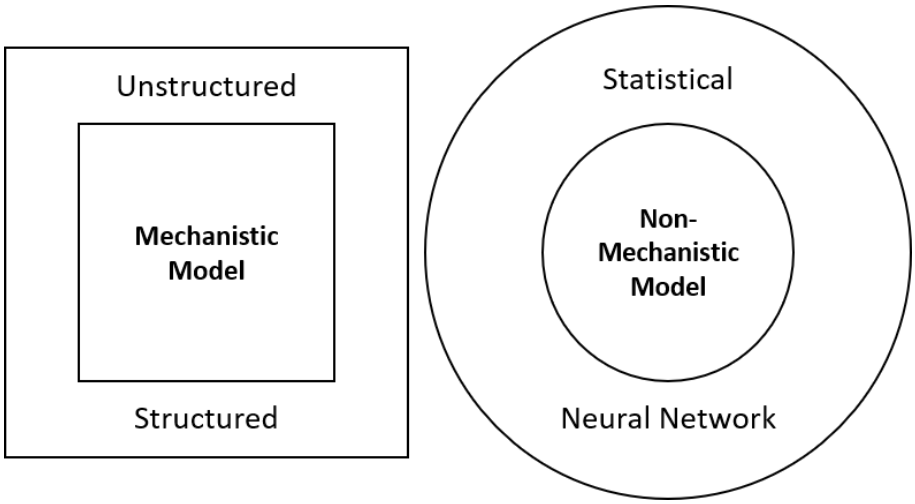

Figure 2.6: A mechanistic model is based on deterministic principles [15]. On the other hand, empirical models represent input-output relations without the knowledge of a mechanism. Fermentation process models are usually represented with a combination of both mechanistic and empirical models.

2.5.1 Unstructured Mechanistic Models

Unstructured mechanistic models or unstructured kinetic models, known as UKMs, provide a general global point of view of the process. These UKMs consist mainly of mathematical descriptions for semi-empirical observations. These descriptions can model the cell and medium concentration as an average using ideal conditions. This assumption is not entirely true, of course, but does allow for a much simpler model system. An example of an UKM being utilized can be seen in the Monod equation in Section 4 which describes the biomass growth as a function of substrate [95]. However, the simplicity of the Monod equation does not capture more complex cellular kinetics such as inhibition. In order to make a UKM dynamic, the model is described as a set of ordinary differential equations, or ODEs [96]. This dynamic morphological UKM is the premise of the model structure presented in Section 4.

2.5.2 Structured Mechanistic Models

Structured mechanistic models or structured kinetic models, known as SKMs, describe the changes in the cell population via modeling the internal structure of the microorganism. Doing so will consequently increase the complexity of variables and parameters mathematically required to model the fermentation processes. A particular SKM, for example, is the morphological SKM, which describes the kinetics of the substrate consumption along with the carbon dioxide and product formation [97].

2.5.3 Non-Mechanistic Models

Non-mechanistic models, known as BBMs, involve artificial intelligence such as neural networks or statistical models. Implementing BBMs are relatively straightforward and are gaining interest for various applications. The downside of these models is understanding the input-output relationship and troubleshooting this nontrivial tool [98]. Lastly, there are also gray box models, or GBMs, which are a hybrid of both mechanistic and non-mechanistic models. GBMs combine WBMs with artificial intelligence which can provide better performance and lessen noise associated with measurements [99].

2.5.4 State Estimator

The main objective of state observers or estimators is to estimate states which are difficult to measure. An example are dynamic parameters which determine growth kinetics, production rate, and cell death rate. These difficulties can be due to the lack of sensors or non-adequate measurement frequency/delay [100, 101]. Using observers in conjunction with a UKM is quite complimentary. The state observer can merge vital information of the UKM and conventional *in-situ* probe measurements. By using both sources of information the accuracy can be dramatically increased. For example, if the model is lacking the measurements the observer can prevent failures and vice versa. The main types of observers currently are: Luenberger based, finite dimensional, Bayesian, interval, and even artificial intelligence [102]. This study will look into the Bayesian Kalman filters [103]. Bayesian observers use the probability distribution estimation of stochastic state variables using the available process data [104]. The particular Kalman filters being tested are the Unscented Kalman filter, or UKF, and the Extended Kalman filter, or EKF. The UKF is a nonlinear observer while the EKF is a linear observer [105]. This hybrid implementation of the Kalman filters with the UKM ultimately makes for a highly versatile and rapid system for various fermentation processes [106]. The details of this filter are discussed in Section 5.

Table 2.3 showcases the various types of parameter estimation methods used for biochemical processes. As seen below the most common observer used in biochemical processes is the sliding mode observer. The Kalman filter is definitely explored less when applied to bioreactors and fermentors. This study showcases another use-case for a Kalman filter in a biochemical application.

Table 2.3: Application of recent observers in strictly biochemical process systems [102].

Observer	Objective/estimate(s)	System	Positive highlight(s)	Ref.
Adaptive state observer	Growth rate, kinetic coefficient	Bioreactor	Guaranteed convergence factor	[107]
Continuous-discrete-interval	Process kinetics	Bioreactor	Avoids growth of interval sizes during estimation	[108]
Continuous-discrete-Extended Kalman filter	Biomass, substrate concentration	Bioreactor	Accurate estimates, reduced error	[109]
Exponential	Microorganisms concentration	Bioreactor	Guaranteed convergence	[110]
Extended Luenberger observer-Asymptotic observer	Biomass concentration	Bioreactor	Stable rate of convergence	[111]
Particle filter	Yield parameter	Fermentor	Good estimation based on maximization algorithm theory	[112]
Reduced-order	Substrate concentration	Bioreactor	Robust estimation	[113]
Sliding mode observer	Substrate concentration, specific growth rate	Fermentation process	Smooth estimates	[114]
Sliding mode observer	Specific growth rate	Fed-batch bioreactor	Accurate and error free estimation	[115]
Sliding mode observer	Substrate concentration	Bioreactor	Proven stability factor	[116]
Sliding mode observer	Biomass and substrate concentration	Bioreactor	Proven stability factor	[117]
Quasi-unknown input observer	Faults in concentration, flow rates, light intensity	Bioreactor	Satisfactory estimates	[118]
Unscented Kalman filter	Biomass concentration	Fermentor	Effective estimation despite using the simplified mechanistic model	[119]

2.5.5 Process Optimization

The goal of every industrial bio-process is to produce quality products at an optimal rate, keep the process in a stable and robust state, and sustain a minimum operating cost which maximizes profits [120]. These goals can be condensed into theories, which if followed correctly, can achieve the industrial bio-processing goals. Seen from Figure 2.7, the "Ring of Fire" method can be explained as follows [121]:

1. Determine the objective functions to optimize which are formulated from various process variables.
2. Analyze the data for quality and consistency.
3. Convert the data to information descriptors and utilize them for the design of experiments.
4. Obtain hypotheses from the various experiments to formulate mechanistic models.
5. Utilize the models for real time predictive control with the objective function in mind as desired.

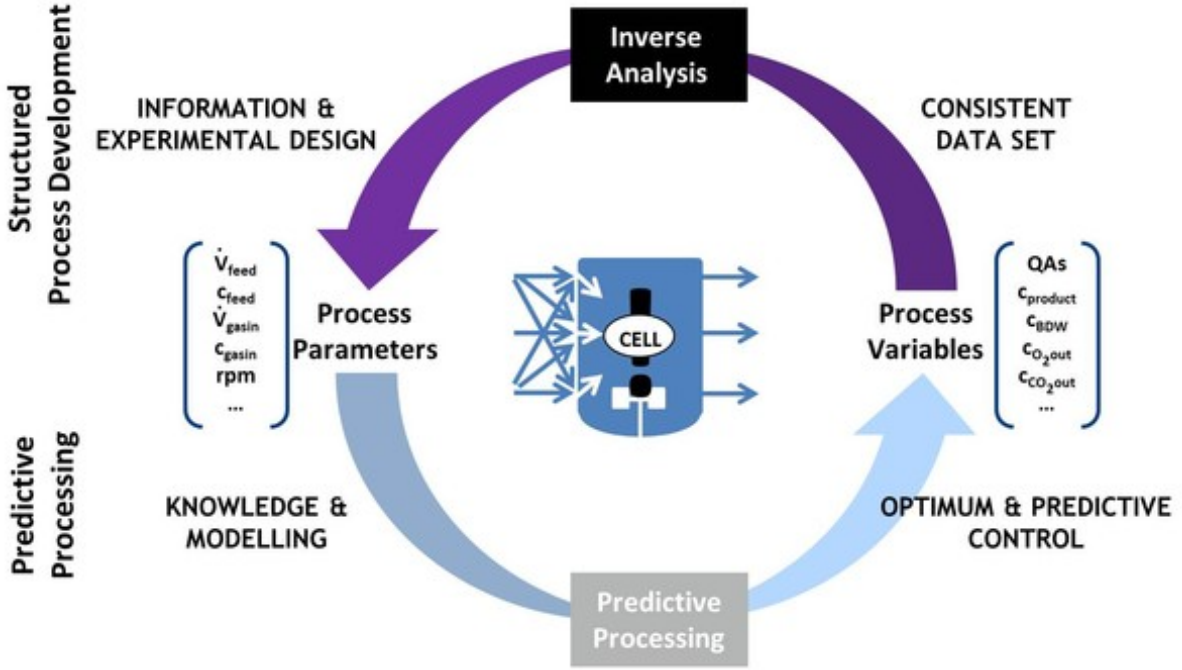

Figure 2.7: Diagram known as the "Ring of Fire" [121]. This method shows the loop in which objective functions are formulated to be accurately converted into scalable information descriptors. These descriptors can then be used in tandem with a controller to manage the process inputs.

3 Materials and Methods

3.1 Bio-process

Fermentation was performed as fed-batch cultivations in stirred tank reactors as seen in Section 3.5. The inoculum for the fed-batch cultivations, also referred to as growth culture, is produced in a flask. The media for the preculture is composed of a complex media 2YT seen in Table 3.1. After 24 hours of aerobic fermentation and depletion of the provided nutrients, the inoculum is ready to start the main culture.

Table 3.1: Inoculum 2xYT microbial medium powder composition [122]. It is an excellent growth medium for culturing Escherichia coli, particularly laboratory or recombinant strains.

2YT Components	Concentration (g/L)
Tryptone	16
Yeast Extract	10
Sodium Chloride	5
Total	31

3.2 Cultivation

Using spore suspension of a newly developed C. glutamicum strain for GABA production multiple separate fed-batch cultivations, denoted by the media glucose, synthetic SSL and non-synthetic SSL, were performed in multiple 2.7 liter parallel bioreactor systems (Infors AG, Switzerland). At the end of the batch processes, indicated by an increase in pO_2 (pO_2 value raised from 30% to 60% for the first time), the cell broth was transferred to the reactors filled with 1425 mL defined fed-batch media. The fed-batch processes were run for 120 hours. Dissolved oxygen was controlled at 30% by stirrer speed (200 - 1100 rpm), while the reactor was aerated with 2.0 $\frac{L}{min}$ of air. The temperature was kept at 30°C and the pH value was maintained at 7 by addition of KOH or H_3PO_4. Glucose (circa 200 $\frac{g}{L}$) or synthetic SSL were supplied as feeds.

3.3 Medium Composition

Once the inoculum is ready the flask broth is added to a defined carbon free minimal fed-batch media (CGXII) with a starting OD value of 1 [123]. Besides inoculum (5% v/v), carbon source (20% v/v) and minimal media (75% v/v), a carbon source feed was used in the fed-batch phase which is detailed in Table 3.2. The pH was controlled at 7 by automatic addition of phosphoric acid (10% (w/w)) and potassium hydroxide (4 M).

Table 3.2: Medium compositions in both the 1.5 L of broth and 500 mL of feed for the fermentation experiments. This composition consists of CGXII, carbon source, and the inoculum.

Overall Broth Components	**Concentration (%), in 1.5 L for broth and 500 mL for feed respectively**
CGXII	75
Carbon Source	20
Inoculum	5

3.3.1 Broth Substrate Composition

There will be four different fermentations using glucose, synthetic SSL, and SSL. The glucose, used as a control, will be an equal amount of carbon source as the synthetic and non-synthetic SSL (glucose, xylose, and mannose), excluding Arabinose, which is seen in Table 3.3.

Table 3.3: Total amount of sugars in the initial broth for the different experiments.

Experiment Type	**Mass of sugars in 300 mL of broth (g)**
Synthetic SSL	60.3
Glucose	57.3
SSL	60.3
Glucose with wild type strain	66.7

The synthetic SSL composition without any dilution used can be seen in Table 3.4. Looking at the dilution column in the table, the total amount of sugars required for a 20% dilution is 40.2 $\frac{g}{L}$. However, considering the Arabinose is not consumed, the total available carbon source concentration becomes 38.2 $\frac{g}{L}$. Consequently, the amount of usable sugars in 1.5 liters is 57.3 grams.

Table 3.4: Synthetic SSL broth composition, which excludes any toxins that can influence the fermentation process of the microorganisms found in non-synthetic SSL.

Monosaccharides in synthetic SSL broth	**Concentration without dilution (g/L)**	**Concentration with 20% dilution (g/L)**	**Weight of sugars in required 1.5 L (g)**
Arabinose (C5)	10	2	3
Xylose (C5)	45	9	13.5
Glucose (C6)	36	7.2	10.8
Mannose (C6)	110	22	33
Total	201	40.2	60.3 (57.3)

3.3.2 Feed Substrate Composition

To compare the four fermentations every feed needs to have the same amount of sugars. In order to get the feed details the second column in Table 3.5, which corresponds to the composition of the non-diluted synthetic SSL, is looked at. This column is then halved in order to correspond to half a liter of feed. These numbers are found in Table 3.5. Excluding the unusable Arabinose the total amount of feed sugars is 95.5 grams. Therefore, 95.5 grams of glucose in 500 mL for the glucose fermentation will be used as well.

Table 3.5: Synthetic and non-synthetic spent sulfite liquor feed compositions used for fed-batch fermentations.

Monosaccharides in synthetic SSL feed	Concentration without dilution (g/L)	Weight of sugars in required 0.5 L (g)
Arabinose (C5)	10	5
Xylose (C5)	45	22.5
Glucose (C6)	36	18
Mannose (C6)	110	55
Total	201	100.5 (95.5)

3.4 Measurements

For online analytics, carbon dioxide and oxygen in the off gas were quantified by a gas analyzer BlueInOne sensor (BlueSens, Germany) using infrared and paramagnetic principle respectively. Offline samples were collected every 2 hours by Numera© (Securecell, Switzerland) autosampler and cooled down to 4°C until use. Dilution of the samples (1:10) and/or filtration were performed automatically by the Numera© system when needed. Optical density of the samples were analyzed via spectrophotometry (Genesys 10S UV-Vis, Thermo Scientific, U.S.), in order to determine the biomass concentration. Sugars were analyzed by high performance liquid chromatography, or HPLC (Agilent Technologies, U.S.). Cell cultures were diluted (1:10) and filtered by the Numera© system (Securecells, Switzerland) and the supernatants were used for analysis or stored at -20°C. The quantification of sugars was done using a 300 × 7.8 mm NUCLEOGEL®SUGAR 810 Pb column (Macherey-Nagel, Germany) pre-warmed at 80ºC and detected by a refractive index detector (RefractoMax 520, Thermo Scientific, U.S.). The system was run isocratically with deionized water at 0.4 $\frac{mL}{min}$ as mobile phase.

3.5 Bioreactor System

The fermentations were performed in Labfors5 bioreactor systems (Infors HT, Switzerland), consisting of a working volume of 2 liters each. The reaction vessels are equipped with stainless steel components. Each bioreactor contains four baffles, an impeller with two six-bladed Rushton turbines, an L-sparger for gassing, an off-gas condenser, four ports for feeding with one for sampling and a heating jacket. Sensors for data collection are as follows: a temperature sensor (Pt element, Pt100 1/3 DIN-B), pH electrode (Hamilton; Reno, USA), and a pO_2 electrode (Hamilton; Reno, USA) were installed. Off-gas measurements, oxygen and carbon dioxide, were determined via a BlueInOne sensor (BlueSens, Germany). For optical density, which can be correlated to biomass, online measurement using a NIR probe (ASD12-N, Optek) was installed. Planning, control, and monitoring of the data was done with the software EVE (Infors HT, Switzerland). The fully equipped reactors, containing the batch media of 1.5 Liters, were sterilized at 121°C for 20 minutes. A depiction of the basic premise for the experimental apparatus can be seen in Figure 3.1.

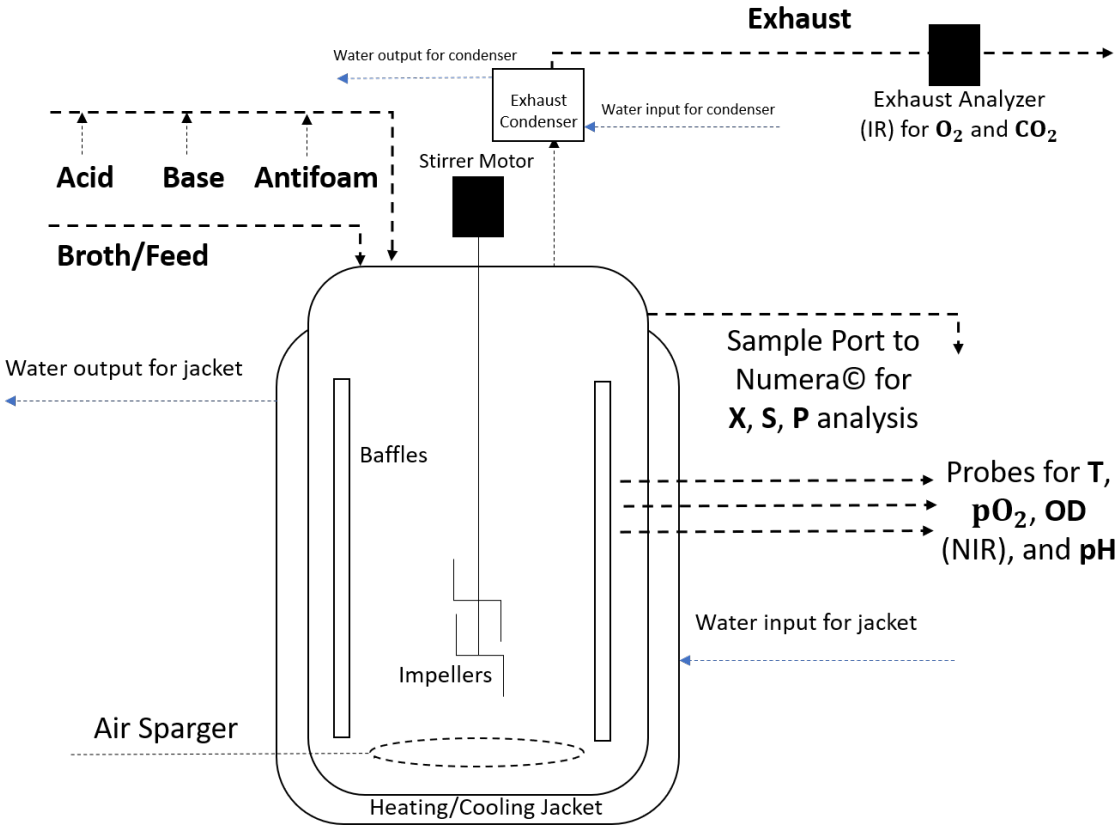

Figure 3.1: Basic experimental stirred tank bioreactor diagram used for simplicity. The labeled equipment are as follows: impellers, stirrer motor, baffles, air sparger, heat exchange jacket, ports for broth/feed, exhaust condenser, exhaust analyzer for carbon dioxide and oxygen, ports for acid, base, and antifoam, probes for temperature, partial pressure of oxygen, optical density, and pH, and lastly the sample port for the analysis of biomass, substrate, and product. Due to the simplification of the diagram, it should not be taken as a 1:1 replica for sizing and/or exact placement of ports/equipment.

3.6 Signal Processing

The signals for NIR and carbon dioxide were collected every 10 seconds and calibrated with the regression curves obtained from previous experiments to convert them to $\frac{g}{L}$ of biomass, or cell dry weight (CDW).

3.6.1 NIR to Cell Dry Weight

The NIR probe is an invasive probe (ASD12-N Absorption Probe, Optek GmbH) which measures absorbance in the culture broth in a range of $0.05 - 4$ concentration units or CU. The calibration curve from NIR to $\frac{g}{L}$ of biomass, or CDW, is seen below in Equation 1.

$$CDW_{NIR} = 110.3 \cdot (NIR)^2 - 3.254 \cdot NIR + 1.878 \tag{1}$$

3.6.2 Carbon Dioxide to Cell Dry Weight

The signals for carbon dioxide were measured with a non-invasive infrared probe (BlueInOne Ferm, BlueSens GmbH). This sensor gives signals for carbon dioxide composition in the off-gas. To relate the signals to the cell growth, the measurements from the off-gas concentration were integrated over time to have the value of total carbon dioxide produced at each time point and divided by the culture volume. In this way the signal was related to the biomass growth since the carbon dioxide is a product in the the aerobic fermentation and is usually a valuable measurement to detect cell activity [124]. The calibration curve from CO_2 to $\frac{g}{L}$ of biomass, or CDW, is seen below in Equation 2.

$$CDW_{CO_2} = 0.759 \cdot CO_2 + 1.817 \tag{2}$$

3.6.3 CDW Sensor Fusion

The two aforementioned sensors in Equations 1 and 2 carry information about the cellular growth. By using nonlinear least-squares data fitting (lsqnonlin) for three different experiments, the two signals are merged in Equation 3 by using a factor $\alpha = 0.6655$ as detailed below.

$$CDW = \alpha \cdot CDW_{NIR} + (1 - \alpha) \cdot CDW_{CO_2} \tag{3}$$

3.6.4 Carbon Dioxide to Substrate

The signals for the carbon dioxide are measured with the non-invasive infrared probe (BlueInOne Ferm, BlueSens GmbH). As mentioned previously, this sensor gives signals for carbon dioxide composition in the off-gas. To relate the signals to the substrate concentration the signal from the off-gas measurement device, which gives the percentage of carbon dioxide in the off-gas, was correlated to the sugar concentration using least-squares regression (lsqnonlin). The measurement of sugar concentrations is normally carried out by HPLC analysis but this method is time consuming and does not allow an online monitoring technique. To overcome this barrier, it may very well be viable to relate the formation of carbon dioxide to the sugar concentration as carbon dioxide is a product of the respiration in aerobic fermentations. Respiration requires the presence of substrate in order to utilize energy making the byproduct carbon dioxide. In this way the infrared, or IR, signal of the percentage of carbon dioxide in the off-gas is related to the substrate concentration. The linear relation between CO_2 % to $\frac{g}{L}$ of glucose is seen below in Equation 4, where $\beta = 4.502$.

$$S_{CO_2} = \beta \cdot CO_2\% \tag{4}$$

3.7 Design of Experiments

Description and explanation of experiments:

1. The first experiment was the wild type strain along with glucose. This experiment used glucose which produced no GABA and is used as a baseline or reference to compare with the other experiments. This baseline experiment will be able to determine differences when other variables are added into the comparison.

2. The second experiment was the new GMO strain with glucose to produce GABA. This experiment is a steppingstone to start investigating a new strain but while also keeping the medium and other variables constant. Thus, the characteristics of the new GMO strain will be compared directly with the established, well tested wild type strain. It is unknown how the production of GABA will influence the behavior of the strain.

3. The third experiment was the new GMO strain with synthetic SSL to produce GABA. This experiment steps further into the fray by introducing another unstudied variable. This variable being the substrate. However, with the synthetic SSL there are no toxins involved. The reasoning for this is to strictly study the consumption behavior the new strain has in the synthetic SSL medium. It is unknown whether it consumes the sugars consecutively or parallel. Leaving out the toxins will also enable an easier analysis of how the toxins inhibit the bacteria which will be done in the final experiment.

4. The fourth experiment was of the new GMO strain with SSL, including toxins, to produce GABA. This experiment will allow the study of how the strain behaves under the influence of toxins and multiple sugar sources.

5. The fifth experiment looks into the cell dry weight, or CDW, of the biomass during fermentation. The experiment uses the same wild type strain with glucose substrate seen in experiment one. The CDW is done by taking the difference of the weight of a filter when passing a liquid biomass sample through it. Doing so verifies if the NIR probe measurements are accurate and true to what is happening during fermentation. It was speculated the NIR measurements were becoming unreliable due to the darkening of the broth.

4 Modeling

4.1 Carbon Dioxide Evolution

The complex network of reactions in which carbon dioxide can partake, seen in Figure 4.1, makes the carbon dioxide state particularly hard to model [125–130]. It can be seen the carbon dioxide produced from the bacteria is first dissolved in the medium and then can undergo reversible side reaction forming bicarbonate. The dissolved carbon dioxide can then transfer from the liquid phase to the gaseous phase in which it may be interpreted by the non-invasive carbon dioxide sensor. Therefore, the complexity of properly measuring carbon dioxide is much harder in reality. The OCER must be reverse engineered in order to understand the CER of the microorganism. Working backwards from OCER enables the CTR to be acquired. Summing the bicarbonate side reactions along with the CTR will then provide the desired CER. The numerous equations presented in Section 4 will showcase how the calculated CER, or CCER, is attained.

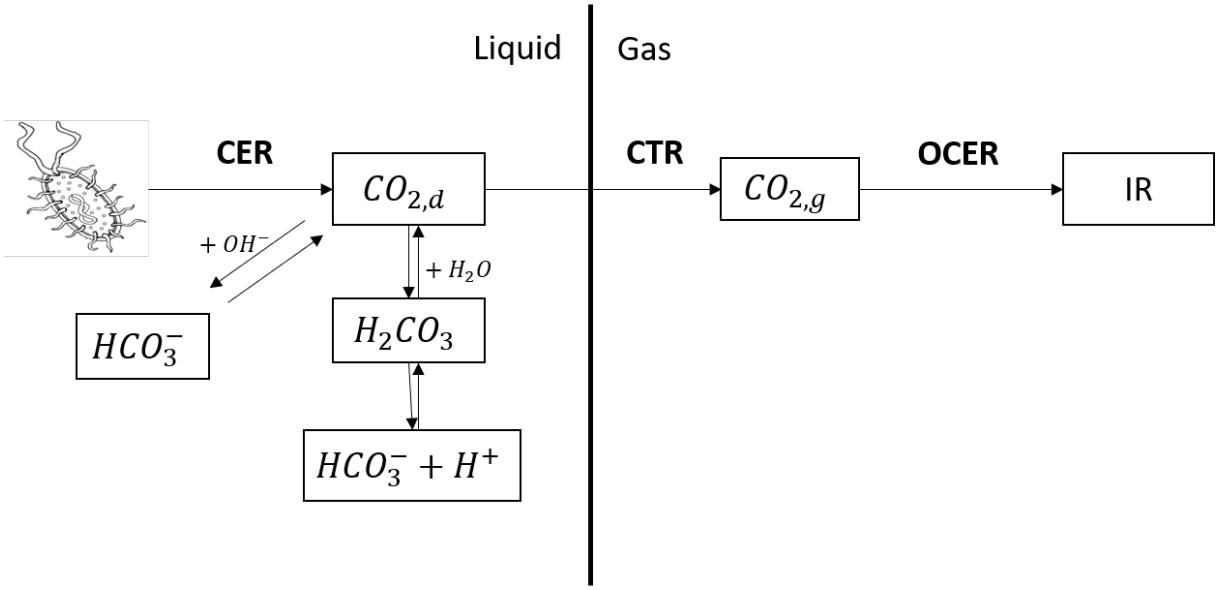

Figure 4.1: Simplified schematic representing the numerous paths carbon dioxide evolution can undergo [126]. The microbial cell produces a specific amount of carbon dioxide based on the CER. This carbon dioxide can reversibly react with hydroxide and/or water which creates bicarbonate. The carbon dioxide can also transfer from the liquid phase to the gaseous phase based on the CTR. Ultimately, the gaseous carbon dioxide is analyzed by the sensor giving the OCER.

Equation 5 is the carbon dioxide and water reaction forming bicarbonate and hydrogen ions [125, 131]. This reaction is portrayed in the left, or liquid, side of Figure 4.1. This is a reversible reaction with reaction constants k_1 and k_{-1}.

$$CO_2 + H_2O \underset{k_{-1}}{\overset{k_1}{\rightleftharpoons}} H^+ + HCO_3^- \tag{5}$$

Equation 6 is the carbon dioxide and hydroxide reaction forming bicarbonate [125, 131]. This reaction is also portrayed in the left, liquid, side of Figure 4.1. This is also a reversible reaction with the reaction constants k_2 and k_{-2}.

$$CO_2 + OH^- \underset{k_{-2}}{\overset{k_2}{\rightleftharpoons}} HCO_3^- \tag{6}$$

Equation 7 are the corresponding equilibrium constants for reaction Equations 5 and 6 [126]. Equating the equilibrium constants will allow for the creation of Equation 8.

$$K_1 = \frac{[H^+][HCO_3^-]}{[CO_2]} \cdot K_2 = \frac{[HCO_3^-]}{[OH^-][CO_2]} = \frac{K_1}{K_W} \tag{7}$$

Equation 8 gives the equilibrium constant K_2, and is created by canceling out the reactant and product terms in Equation 7. This equation enables the relationship between K_1 and K_2 using the water dissociation constant, K_W.

$$K_2 = \frac{K_1}{K_W} \tag{8}$$

Equation 9 is the equation for the equilibrium constant, K_1 , as a function of temperature inside the bioreactor [132].

$$K_1 = \exp(-11.582 - \frac{918.9}{T}) \tag{9}$$

Equation 10 is the rate of reaction one as seen in Equation 5. The rate, r_1, is a function of the forward reaction minus the reverse reaction [126].

$$r_1 = k_1 \cdot [CO_2] - k_{-1} \cdot [HCO_3^-] \cdot [H^+] = k_1 \cdot [CO_2] - k_{-1} \cdot 10^{(-pH)} \cdot [H^+] \tag{10}$$

Equation 11 is the rate of reaction two as seen in Equation 6. The rate, r_2, is a function of the forward reaction minus the reverse reaction [126].

$$r_2 = k_2 \cdot [CO_2] \cdot [OH^-] - k_{-2} \cdot [HCO_3^-] = k_2 \cdot [CO_2] \cdot 10^{(pH-14)} - k_{-2} \cdot [HCO_3^-] \quad (11)$$

Equation 12 is the equation for the reverse reaction constant, k_{-1}, as a function of the forward reaction constant, k_1 and the equilibrium constant, K_1 [133].

$$k_{-1} = \frac{k_1}{K_1} \quad (12)$$

Equation 13 is the equation for the reverse reaction constant, k_{-2}, as a function of the forward reaction constant, k_2 and the equilibrium constant, K_2 [133].

$$k_{-2} = \frac{k_2}{K_2} \quad (13)$$

4.2 Carbon Dioxide Solubility and Phase Transfer

Equation 14 is the formula for the saturation concentration of carbon dioxide. This equation is necessary for the experiments as there was no measurement device that records the saturation concentration of carbon dioxide. This equation uses Henry's law which is able to convert the partial pressure of carbon dioxide into the saturation concentration of carbon dioxide [134].

$$CO_2^* = \frac{P_{CO_2}}{H} \tag{14}$$

Equation 15 involves ideal gas law which substitutes the partial pressure of carbon dioxide with the molar concentration of carbon dioxide, ideal gas constant, and temperature. At a relatively constant temperature, Henry's law claims the amount of a given gas which dissolves in a given type and volume of liquid is directly proportional to the partial pressure of that gas in equilibrium with that liquid [135].

$$CO_2^* = \frac{CO_{2_{mol}}}{H} \cdot R \cdot T \tag{15}$$

Equation 16 is an expression for the value of Henry's constant, H, depending on temperature [132]. The constants at the end of the equation change the units from $\frac{Pa \cdot L}{mol}$ to $\frac{atm \cdot m^3}{mol}$ for unit consistency.

$$H = [101330 \cdot \exp(11.549 - \frac{2440.4}{T})] \cdot \frac{1}{101325} \cdot \frac{1}{1000} \tag{16}$$

Equation 17 is the equation for the volumetric carbon dioxide transfer coefficient, $k_L a_{CO_2}$ [136, 137]. This equation is a function of the RPS of the impeller, the minimum impeller speed for complete dispersion of the sparged gas, and the superficial gas velocity. Lastly, the units are converted from $\frac{1}{s}$ to $\frac{1}{hr}$.

$$k_L a_{CO_2} = [1.59 \cdot (\frac{N}{N_{cd}})^{1.342} \cdot (V_G)^{0.93}] \cdot 3600 \tag{17}$$

Equation 18 is the equation for the minimum impeller speed for complete dispersion of the sparged gas [136, 137]. It is a function of the volumetric gas flow rate, the diameter of the bioreactor, and the diameter of the impeller.

$$N_{cd} = \frac{4 \cdot (Q_G)^{0.5} \cdot (D_B)^{0.25}}{D^2} \tag{18}$$

Equation 19 is the equation for the superficial gas velocity [138, 139]. This is determined by taking the volumetric gas flow rate and dividing it by the cross-sectional area of the bioreactor.

$$V_G = \frac{Q_G}{A} = \frac{A_f/(60 \cdot 100)}{\pi \cdot (\frac{D_B}{2})^2} \tag{19}$$

Equation 20 is the expression for the driving force potential. This is calculated by taking the difference of the saturation concentration of carbon dioxide based off the carbon dioxide concentration leaving the bioreactor, CO_2^*, and the carbon dioxide dissolved in the liquid phase, CO_{2_d}.

$$\Delta C_{moy} = CO_2^* - CO_{2_d} \tag{20}$$

4.3 Simplified Microorganism Kinetics

Equation 21 is the formula for the specific rate of biomass growth. This is equation is termed the "Monod" equation [95]. It has become a popular method to describe how the rate of biomass grows. The growth is dependent on maximum growth rate and the available substrate. The substrate specific constant determines the optimum substrate concentration for the bacteria. For example, when the substrate concentration is lower than the substrate specific constant, μ becomes smaller than the maximum.

$$\mu = \mu_{max} \cdot \frac{S}{(k_S + S)} \tag{21}$$

4.4 Model Equations

Equation 22 is the differential equation describing how the volume changes as a function of time. It is simply how much feed is put into the system as this is a batch-fed reaction. If there is no feed going into the reactor the volume in the reactor stays constant. However, in practice this is technically not the case as samples are taken from the reactor. These sample volumes are assumed to be negligible compared to the reactor volume. If even greater precision is desired, implementing the change of volume due to samples taken could be easily added into the model [140].

$$\frac{dV}{dt} = F \tag{22}$$

Equation 23 is the differential equation which describes how the biomass changes as a function of time. This equation has three terms in total. The first term describes how the biomass grows given the substrate concentration. The second term involves the cell death coefficient and the biomass concentration. This term describes how the bacteria dies thus the negative sign. The third term considers the dilution of biomass due to feeding [140].

$$\frac{dX}{dt} = \mu \cdot X - k_d \cdot X - \frac{F}{V} \cdot X \tag{23}$$

Equation 24 is the differential equation describing how the substrate changes as a function of time. This equation includes two terms in total. The first term accounts for the substrate taken by the bacteria to produce biomass thus the negative sign. The amount of biomass formed per grams of substrate is defined by the yield coefficient. The second term accounts for the addition of sugar from the feed as well as the dilution due to the feed. The substrate concentration influences the specific rate of biomass growth as seen in Equation 4-3. Therefore there is an optimal concentration of substrate which the bacterium prefers for biomass growth [140].

$$\frac{dS}{dt} = -\frac{1}{Y_{\frac{X}{S}}} \cdot \mu \cdot X + \frac{F}{V} \cdot S_{in} - \frac{F}{V} \cdot S \tag{24}$$

Equation 25 is the differential equation which describes how carbon dioxide changes as a function of time [140]. This equation is also equivalent to the carbon dioxide transfer rate or CTR. This equation has two terms in total. The first term considers the carbon dioxide formation due to growth. The second term describes the dilution of carbon dioxide concentration in the broth due to feeding.

$$\frac{dCO_2}{dt} = CTR = \frac{\mu \cdot X}{Y_{\frac{CO_2}{X}}} - \frac{F}{V} \cdot CO_2 \tag{25}$$

Equation 26 is the differential equation which describes the bicarbonate formation during the fermentation process. This equation has two terms in total. The first term takes the reaction of carbon dioxide in account as seen in Equations 5 and 6. The second term takes into account the reverse of reactions [126].

$$\frac{dHCO_3^-}{dt} = (k_1 + k_2 \cdot 10^{pH-14}) \cdot CO_{2_d} - (k_{-2} + k_{-1} \cdot 10^{-pH}) \cdot HCO_3^- \tag{26}$$

Equation 27 is the differential equation for the change of the carbon dioxide concentration dissolved in the liquid phase. This equation considers the diffusion of the carbon dioxide concentration from the liquid phase to the gaseous phase. The higher the transfer coefficient and driving force potential results in more carbon dioxide which can be expelled from the broth and allows the broth to be oxygenated for more bacterial respiration. [126]

$$\frac{dCO_{2_d}}{dt} = k_L a_{CO_2} \cdot \Delta C_{moy} \tag{27}$$

Equation 28 is the carbon dioxide evolution rate equation. There are three terms in total for this equation. The first is the change of the dissolved carbon dioxide concentration term found in Equation 27. The second and third terms are the same forward and reverse carbon dioxide reactions seen in Equation 26 [126]. Lastly, the equation is converted from moles to grams for easy structure compilation.

$$CER = M_{CO_2} \cdot [dCO_{2_d} + (k_1 + k_2 \cdot 10^{pH-14}) \cdot CO_{2_d} - (k_{-2} + k_{-1} \cdot 10^{-pH}) \cdot HCO_3^-] \tag{28}$$

Equation 29 is the calculated CER or CCER. This equation takes into account the carbon dioxide in the gaseous phase, the bicarbonate in the liquid phase, and the carbon dioxide dissolved in the liquid phase. Looking again at Figure 4.1, the summation of these three terms derives the CCER of the microorganism.

$$CCER = CO_2 + HCO_3 + CO_{2_d} \tag{29}$$

Equation 30 is the differential equation which describes how the product, in this case GABA, changes as a function of time [140]. The equation has two terms in total. The first term describes the substrate consumption by defining how much product the bacterium can yield given the amount of biomass. The second term describes the dilution of product concentration due to feed into the bioreactor.

$$\frac{dP}{dt} = \frac{1}{Y_{\frac{P}{X}}} \cdot \mu \cdot X - \frac{F}{V} \cdot P \tag{30}$$

Table 4.1 displays the constants used in the equations found in Section 4. These terms are given a description, a value along with their units, and a reference. Estimated parameter values are found in Section 4.5.

Table 4.1: Model constants for the glucose experiment with no GABA production

Term	Description	Value	Units	Ref.
D	Diameter of impeller	0.046	m	[141]
D_B	Diameter of bioreactor	0.115	m	[141]
k_1	Forward rate constant for r_1	129.6	$\frac{1}{hr}$	[142]
k_2	Forward rate constant for r_2	$4176 \cdot 10^4$	$\frac{L}{mol \cdot hr}$	[142]
K_W	Water dissociation constant	$1.5849 \cdot 10^{-14}$	$\frac{mol^2}{L^2}$	[143]
M_{CO_2}	Molar mass of carbon dioxide	44	$\frac{g}{mol}$	[144]
R	Ideal gas constant	$8.205736 \cdot 10^{-5}$	$\frac{atm \cdot m^3}{K \cdot mol}$	[145]
ρ_{CO_2}	Density of carbon dioxide	1.98	$\frac{g}{L}$	[146]

Table 4.2 displays the most important equations in Section 4 pertaining to the dynamic UKM. This includes the nonlinear ordinary differential equations for volume, biomass, substrate, carbon dioxide, bicarbonate, and product. This ODE is solved via the *ode15s* function in Matlab.

Table 4.2: Main equation of states model overview for Section 4.

$$\frac{dV}{dt} = F \tag{22 revisited}$$

$$\frac{dX}{dt} = \mu \cdot X - k_d \cdot X - \frac{F}{V} \cdot X \tag{23 revisited}$$

$$\frac{dS}{dt} = -\frac{1}{Y_{\frac{X}{S}}} \cdot \mu \cdot X + \frac{F}{V} \cdot S_{in} - \frac{F}{V} \cdot S \tag{24 revisited}$$

$$\frac{dCO_2}{dt} = \frac{\mu \cdot X}{Y_{\frac{CO_2}{X}}} - \frac{F}{V} \cdot CO_2 \tag{25 revisited}$$

$$\frac{dHCO_3^-}{dt} = (k_1 + k_2 \cdot 10^{pH-14}) \cdot CO_{2_d} - (k_2 + k_1 \cdot 10^{-pH}) \cdot HCO_3^- \tag{26 revisited}$$

$$\frac{dCO_{2_d}}{dt} = k_L a_{CO_2} \cdot \Delta C_{moy} \tag{27 revisited}$$

$$\frac{dP}{dt} = \frac{1}{Y_{\frac{P}{X}}} \cdot \mu \cdot X - \frac{F}{V} \cdot P \tag{30 revisited}$$

4.5 Parameter Estimation

Parameter estimation is necessary to be able to properly and adequately use the models given above. This is due to many of these parameters being difficult to calculate and, also, can change from experiment to experiment. Therefore the best way to obtain a value is by parameter estimation. Equation 31 is the general optimization equation which finds the minimal distance between the experimental and model parameters of interest, represented as the vector y. Where M is the number of parameters, N is the number of data for each parameter, and y being the states of interest for both the model and the experiment. This iterative process works towards a solution which "matches" these experimental and model states. Which should, in theory, provide accurate parameter values for the processes if the model is completely correct [140].

$$J = min(\sum_{i=1}^{N}\sum_{j=1}^{M}[(y_{exp,i} - y_{model,i})_j]^2) \tag{31}$$

The estimated parameter values of the model structure are found in Table 4.3. These parameters involve values obtained using the Kalman filters detailed in Section 5.

Table 4.3: Model parameters estimated by the Kalman filter for the glucose experiment with no GABA production

Term	Description	Value	Units
k_d	Cell death coefficient	0.0074	$\frac{1}{hr}$
k_S	Substrate specific constant	0.006	$\frac{g}{L}$
μ_{max}	Maximum specific growth rate	0.1529	$\frac{1}{hr}$
$Y_{\frac{X}{S}}$	Yield coefficient of biomass per substrate consumed	0.4719	$\frac{g_{biomass}}{g_{Substrate}}$
$Y_{\frac{CO_2}{X}}$	Yield coefficient of CO_2 per biomass consumed	0.788	$\frac{g_{CO_2}}{g_{biomass}}$

5 Kalman Filters

5.1 Extended Kalman Filter

The Extended Kalman filter, or EKF, is implemented as in Simon's "Optimal state estimation" [147]. The system is given with continuous-time dynamics and discrete-time measurements as follows:

$$\dot{x} = f(x, u, \omega) \tag{32}$$

$$y_k = Hx_k \tag{33}$$

$$\omega \sim (0, Q) \tag{34}$$

$$v_k \sim (0, R) \tag{35}$$

For k $= 1, \cdots, N_{end}$, state estimate and its covariance are calculated as:

$$\dot{\hat{x}} = f(\hat{x}, u, 0) \tag{36}$$

$$\dot{P} = AP + PA^T + Q \tag{37}$$

Equations 36 and 37 are integrated from $(k-1)^+$ to k^- where:

$$A = \frac{\partial f}{\partial x}$$

The measurements y_k are incorporated at time k as follows:

$$K_k = P_k^- H^T (H P_k^- H^T + R)^{-1} \tag{38}$$

$$\hat{x}_k^+ = \hat{x}_k^- + K_k(y_k - H\hat{x}_k^-) \tag{39}$$

$$P_k^+ = (I - K_k H) P_k^- (I - K_k H)^T + K_k R K_k^T \tag{40}$$

5.2 Unscented Kalman Filter

The system is given as in Equations 32-35. The state estimate and the covariance for the Unscented Kalman filter, or UKF, are implemented as follows [147]. To propagate the system from time $(k-1)^+$ to k^-, we choose the sigma points as:

$$\hat{x}_{k-1}^{(i)} = \hat{x}_{k-1}^{(+)} + \tilde{x}^{(i)} \qquad i = 1, \cdots, 2n$$

$$\tilde{x}^{(i)} = \left(\sqrt{nP_{k-1}{}^{+}}\right)_i^T \qquad i = 1, \cdots, n$$

$$\tilde{x}^{(n+i)} = -\left(\sqrt{nP_{k-1}{}^{+}}\right)_i^T \qquad i = 1, \cdots, n \tag{41}$$

The matrix square root was calculated by using Cholesky factorization. We transform the sigma points using the non-linear system $f(\cdot)$:

$$\hat{x}_k^{(i)} = f(\hat{x}_{k-1}^{(i)}, u_k) \tag{42}$$

Combine them to obtain the a priori state estimate at time k:

$$\hat{x}_k^- = \frac{1}{2n}\sum_{i=1}^{2n} \hat{x}_k^{(i)} \tag{43}$$

And estimate the a priori error covariance as:

$$\hat{P}_k^- = \frac{1}{2n}\sum_{i=1}^{2n} (\hat{x}_k^{(i)} - \hat{x}_k^-)(\hat{x}_k^{(i)} - \hat{x}_k^-)^T + Q \tag{44}$$

For the measurement updates, we transform the sigma points into $\hat{y}_k^{(i)}$:

$$\hat{y}_k^{(i)} = H\hat{x}_k^{(i)} \tag{45}$$

And combine them to obtain the predicted measurement at time k:

$$\hat{y}_k = \frac{1}{2n} \sum_{i=1}^{2n} \hat{y}_k^{(i)} \tag{46}$$

We estimate the covariance of the predicted measurements as:

$$P_y = \frac{1}{2n} \sum_{i=1}^{2n} (\hat{y}_k^{(i)} - \hat{y}_k)(\hat{y}_k^{(i)} - \hat{y}_k)^T + R \tag{47}$$

And the cross covariance between $\hat{x}_k^-$ and $\hat{y}_k$ as:

$$P_{xy} = \frac{1}{2n} \sum_{i=1}^{2n} (\hat{x}_k^{(i)} - \hat{x}_k^-)(\hat{y}_k^{(i)} - \hat{y}_k)^T \tag{48}$$

The measurement update is:

$$K_k = P_{xy} {P_y}^{-1} \tag{49}$$

$$\hat{x}_k^+ = \hat{x}_k^- + K_k(y_k - \hat{y}_k) \tag{50}$$

$${P_k}^+ = {P_k}^- + K_k P_y {K_k}^T \tag{51}$$

6 Results and Discussion

6.1 GABA Production

Table 6.1 shows the production and productivity of the *C. glutamicum* strain tested using glucose, synthetic SSL, and SSL as substrates. It can be seen the synthetic SSL medium allows for a higher productivity of GABA compared to simply utilizing glucose. The diversity of sugars involved in the synthetic SSL allows the bacteria to be more efficient when using solely glucose. However, the results showcased in this table may not be entirely correct due to saturated HPLC peaks. The saturated GABA peaks on the HPLC most likely mean the numbers presented are in reality conservative. These obtained conservative results are 2.473 $\frac{g}{L}$ and 0.055 $g/L/hr$ for the glucose experiment and 6.832 $\frac{g}{L}$ and 0.152 $g/L/hr$ for the synthetic SSL experiment. Unfortunately, due to laboratory constraints mandated by the Covid-19 pandemic, the SSL experiment was not able to be fully analyzed. These GABA results are quite small when looking at the results from other experiments in Table 2.1. Therefore, the method for HPLC analysis should be modified and tried again in order to fully encapsulate the GABA peaks. That in turn should provide the correct results for the fermentations investigated.

Table 6.1: GABA production with GMO strain, substrates, fermentation condition, and productivity.

Strains	**Substrates**	**Fermentation conditions**	**GABA**		**Ref.**
			Titer (g/L)	**Productivity** (g/L/hr)	
Corynebacterium glutamicum ATCC13032	Glucose medium	Fed-batch	2.473	0.055	This Study
C. glutamicum ATCC13032	Synthetic SSL medium	Fed-batch	6.832	0.152	This Study
C. glutamicum ATCC13032	SSL medium	Fed-batch	TBD	TBD	This Study

6.2 Biomass and Carbon Dioxide Production

Figure 6.1 details the carbon dioxide and biomass concentrations throughout the duration of the experiment. This fed-batch experiment was given the feed from hours 20 to 24. It can be seen the carbon dioxide closely follows the same growth as the biomass concentration. The stagnant stages of carbon dioxide indicate there is no energy usage during the aerobic fermentation. Consequently, the biomass population is slowly dying given by the slightly negative curve. This confirms the assumption which correlates the fast, easily measurable carbon dioxide concentrations with the noise-laden NIR probe measures for biomass concentration. The end phase of the fermentation shows the biomass peak and then decay to what looks to be at least a partial steady state concentration.

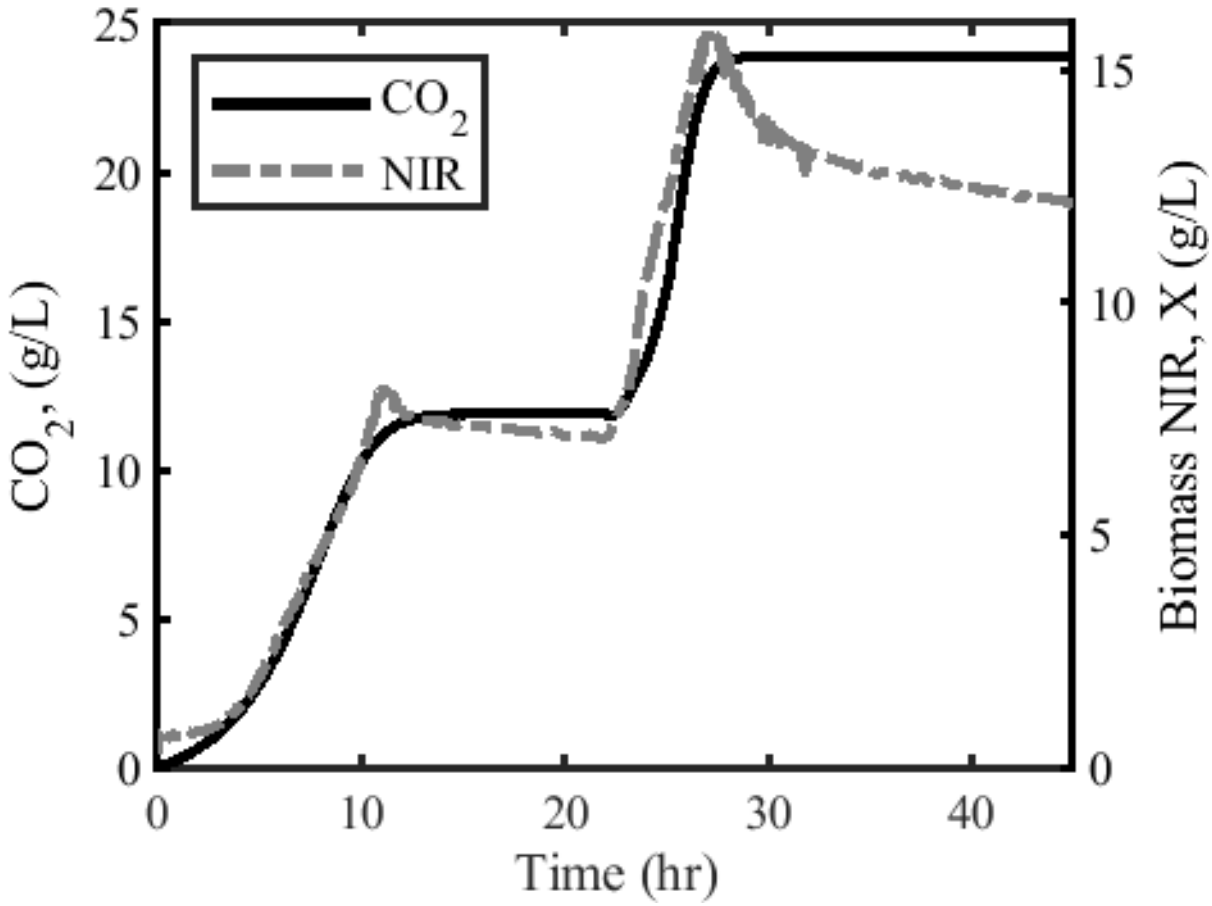

Figure 6.1: Carbon dioxide concentration versus biomass concentration, which is calculated via the NIR probe, for the wild type non-product fed-batch fermentation experiment. The units for the concentrations are in grams per liter. The slope increases when substrate is available and levels off when the biomass is substrate starved.

6.2.1 Bicarbonate and Carbon Dioxide Analysis

Figure 6.2 demonstrates the carbon dioxide concentration along with the base, KOH, fed throughout the time of the experiment. It can be seen the base fed into the reactor follows quite closely with the carbon dioxide emitted. This should be the case as a solution of carbon dioxide is slightly acidic. This acidity derives from the bicarbonate formation seen in Equations 5 and 6. The reason why carbon dioxide solutions are slightly acidic is due to the equilibrium with water which produces hydrogen ions which are acidic. This plot depicts the direct relationship during the experiment and shows that CER is occurring.

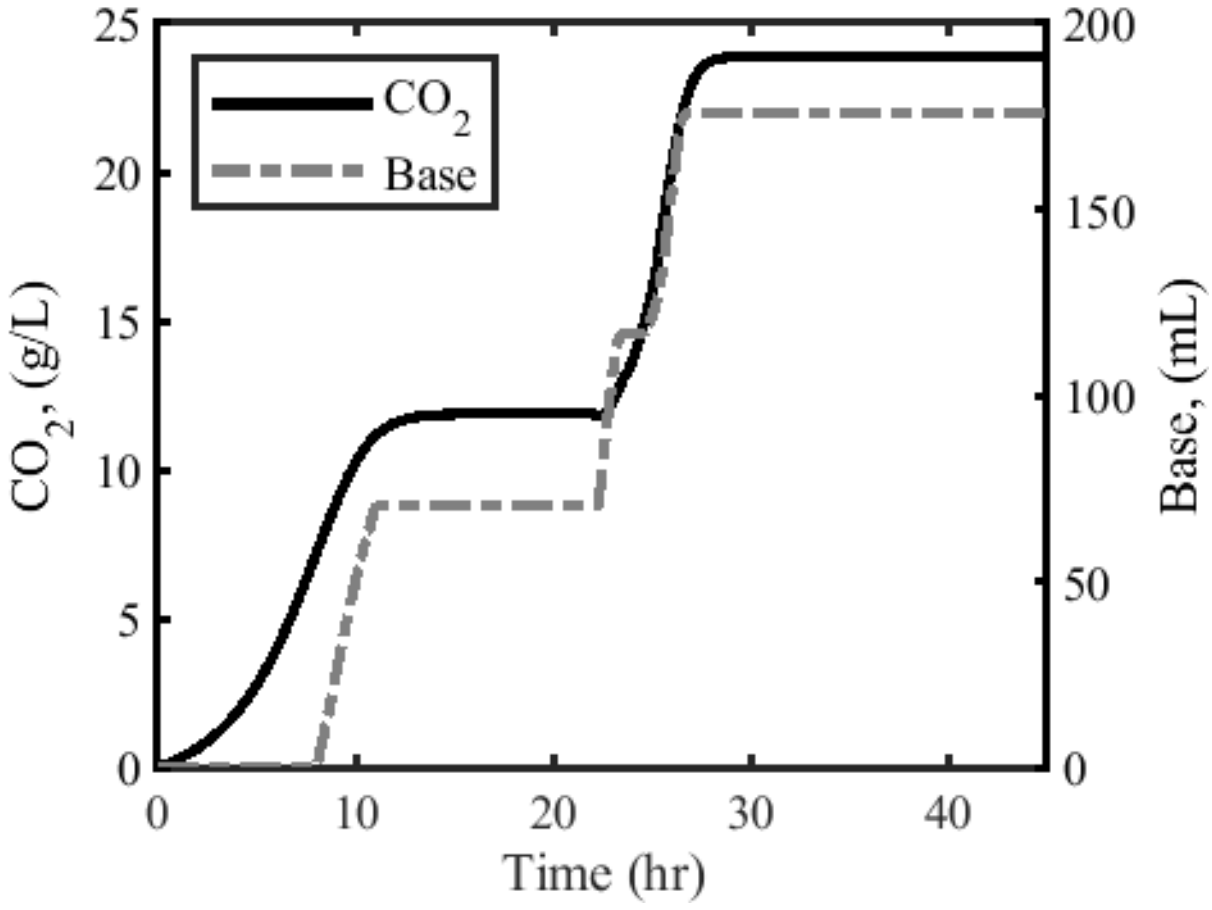

Figure 6.2: Carbon dioxide concentration versus base concentration for the wild type non-product fed-batch fermentation experiment. The units for the carbon dioxide concentration is in grams per liter. The amount of base supplied to the system is shown in units of mL. The slope increases when substrate is available and levels off when the biomass is substrate starved.

Figure 6.3 shows both the carbon dioxide off-gas and the carbon dioxide via the calculated CER. It can be seen the CCER follows the measured carbon dioxide off-gas perfectly! Thus, the modeling and formulation which were utilized worked successfully. This also shows that Equation 29, the formula for CCER, has negligible dissociated and dissolved carbon dioxide terms. This is due to the small magnitudes of the dissolved carbon dioxide and bicarbonate seen in Figure 6.4. Consequently, modeling the liquid phase of bicarbonate and carbon dioxide is not required to perfectly model the fermentation process.

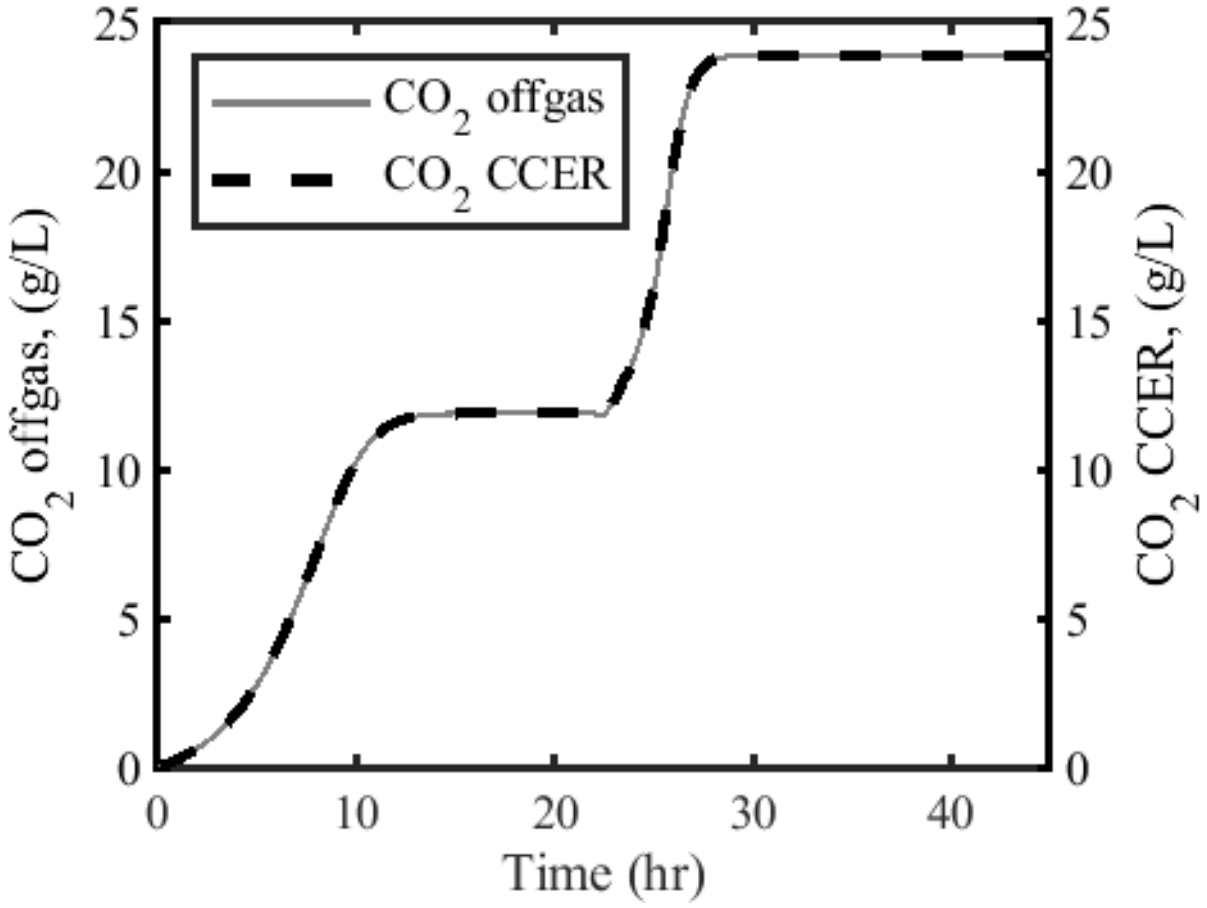

Figure 6.3: Carbon dioxide off-gas concentration versus carbon dioxide concentration, calculated by using the carbon dioxide evolution rate, for the wild type non-product fed-batch fermentation. The units for the concentrations are in grams per liter. The slope increases when substrate is available and levels off when the biomass is substrate starved.

Figure 6.4 displays the bicarbonate and dissolved carbon dioxide concentrations throughout the duration of the experiment. These results were simulated within the model and the states of both during the experiment are provided. It can be seen the order of magnitude, 10^{-3}, for the concentrations are relatively the same. The beginning of the experiment starts at a concentration close to zero and ends with the concentration also very close to zero. Therefore, the carbon dioxide and bicarbonate which enters the system also leaves the system. As detailed, the dissolved carbon dioxide terms used in the model are negligible and do not need to be considered.

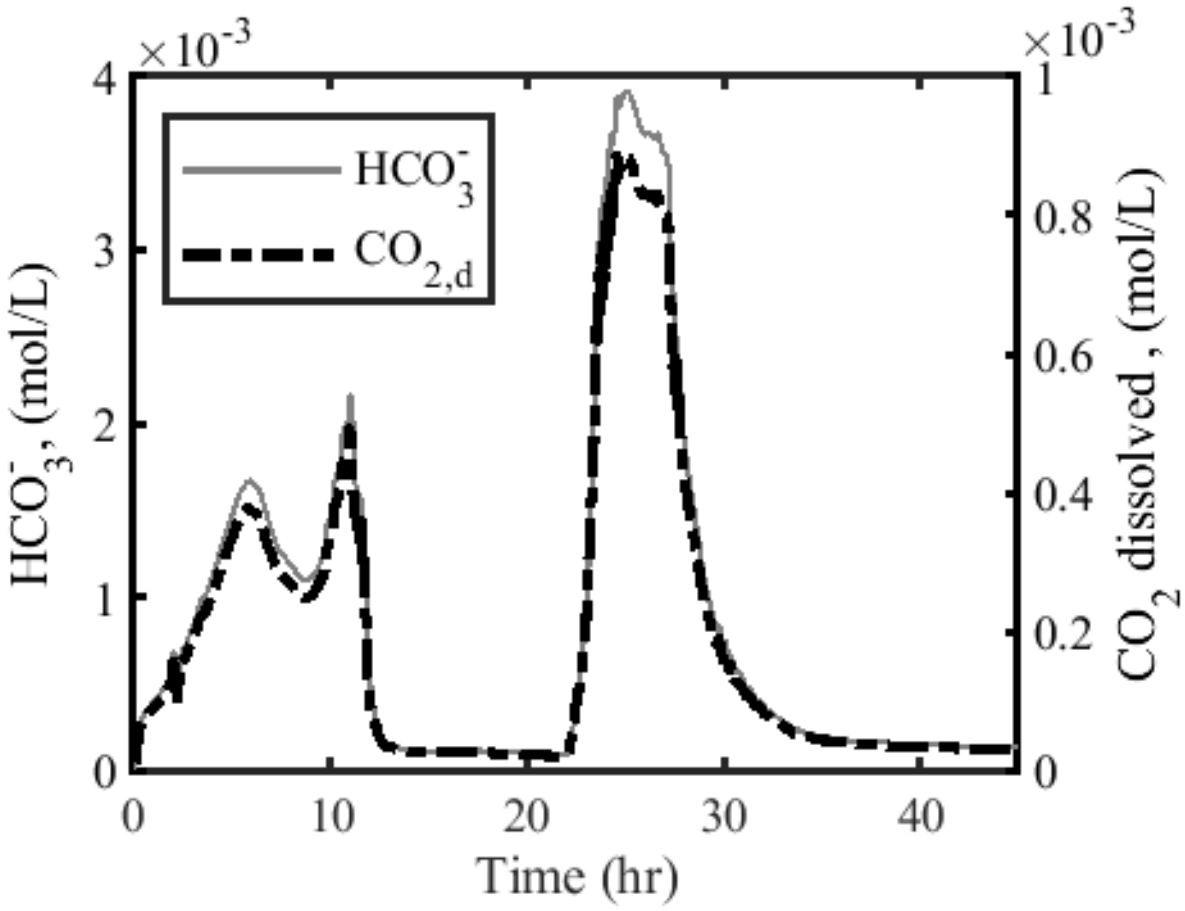

Figure 6.4: Bicarbonate concentration versus dissolved carbon dioxide concentration for the wild type non-product fermentation fed-batch fermentation. The units for the concentrations are in moles per liter. Peaks can be seen when the biomass converts substrate to cellular energy.

6.3 Kalman Filters

Below details the results of the Kalman filters. The initial conditions of volume, CDW, substrate, and carbon dioxide were given as:

$$[ht]x_0 = \begin{bmatrix} 1.5 & 1.2 & 20 & 0 \end{bmatrix}^T$$

$$\hat{x}_0^+ = x_0$$

$$P_0{}^+ = \begin{bmatrix} 1 & 0 & 0 & 0 \\ 0 & 1 & 0 & 0 \\ 0 & 0 & 1 & 0 \\ 0 & 0 & 0 & 1 \end{bmatrix} \tag{52}$$

And the measurement and process noises are:

$$R = \begin{bmatrix} 10^{-4} & 0 & 0 & 0 \\ 0 & 1.954 & 0 & 0 \\ 0 & 0 & 10^{-2} & 0 \\ 0 & 0 & 0 & 0.2 \end{bmatrix}$$

$$Q = \begin{bmatrix} 0.1 & 0 & 0 & 0 \\ 0 & 1.954 \cdot 10^{-2} & 0 & 0 \\ 0 & 0 & 10^{-4} & 0 \\ 0 & 0 & 0 & 1 \end{bmatrix} \tag{53}$$

With the measurement matrix simply as:

$$H = \begin{bmatrix} 1 & 0 & 0 & 0 \\ 0 & 1 & 0 & 0 \\ 0 & 0 & 1 & 0 \\ 0 & 0 & 0 & 1 \end{bmatrix} \tag{54}$$

The measurements available for the filter are the volume, the CDW as defined in Equation 3, the substrate, and the carbon dioxide:

$$y = \begin{bmatrix} V \\ CDW \\ S \\ CO_2 \end{bmatrix} \tag{55}$$

6.3.1 Biomass Analysis

The filters receive signals from the sensors every 60 seconds. The results for the biomass are reported in Figure 6.5. The UKF is able to filter the signal and remove the noise following the measurements while the EKF results gain trust in the predictions over the observations. This makes it difficult to regain the correct variance and makes the filter divergent. The actual errors between the true and estimated states tend to be larger than those predicted by the calculated covariance matrix. This deviation is observed when the system at steady state is perturbed by the input (around 23 hrs Fig. 6.5). The performance of the UKF shows if higher order information is available about the distribution it can then be incorporated to improve the estimate.

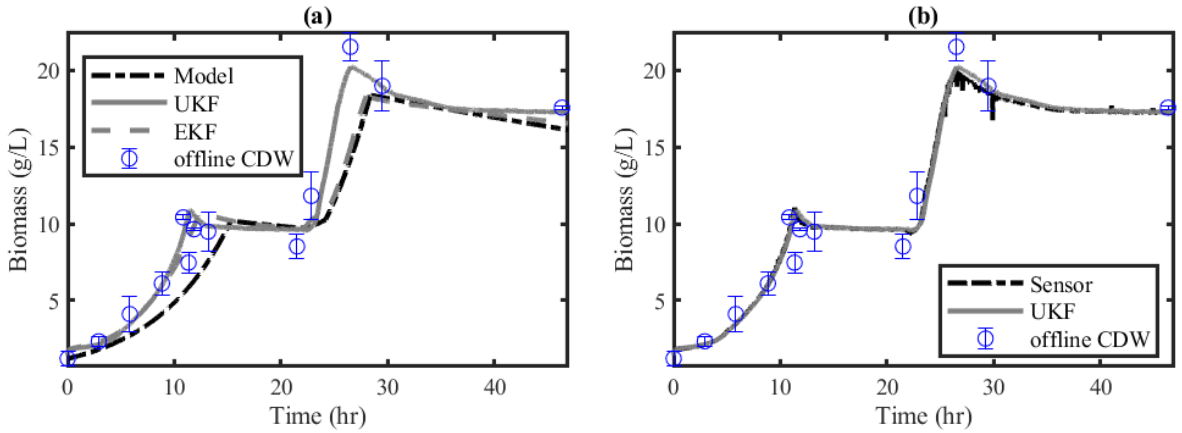

Figure 6.5: Biomass plots for the CDW experiment with the model, EKF and UKF implemented. The Kalman filters are used to smooth the signal from the biomass sensor. The filters are compared with the performances of the model in (a). The UKF is able to filter out the noise while the EKF diverges from the off-line measurements. The UKF performance is then directly compared in (b) with the sensor measurements. Utilizing the UKF, noise from the sensor following the measurements is able to filtered out.

6.3.2 Substrate Analysis

By exploiting the information carried by the IR off-gas measurement, it is also possible to have online measurements of the substrate. However, this is possible only during the fed-batch phase and not during the batch phase. This is because during that phase the carbon dioxide production is not linearly related to the substrate concentration. The filter therefore starts receiving measurements at the end of the batch as visible in Figure 6.6. The results demonstrate the filter can be tuned appropriately and allows for online measurements of the substrate as well. However, it is preferable to add the information from the real measurement to prevent any possible failure. The observability of the system can be investigated by using Lie derivatives [148]. The limitation of the estimation for the sugars derives from an inaccurate measurement of the volume. The volume measurement needs to be improved to allow for more accurate estimates. Taking into account the volume increase due to the acid, base and antifoam is most likely the best solution.

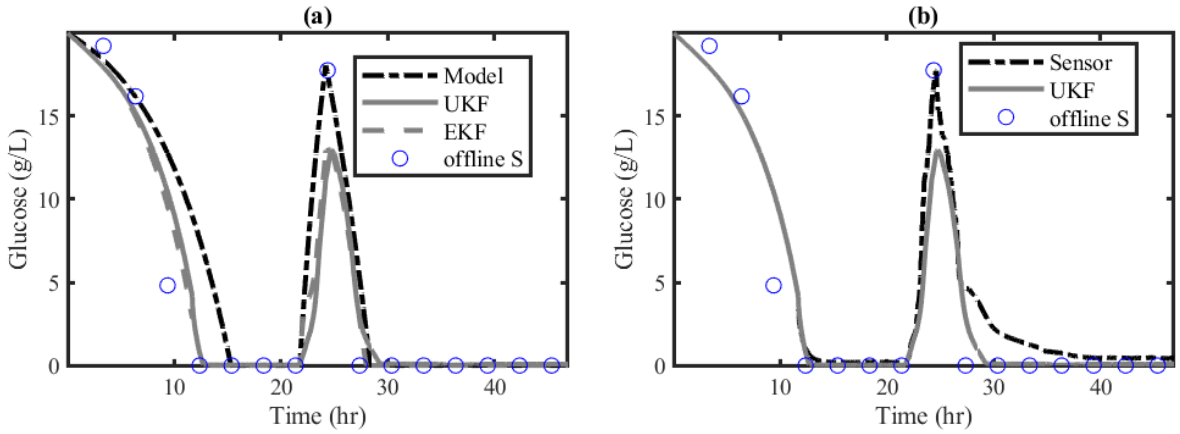

Figure 6.6: Substrate plots for the CDW experiment with the model, EKF and UKF implemented. In this case, the model dynamics seem to accurately describe the sugar consumption. However, it is preferable to add the information from the real measurement to prevent any possible failure. Both filters here have a comparable performance. The filter is used as a smother to correct the signal from the substrate sensor. The estimation results are compared with the performances of the model in (a) and then in (b) with the sensor measurements. As already said for the biomass, and in this case, the estimator is blind to the offline measurements. The limitation on the estimation of the sugars comes from an inaccurate measurement of the volume which needs to be improved to allow the filters to give accurate estimates.

7 Conclusion

The results of this work demonstrates successful implementation of a non-linear unstructured kinetic model used alongside both an Unscented and an Extended Kalman filter for state estimation. The available online measurements were shown to effectively describe the dynamic behavior of the process which can lead to closer estimations of all the important states of interest. The results from the estimators show, in this specific case, the Unscented Kalman Filter seems to be a suitable estimator for monitoring of biomass and substrate. The estimator allows for frequent measurement without the presence of noise or the use of any offline measurements. Parameter estimation can be included to correct the uncertainty of the model and allow for using the filters for more accurate prediction of the states. The results from the present approach are quite promising and can be further exploited by increasing the number of measurements and thus the estimated states like product formation. The initial aim was to test the estimators for the GABA producing strain which includes product estimation under the presence of a complex sugar mixture such as SSL. However, this was not possible due to the University and laboratory restrictions which became necessary during the spread of the COVID-19 pandemic.

8 Further Work

Further work involving this research includes verifying HPLC measurements for the sugars and GABA from the SSL experiment, verifying fermentation results by doing duplicate identical experiments, implementing the product model in the UKM, and looking into the possibility to estimate the product in a strain developed to deplete multiple sugars such as SSL. Unfortunately, the product model could not be investigated due to the lab being at capacity for use of the HPLC after the lab restrictions were put into place due to the COVID-19 pandemic. This product state will be studied once the results have been obtained from the HPLC. Multiple identical experiments should be accomplished in order to properly verify the effectiveness of the estimator. The results of the present approach can be exploited further by increasing the number of measurements which will then allow for more estimated states. This is another way to accomplish the determination of product formation.

References

[1] Karin Kovárová-Kovar and Thomas Egli. Growth kinetics of suspended microbial cells: from single-substrate-controlled growth to mixed-substrate kinetics. *Microbiol. Mol. Biol. Rev.*, 62(3):646–666, 1998.

[2] Manoj Kumar Enamala, Divya Sruthi Pasumarthy, Pavan Kumar Gandrapu, Murthy Chavali, Harika Mudumbai, and Chandrasekhar Kuppam. Production of a variety of industrially significant products by biological sources through fermentation. In *Microbial Technology for the Welfare of Society*, pages 201–221. Springer, 2019.

[3] Joseph A Chemler and Mattheos AG Koffas. Metabolic engineering for plant natural product biosynthesis in microbes. *Current opinion in biotechnology*, 19(6):597–605, 2008.

[4] Michael J Waites, Neil L Morgan, John S Rockey, and Gary Higton. *Industrial microbiology: an introduction*. John Wiley & Sons, 2009.

[5] Gaurav Kumar Pal and PV Suresh. Microbial collagenases: challenges and prospects in production and potential applications in food and nutrition. *RSC advances*, 6(40):33763–33780, 2016.

[6] Dominik Krämer and Rudibert King. On-line monitoring of substrates and biomass using near-infrared spectroscopy and model-based state estimation for enzyme production by *S. cerevisiae*. *IFAC-PapersOnLine*, 49(7):609–614, 2016.

[7] RD Gudi, SL Shah, and MR Gray. Multirate state and parameter estimation in an antibiotic fermentation with delayed measurements. *Biotechnology and Bioengineering*, 44(11):1271–1278, 1994.

[8] Gregory Stephanopoulos and Ka-Yiu San. Studies on on-line bioreactor identification. i. theory. *Biotechnology and Bioengineering*, 26(10):1176–1188, 1984.

[9] D Krämer and R King. A hybrid approach for bioprocess state estimation using nir spectroscopy and a sigma-point kalman filter. *Journal of Process Control*, 82:91–104, 2019.

[10] Jae Woong Choi, Sung Sun Yim, Seung Hwan Lee, Taek Jin Kang, Si Jae Park, and Ki Jun Jeong. Enhanced production of gamma-aminobutyrate (gaba) in recombinant corynebacterium glutamicum by expressing glutamate decarboxylase active in expanded ph range. *Microbial cell factories*, 14(1):21, 2015.

[11] Naoko Okai, Chihiro Takahashi, Kazuki Hatada, Chiaki Ogino, and Akihiko Kondo. Disruption of pkng enhances production of gamma-aminobutyric acid by corynebacterium glutamicum expressing glutamate decarboxylase. *AMB Express*, 4(1):1–8, 2014.

[12] Feng Shi, Junjun Jiang, Yongfu Li, Youxin Li, and Yilong Xie. Enhancement of γ-aminobutyric acid production in recombinant corynebacterium glutamicum by co-expressing two glutamate decarboxylase genes from lactobacillus brevis. *Journal of industrial microbiology & biotechnology*, 40(11):1285–1296, 2013.

[13] Nannan Wang, Yalan Ni, and Feng Shi. Deletion of odha or pyc improves production of γ-aminobutyric acid and its precursor l-glutamate in recombinant corynebacterium glutamicum. *Biotechnology letters*, 37(7):1473–1481, 2015.

[14] Chihiro Takahashi, Junki Shirakawa, Takeyuki Tsuchidate, Naoko Okai, Kazuki Hatada, Hideki Nakayama, Toshihiro Tateno, Chiaki Ogino, and Akihiko Kondo. Robust production of gamma-amino butyric acid using recombinant corynebacterium glutamicum expressing glutamate decarboxylase from escherichia coli. *Enzyme and microbial technology*, 51(3):171–176, 2012.

[15] Carlos González-Figueredo, René Alejandro Flores-Estrella, and Oscar A Rojas-Rejón. Fermentation: Metabolism, kinetic models, and bioprocessing. In *Current topics in biochemical engineering*. IntechOpen, 2018.

[16] Hans F Ebel, Claus Bliefert, and William E Russey. *The Art of Scientific Writing: From Student Reports to Professional Publications in Chemistry and Related Fields*. John Wiley & Sons, 2004.

[17] Sarah C Watkinson, Lynne Boddy, and Nicholas Money. *The fungi*. Academic Press, 2015.

[18] Sudhanshu S Behera, Ramesh C Ray, Urmimala Das, Sandeep K Panda, and P Saranraj. Microorganisms in fermentation. In *Essentials in Fermentation Technology*, pages 1–39. Springer, 2019.

[19] Soumya Mukherjee. Isolation and purification of industrial enzymes: Advances in enzyme technology. In *Advances in Enzyme Technology*, pages 41–70. Elsevier, 2019.

[20] Kenneth P Clapp, Andreas Castan, and Eva K Lindskog. Upstream processing equipment. In *Biopharmaceutical Processing*, pages 457–476. Elsevier, 2018.

[21] Akinori Matsushika, Atsushi Nagashima, Tetsuya Goshima, and Tamotsu Hoshino. Fermentation of xylose causes inefficient metabolic state due to carbon/energy starvation and reduced glycolytic flux in recombinant industrial saccharomyces cerevisiae. *PLoS One*, 8(7), 2013.

[22] RH De Deken. The crabtree effect: a regulatory system in yeast. *Microbiology*, 44(2):149–156, 1966.

[23] PR Rich. The molecular machinery of keilin's respiratory chain, 2003.

[24] Wei-Cho Huang and I-Ching Tang. Bacterial and yeast cultures–process characteristics, products, and applications. In *Bioprocessing for value-added products from renewable resources*, pages 185–223. Elsevier, 2007.

[25] Klaus Schmidt-Rohr. Oxygen is the high-energy molecule powering complex multicellular life: Fundamental corrections to traditional bioenergetics. *ACS omega*, 5(5):2221–2233, 2020.

[26] Donika Ivanova, Zhivko Zhelev, Plamen Getsov, Biliana Nikolova, Ichio Aoki, Tatsuya Higashi, and Rumiana Bakalova. Vitamin k: redox-modulation, prevention of mitochondrial dysfunction and anticancer effect. *Redox biology*, 16:352–358, 2018.

[27] Judith Becker and Christoph Wittmann. Systems and synthetic metabolic engineering for amino acid production–the heartbeat of industrial strain development. *Current opinion in biotechnology*, 23(5):718–726, 2012.

[28] Volker F Wendisch, Joao MP Jorge, Fernando Pérez-García, and Elvira Sgobba. Updates on industrial production of amino acids using *Corynebacterium glutamicum*. *World Journal of Microbiology and Biotechnology*, 32(6):105, 2016.

[29] Lothar Eggeling and Michael Bott. *Handbook of Corynebacterium glutamicum*. CRC press, 2005.

[30] Bastian Blombach and Gerd M Seibold. Carbohydrate metabolism in corynebacterium glutamicum and applications for the metabolic engineering of l-lysine production strains. *Applied microbiology and biotechnology*, 86(5):1313–1322, 2010.

[31] Muriel Cocaign, Christophe Monnet, and Nicholas D Lindley. Batch kinetics of corynebacterium glutamicum during growth on various carbon substrates: use of substrate mixtures to localise metabolic bottlenecks. *Applied microbiology and biotechnology*, 40(4):526–530, 1993.

[32] H Dominguez, M Cocaign-Bousquet, and ND Lindley. Simultaneous consumption of glucose and fructose from sugar mixtures during batch growth of corynebacterium glutamicum. *Applied microbiology and biotechnology*, 47(5):600–603, 1997.

[33] Thomas Hermann. Industrial production of amino acids by coryneform bacteria. *Journal of biotechnology*, 104(1-3):155–172, 2003.

[34] Jens Schneider, Karin Niermann, and Volker F Wendisch. Production of the amino acids l-glutamate, l-lysine, l-ornithine and l-arginine from arabinose by recombinant corynebacterium glutamicum. *Journal of biotechnology*, 154(2-3):191–198, 2011.

[35] Jens Schneider and Volker F Wendisch. Putrescine production by engineered corynebacterium glutamicum. *Applied microbiology and biotechnology*, 88(4):859–868, 2010.

[36] Bastian Blombach, Tanja Riester, Stefan Wieschalka, Christian Ziert, Jung-Won Youn, Volker F Wendisch, and Bernhard J Eikmanns. Corynebacterium glutamicum tailored for efficient isobutanol production. *Appl. Environ. Microbiol.*, 77(10):3300–3310, 2011.

[37] Miho Sasaki, Toru Jojima, Masayuki Inui, and Hideaki Yukawa. Xylitol production by recombinant corynebacterium glutamicum under oxygen deprivation. *Applied microbiology and biotechnology*, 86(4):1057–1066, 2010.

[38] Deo Rashmi, Rahul Zanan, Sheeba John, Kiran Khandagale, and Altafhusain Nadaf. γ-aminobutyric acid (gaba): biosynthesis, role, commercial production, and applications. In *Studies in Natural Products Chemistry*, volume 57, pages 413–452. Elsevier, 2018.

[39] Michaela Graf, Thorsten Haas, Felix Müller, Julia Harm-Bekbenbetova, Andreas Freund, Alexander Nieß, Marcus Persicke, Joern Kalinowski, Bastian Blombach, and Ralf Takors. Continuous adaptive

evolution of a fast-growing corynebacterium glutamicum strain independent of protocatechuate. *Frontiers in microbiology*, 10:1648, 2019.

[40] Judith Becker and Christoph Wittmann. Industrial microorganisms: Corynebacterium glutamicum. *Industrial biotechnology: microorganisms*, 1:183–220, 2017.

[41] Jeffrey C Pommerville. *Alcamo's laboratory fundamentals of microbiology*. Jones & Bartlett Publishers, 2010.

[42] Uri Alon, Michael G Surette, Naama Barkai, and Stanislas Leibler. Robustness in bacterial chemotaxis. *Nature*, 397(6715):168–171, 1999.

[43] Ebru Altiındağ and Betul Baykan. Discover the world's research. *Turk J Neurol*, 23:88–89, 2017.

[44] Haixing Li and Yusheng Cao. Lactic acid bacterial cell factories for gamma-aminobutyric acid. *Amino acids*, 39(5):1107–1116, 2010.

[45] David L Martin. Mechanisms controllign gaba synthesis and degradation in the brain. *GABA in the nervous system: the view at fifty years*, pages 25–41, 2000.

[46] Javier DeFelipe. Neocortical neuronal diversity: chemical heterogeneity revealed by colocalization studies of classic neurotransmitters, neuropeptides, calcium-binding proteins, and cell surface molecules. *Cerebral cortex*, 3(4):273–289, 1993.

[47] James H Wood, Theodore A Hare, Bruce S Glaeser, James C Ballenger, and Robert M Post. Low cerebrospinal fluid γ-aminobutyric acid content in seizure patients. *Neurology*, 29(9 Part 1):1203–1203, 1979.

[48] Si Jae Park, Eun Young Kim, Won Noh, Young Hoon Oh, Hye Young Kim, Bong Keun Song, Kwang Myung Cho, Soon Ho Hong, Seung Hwan Lee, and Jonggeon Jegal. Synthesis of nylon 4 from gamma-aminobutyrate (gaba) produced by recombinant escherichia coli. *Bioprocess and biosystems engineering*, 36(7):885–892, 2013.

[49] Norioki Kawasaki, Atsuyoshi Nakayama, Naoko Yamano, Sahori Takeda, Yoshikazu Kawata, Noboru Yamamoto, and Sei-ichi Aiba. Synthesis, thermal and mechanical properties and biodegradation of branched polyamide 4. *Polymer*, 46(23):9987–9993, 2005.

[50] Kazuhiko Hashimoto, Tsuyoshi Hamano, and Masahiko Okada. Degradation of several polyamides in soils. *Journal of applied polymer science*, 54(10):1579–1583, 1994.

[51] Yutaka Tokiwa, Buenaventurada P Calabia, Charles U Ugwu, and Seiichi Aiba. Biodegradability of plastics. *International journal of molecular sciences*, 10(9):3722–3742, 2009.

[52] Radhika Dhakal, Vivek K Bajpai, and Kwang-Hyun Baek. Production of gaba (γ-aminobutyric acid) by microorganisms: a review. *Brazilian Journal of Microbiology*, 43(4):1230–1241, 2012.

[53] João MP Jorge, Christian Leggewie, and Volker F Wendisch. A new metabolic route for the production of gamma-aminobutyric acid by corynebacterium glutamicum from glucose. *Amino acids*, 48(11):2519–2531, 2016.

[54] Barry J Shelp, Alan W Bown, and Michael D McLean. Metabolism and functions of gamma-aminobutyric acid. *Trends in plant science*, 4(11):446–452, 1999.

[55] Taowei Yang, Zhiming Rao, Xian Zhang, Qing Lin, Haifeng Xia, Zhenghong Xu, and Shangtian Yang. Production of 2, 3-butanediol from glucose by gras microorganism bacillus amyloliquefaciens. *Journal of basic microbiology*, 51(6):650–658, 2011.

[56] Tao-Wei Yang, Zhi-Ming Rao, Xian Zhang, Mei-Juan Xu, Zheng-Hong Xu, and Shang-Tian Yang. Fermentation of biodiesel-derived glycerol by bacillus amyloliquefaciens: effects of co-substrates on 2, 3-butanediol production. *Applied microbiology and biotechnology*, 97(17):7651–7658, 2013.

[57] Noriko Komatsuzaki, Jun Shima, Shinichi Kawamoto, Hiroh Momose, and Toshinori Kimura. Production of γ-aminobutyric acid (gaba) by lactobacillus paracasei isolated from traditional fermented foods. *Food microbiology*, 22(6):497–504, 2005.

[58] Haixing Li, Ting Qiu, Guidong Huang, and Yusheng Cao. Production of gamma-aminobutyric acid by lactobacillus brevis ncl912 using fed-batch fermentation. *Microbial Cell Factories*, 9(1):85, 2010.

[59] Lingzhi Tian, M Xu, and Zhiming Rao. Construction of a recombinant escherichia coli bl21/pet-28a-lpgad and the optimization of transformation conditions for the efficient production of gamma-aminobutyric acid. *Sheng wu gong cheng xue bao= Chinese journal of biotechnology*, 28(1):65–75, 2012.

[60] Taek Jin Kang, Ngoc Anh Thu Ho, and Seung Pil Pack. Buffer-free production of gamma-aminobutyric acid using an engineered glutamate decarboxylase from escherichia coli. *Enzyme and microbial technology*, 53(3):200–205, 2013.

[61] Mineka Yoshimura, Tohru Toyoshi, Atsushi Sano, Toru Izumi, Takashi Fujii, Chiaki Konishi, Shuji Inai, Chiaki Matsukura, Naoya Fukuda, Hiroshi Ezura, et al. Antihypertensive effect of a γ-aminobutyric acid rich tomato cultivar 'dg03-9'in spontaneously hypertensive rats. *Journal of Agricultural and Food Chemistry*, 58(1):615–619, 2010.

[62] Taowei Yang, Zhiming Rao, Bernard Gitura Kimani, Meijuan Xu, Xian Zhang, and Shang-Tian Yang. Two-step production of gamma-aminobutyric acid from cassava powder using corynebacterium glutamicum and lactobacillus plantarum. *Journal of industrial microbiology & biotechnology*, 42(8):1157–1165, 2015.

[63] E Barrett, RP Ross, PW O'toole, GF Fitzgerald, and C Stanton. γ-aminobutyric acid production by culturable bacteria from the human intestine. *Journal of applied microbiology*, 113(2):411–417, 2012.

[64] Saoharit Nitayavardhana, Prachand Shrestha, Mary L Rasmussen, Buddhi P Lamsal, J Hans van Leeuwen, and Samir Kumar Khanal. Ultrasound improved ethanol fermentation from cassava chips in cassava-based ethanol plants. *Bioresource technology*, 101(8):2741–2747, 2010.

[65] Myung-Ji Seo, Young-Do Nam, So-Young Lee, So-Lim Park, Sung-Hun YI, and Seong-Il Lim. Expression and characterization of a glutamate decarboxylase from lactobacillus brevis 877g producing γ-aminobutyric acid. *Bioscience, biotechnology, and biochemistry*, 77(4):853–856, 2013.

[66] Ying Zhang, Lei Song, Qiang Gao, Shao Mei Yu, Lei Li, and Nian Fa Gao. The two-step biotransformation of monosodium glutamate to gaba by lactobacillus brevis growing and resting cells. *Applied microbiology and biotechnology*, 94(6):1619–1627, 2012.

[67] Sadaji Yokoyama, Jun-ichi Hiramatsu, and Kiyoshi Hayakawa. Production of γ-aminobutyric acid from alcohol distillery lees by lactobacillus brevis ifo-12005. *Journal of bioscience and bioengineering*, 93(1):95–97, 2002.

[68] SANG-MIN PARK, MOO-YOUNG LEE, GEUN-EOG JI, JAE-WON LEE, MYEONG-SOO PARK, TAE-RYEON HEO, et al. Improvement of γ-aminobutyric acid (gaba) production using cellentrapment of lactobacillus brevis gaba 057. *Journal of microbiology and biotechnology*, 16(4):562–568, 2006.

[69] Jun Huang, Le-he Mei, Hong Wu, and Dong-qiang Lin. Biosynthesis of γ-aminobutyric acid (gaba) using immobilized whole cells of lactobacillus brevis. *World Journal of Microbiology and Biotechnology*, 23(6):865–871, 2007.

[70] Haixing Li, Dandan Gao, Yusheng Cao, and Hengyi Xu. A high γ-aminobutyric acid-producinglactobacillus brevis isolated from chinese traditionalpaocai. *Annals of microbiology*, 58(4):649–653, 2008.

[71] Ja Young Kim, Moo Young Lee, Geun Eog Ji, Yeon Sook Lee, and Keum Taek Hwang. Production of γ-aminobutyric acid in black raspberry juice during fermentation by lactobacillus brevis gaba100. *International Journal of Food Microbiology*, 130(1):12–16, 2009.

[72] Haixing Li, Ting Qiu, Dandan Gao, and Yusheng Cao. Medium optimization for production of gamma-aminobutyric acid by lactobacillus brevis ncl912. *Amino acids*, 38(5):1439–1445, 2010.

[73] Ji-Kang Jeong, Young-Wook Kim, Hye-Sun Choi, Dong Sun Lee, Soon-Ah Kang, and Kun-Young Park. Increased quality and functionality of kimchi when fermented in korean earthenware (onggi). *International journal of food science & technology*, 46(10):2015–2021, 2011.

[74] Y Ran Cho, Ji-Yoon Chang, and Hae-Choon Chang. Production of gamma-aminobutyric acid (gaba) by lactobacillus buchneri isolated from kimchi and its neuroprotective effect on neuronal cells. *Journal of Microbiology and Biotechnology*, 17(1):104–109, 2007.

[75] XiaoXue Lu, CH Xie, and ZhenXin Gu. Optimisation of fermentative parameters for gaba enrichment by lactococcus lactis. *Czech Journal of Food Sciences*, 27(6):433–442, 2009.

[76] M Nomura, H Kimoto, Y Someya, S Furukawa, and I Suzuki. Production of γ-aminobutyric acid by cheese starters during cheese ripening. *Journal of Dairy Science*, 81(6):1486–1491, 1998.

[77] Xiaoxue Lu, Zhigang Chen, Zhenxin Gu, and Yongbin Han. Isolation of γ-aminobutyric acid-producing bacteria and optimization of fermentative medium. *Biochemical Engineering Journal*, 41(1):48–52, 2008.

[78] Edward A Kravitz. Enzymic formation of gamma-aminobutyric acid in the peripheral and central nervous system of lobsters. *Journal of neurochemistry*, 9(4):363–370, 1962.

[79] S-Y Yang, F-X Lü, Z-X Lu, X-M Bie, Y Jiao, L-J Sun, and B Yu. Production of γ-aminobutyric acid by streptococcus salivarius subsp. thermophilus y2 under submerged fermentation. *Amino acids*, 34(3):473–478, 2008.

[80] Ahmed Zahoor, Steffen N Lindner, and Volker F Wendisch. Metabolic engineering of corynebacterium glutamicum aimed at alternative carbon sources and new products. *Computational and structural biotechnology journal*, 3(4):e201210004, 2012.

[81] SN Lindner, KM Nampoothiri, TM Meiswinkel, VF Wendisch, and Vipin Gopinath. Accelerated pentose utilization by corynebacterium glutamicum for accelerated production of lysine, glutamate, ornithine and putrescine. *Microbial Biotechnology*, 2013.

[82] Eoin Barrett, Catherine Stanton, Oskar Zelder, Gerald Fitzgerald, and R Paul Ross. Heterologous expression of lactose-and galactose-utilizing pathways from lactic acid bacteria in corynebacterium glutamicum for production of lysine in whey. *Appl. Environ. Microbiol.*, 70(5):2861–2866, 2004.

[83] Hideo Kawaguchi, Miho Sasaki, Alain A Vertès, Masayuki Inui, and Hideaki Yukawa. Identification and functional analysis of the gene cluster for l-arabinose utilization in corynebacterium glutamicum. *Appl. Environ. Microbiol.*, 75(11):3419–3429, 2009.

[84] Ranjana Sharma, Krysty Munns, Trevor Alexander, Toby Entz, Parasto Mirzaagha, L Jay Yanke, Michael Mulvey, Edward Topp, and Tim McAllister. Diversity and distribution of commensal fecal escherichia coli bacteria in beef cattle administered selected subtherapeutic antimicrobials in a feedlot setting. *Appl. Environ. Microbiol.*, 74(20):6178–6186, 2008.

[85] Gudbrand Rødsrud, Martin Lersch, and Anders Sjöde. History and future of world's most advanced biorefinery in operation. *Biomass and bioenergy*, 46:46–59, 2012.

[86] Martin Börjesson and Erik Ahlgren. Pulp and paper industry. Technology brief, IEA ETSAP, 2015.

[87] Steve S Helle, Tony Lin, and Sheldon JB Duff. Optimization of spent sulfite liquor fermentation. *Enzyme and microbial Technology*, 42(3):259–264, 2008.

[88] Mariya Marinova, Enrique Mateos-Espejel, Naceur Jemaa, and Jean Paris. Addressing the increased energy demand of a kraft mill biorefinery: The hemicellulose extraction case. *Chemical engineering research and design*, 87(9):1269–1275, 2009.

[89] Størker T Moe, Kando K Janga, Terje Hertzberg, May-Britt Hägg, Karin Øyaas, and Nils Dyrset. Saccharification of lignocellulosic biomass for biofuel and biorefinery applications–a renaissance for the concentrated acid hydrolysis? *Energy Procedia*, 20:50–58, 2012.

[90] Swarnima Agnihotri, Ingvild A Johnsen, Maren S Bøe, Karin Øyaas, and Størker Moe. Ethanol organosolv pretreatment of softwood (picea abies) and sugarcane bagasse for biofuel and biorefinery applications. *Wood science and technology*, 49(5):881–896, 2015.

[91] Cristina Rueda, Pedro A Calvo, Gabriel Moncalián, Gema Ruiz, and Alberto Coz. Biorefinery options to valorize the spent liquor from sulfite pulping. *Journal of Chemical Technology & Biotechnology*, 90(12):2218–2226, 2015.

[92] Herbert Sixta. *Handbook of pulp*. Wiley-vch, 2006.

[93] Dan Stanescu and Benito M Chen-Charpentier. Random coefficient differential equation models for bacterial growth. *Mathematical and Computer Modelling*, 50(5-6):885–895, 2009.

[94] JF Van Impe, Filip Poschet, AH Geeraerd, and KM Vereecken. Towards a novel class of predictive microbial growth models. *International journal of food microbiology*, 100(1-3):97–105, 2005.

[95] Jacques Monod. The growth of bacterial cultures. *Annual review of microbiology*, 3(1):371–394, 1949.

[96] Thomas Millat and Klaus Winzer. Mathematical modelling of clostridial acetone-butanol-ethanol fermentation. *Applied microbiology and biotechnology*, 101(6):2251–2271, 2017.

[97] Prashant M Bapat, Sharad Bhartiya, KV Venkatesh, and Pramod P Wangikar. Structured kinetic model to represent the utilization of multiple substrates in complex media during rifamycin b fermentation. *Biotechnology and bioengineering*, 93(4):779–790, 2006.

[98] Jerome G Hust. A fine-grained, isotropic graphite for use as nbs thermophysical property rm's from 5 to 2500 k. *National Bureau of Standards Special Publication*, 1984.

[99] Gonzalo Acuña, Francisco Cubillos, Jules Thibault, and Eric Latrille. Comparison of methods for training grey-box neural network models. *Computers & Chemical Engineering*, 23:S561–S564, 1999.

[100] Denis Dochain, Françoise Couenne, and Christian Jallut. Enthalpy based modelling and design of asymptotic observers for chemical reactors. *International Journal of Control*, 82(8):1389–1403, 2009.

[101] Amiya K Jana. A nonlinear exponential observer for a batch distillation. In *2010 11th International Conference on Control Automation Robotics & Vision*, pages 1393–1396. IEEE, 2010.

[102] Jarinah Mohd Ali, N Ha Hoang, Mohamed Azlan Hussain, and Denis Dochain. Review and classification of recent observers applied in chemical process systems. *Computers & Chemical Engineering*, 76:27–41, 2015.

[103] Greg Welch, Gary Bishop, et al. An introduction to the kalman filter, 1995.

[104] Wen-shiang Chen, Bhavik R Bakshi, Prem K Goel, and Sridhar Ungarala. Bayesian estimation via sequential monte carlo sampling: unconstrained nonlinear dynamic systems. *Industrial & engineering chemistry research*, 43(14):4012–4025, 2004.

[105] Z Gejic. Introduction to linear and nonlinear observers. *Rutgers University*, 2003.

[106] Sachin C Patwardhan and Sirish L Shah. From data to diagnosis and control using generalized orthonormal basis filters. part i: Development of state observers. *Journal of Process control*, 15(7):819–835, 2005.

[107] T Zhang and M Guay. Adaptive nonlinear observers of microbial growth processes. *Journal of process control*, 12(5):633–643, 2002.

[108] Guillaume Goffaux, A Vande Wouwer, and Olivier Bernard. Improving continuous–discrete interval observers with application to microalgae-based bioprocesses. *Journal of Process Control*, 19(7):1182–1190, 2009.

[109] Ph Bogaerts and A Vande Wouwer. Parameter identification for state estimation—application to bioprocess software sensors. *Chemical engineering science*, 59(12):2465–2476, 2004.

[110] A El Assoudi, EH El Yaagoubi, and H Hammouri. Non-linear observer based on the euler discretization. *International Journal of Control*, 75(11):784–791, 2002.

[111] Xavier Hulhoven, A Vande Wouwer, and Ph Bogaerts. Hybrid extended luenberger-asymptotic observer for bioprocess state estimation. *Chemical engineering science*, 61(21):7151–7160, 2006.

[112] Saneej B Chitralekha, J Prakash, H Raghavan, RB Gopaluni, and Sirish L Shah. A comparison of simultaneous state and parameter estimation schemes for a continuous fermentor reactor. *Journal of Process Control*, 20(8):934–943, 2010.

[113] Nikolaos Kazantzis, Nguyen Huynh, and Raymond A Wright. Nonlinear observer design for the slow states of a singularly perturbed system. *Computers & Chemical Engineering*, 29(4):797–806, 2005.

[114] Jesús Picó, Hernán De Battista, and Fabricio Garelli. Smooth sliding-mode observers for specific growth rate and substrate from biomass measurement. *Journal of Process Control*, 19(8):1314–1323, 2009.

[115] Hernán De Battista, Jesús Picó, Fabricio Garelli, and Alejandro Vignoni. Specific growth rate estimation in (fed-) batch bioreactors using second-order sliding observers. *Journal of Process Control*, 21(7):1049–1055, 2011.

[116] J Gonzalez, G Fernandez, R Aguilar, M Barron, and J Alvarez-Ramirez. Sliding mode observer-based control for a class of bioreactors. *Chemical Engineering Journal*, 83(1):25–32, 2001.

[117] M Hajatipour and M Farrokhi. Chattering free with noise reduction in sliding-mode observers using frequency domain analysis. *Journal of Process Control*, 20(8):912–921, 2010.

[118] E Rocha-Cózatl and A Vande Wouwer. State and input estimation in phytoplanktonic cultures using quasi-unknown input observers. *Chemical engineering journal*, 175:39–48, 2011.

[119] Wang Jianlin, Zhao Liqiang, and Yu Tao. On-line estimation in fed-batch fermentation process using state space model and unscented kalman filter. *Chinese Journal of Chemical Engineering*, 18(2):258–264, 2010.

[120] Repligen. Continuous bioprocessing, 2018.

[121] Christoph Herwig. Bioprocess technology. `https://www.vt.tuwien.ac.at/bioprocess_engineering/bioprocess_technology/EN/`. Accessed: 2019-09-15.

[122] Sigma Aldrich. 2xyt microbial growth medium. `https://www.sigmaaldrich.com/catalog/product/sigma/y2377?lang=en&region=NO`. Accessed: 2019-11-30.

[123] Fernando Pérez-García, João MP Jorge, Annika Dreyszas, Joe Max Risse, and Volker F Wendisch. Efficient production of the dicarboxylic acid glutarate by *Corynebacterium glutamicum* via a novel synthetic pathway. *Frontiers in microbiology*, 9, 2018.

[124] Germán Buitrón, André Koefoed, and Bernard Capdeville. Control of phenol biodegradation by using co2 evolution rate as an activity indicator. *Environmental technology*, 14(3):227–236, 1993.

[125] Patrick N Royce. Effect of changes in the ph and carbon dioxide evolution rate on the measured respiratory quotient of fermentations. *Biotechnology and bioengineering*, 40(10):1129–1138, 1992.

[126] Mathieu Spérandio and Etienne Paul. Determination of carbon dioxide evolution rate using on-line gas analysis during dynamic biodegradation experiments. *Biotechnology and bioengineering*, 53(3):243–252, 1997.

[127] R Neeleman, EJ van den End, and AJB Van Boxtel. Estimation of the respiration quotient in a bicarbonate buffered batch cell cultivation. *Journal of biotechnology*, 80(1):85–94, 2000.

[128] LP De Jonge, JJ Heijnen, and WM Van Gulik. Reconstruction of the oxygen uptake and carbon dioxide evolution rates of microbial cultures at near-neutral ph during highly dynamic conditions. *Biochemical engineering journal*, 83:42–54, 2014.

[129] Róbert Kovács, Ferenc Házi, Zsolt Csikor, and Pál Miháltz. Connection between oxygen uptake rate and carbon dioxide evolution rate in aerobic thermophilic sludge digestion. *Periodica Polytechnica Chemical Engineering*, 51(1):17–22, 2007.

[130] L Wu, HC Lange, WM Van Gulik, and JJ Heijnen. Determination of in vivo oxygen uptake and carbon dioxide evolution rates from off-gas measurements under highly dynamic conditions. *Biotechnology and bioengineering*, 81(4):448–458, 2003.

[131] Jeffrey M Smith, Stowell W Davison, and Gregory F Payne. Development of a strategy to control the dissolved concentrations of oxygen and carbon dioxide at constant shear in a plant cell bioreactor. *Biotechnology and bioengineering*, 35(11):1088–1101, 1990.

[132] IG Minkevich and M Neubert. Influence of carbon dioxide solubility on the accuracy of measurements of carbon dioxide production rate by gas balance technique. *Acta biotechnologica*, 5(2):137–143, 1985.

[133] Jessie A Key and David W Ball. *Introductory Chemistry-1st Canadian Edition*. BCcampus, 2014.

[134] William Henry. Iii. experiments on the quantity of gases absorbed by water, at different temperatures, and under different pressures. *Philosophical Transactions of the Royal Society of London*, pages 29–274, 1803.

[135] Clifford Pickover. *Archimedes to Hawking: laws of science and the great minds behind them*. Oxford University Press, 2008.

[136] D Moutafchieva, D Popova, M Dimitrova, and S Tchaoushev. Experimental determination of the volumetric mass transfer coefficient. *Journal of Chemical Technology and Metallurgy*, 48(4):351–356, 2013.

[137] Archis A Yawalkar, Albertus BM Heesink, Geert F Versteeg, and Vishwas G Pangarkar. Gas—liquid mass transfer coefficient in stirred tank reactors. *The Canadian Journal of Chemical Engineering*, 80(5):840–848, 2002.

[138] DOE Fundamentals Handbook. Thermodynamics, heat transfer and fluid flow. *US Department of Energy*, 1:53–96, 1992.

[139] Mark Ramsey et al. Schlumberger oilfield glossary, 2019.

[140] Olympia Roeva and Stoyan Tzonkov. Modelling of escherichia coli cultivations: acetate inhibition in a fed-batch culture. *Bioautomation*, 4:1–11, 2006.

[141] Infors HT. *Infors HT Labfors 5 Operating Manual*. Infors HT.

[142] BRW Pinsent, L Pearson, and FJW Roughton. The kinetics of combination of carbon dioxide with hydroxide ions. *Transactions of the Faraday Society*, 52:1512–1520, 1956.

[143] Daniel L Purich and R Donald Allison. *Handbook of biochemical kinetics: a guide to dynamic processes in the molecular life sciences*. Elsevier, 1999.

[144] Daniel L Reger, Scott R Goode, and David W Ball. *Chemistry: principles and practice*. Cengage Learning, 2009.

[145] Barry N Taylor, Peter J Mohr, and M Douma. The nist reference on constants, units, and uncertainty. *available online from:. physics. nist. gov/cuu/index*, 2007.

[146] Spencer L Seager and Michael R Slabaugh. *Chemistry for today: General, organic, and biochemistry*. Cengage learning, 2013.

[147] Dan Simon. *Optimal state estimation: Kalman, H infinity, and nonlinear approaches*. John Wiley & Sons, 2006.

[148] Henk Nijmeijer and Arjan Van der Schaft. *Nonlinear dynamical control systems*, volume 175. Springer, 1990.

[149] Alexandra Hofer, Paul Kroll, and Christoph Herwig. Glucose monitoring and control using numera, lucullus pims and cedex® bio ht analyzer, 2018.

[150] Securecell. Numera – the unique pat solution. `https://securecell.ch/wp-content/uploads/2019/09/Numera_Flyer.pdf`. Accessed: 2019-12-13.

Appendices

A Auto-Sampling Experimental Setup

A.1 Numera and Lucullus Overview

The Ring of Fire method can be implemented in the same manner for the hardware and software which pertains to Numera© and Lucullus© . The resemblance between Figure 2.7 and Figure A.1 is striking. Therefore, this configuration of Numera© and Lucullus© should be able to accomplish the ultimate goals of an industrial bio-process. The intricacies of the hardware mentioned can be found in Section A.2.

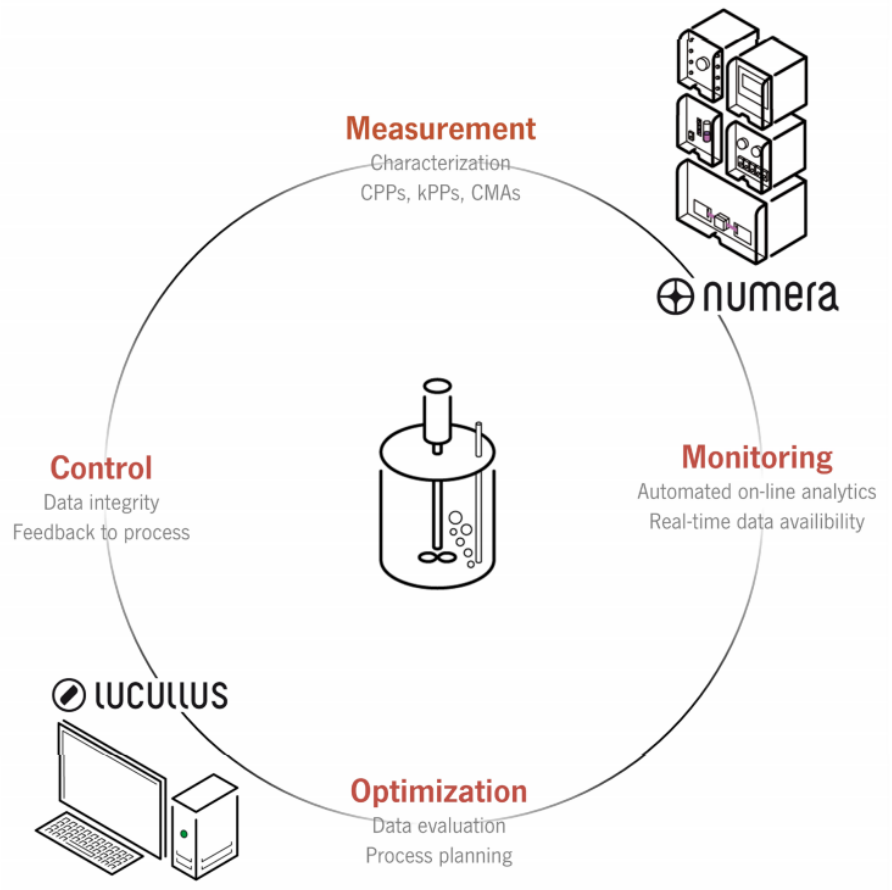

Figure A.1: With the ”Ring of Fire” theory in mind, the Numera and Lucullus modules can effectively achieve the same steps. These steps include: monitoring, measuring, control, and optimization [149].

A.2 Numera© Setup

The hardware required for the Numera© and Lucullus© system described in Section A.1 can be configured as seen in Figure A.2. This system is very modular and can be quite complex depending on the desired outcome. Starting from the left, the system can have up to twelve bioreactors working simultaneously. In the middle of the figure, the Numera© modules involve various operations that can be done to the process. For example, the multiplexer brings the samples from the bioreactor to the other modules. The dilution module simply dilutes the sample to make it readily available for testing. The filtering module can separate the biomass from the substrates and products in the samples. This separation is useful for testing samples in the HPLC for an accurate concentration of substrate and/or products. Once the sample has been diluted and/or filtered, the sample is injected into vials by the autosampler. These modules are overseen and controlled via the control module which is connected to the Lucullus© software and the bioreactors. Once the samples are collected, Lucullus© can control third party analyzers and automatically start taking data from it. Along with the automatic sampling and analysis, the system still allows for manual samples for offline analysis as well. Therefore, in theory, this system can take samples, analyze samples, interpret the samples, and control the bio-process via the results. Thus, if implemented correctly, drastically reduces the effort required for experiments. Once this system and knowledge is perfected, it may be able to play a much greater role in how industrial microbiology evolves.

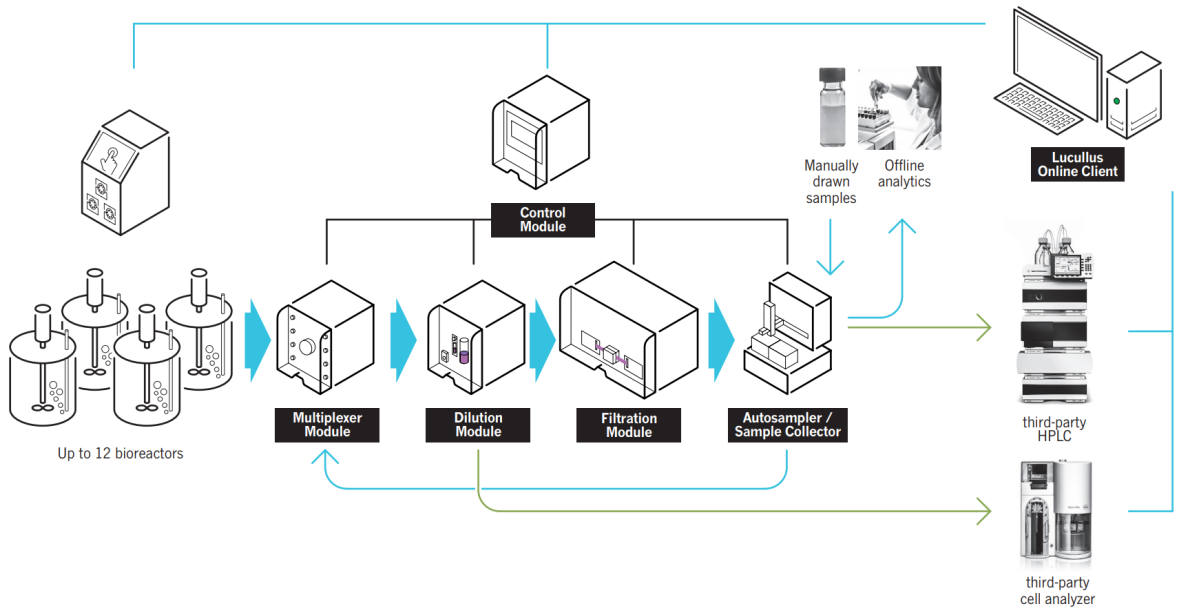

Figure A.2: Diagram of physical equipment, interaction, and setup for the combination Numera© and Lucullus© [150]. This automated sampling configuration starts with the bioreactors on the left, with the various modules in the middle, and the sample injector on the right. This process is choreographed and controlled with the Lucullus software, which can control the entire workflow process of Numera©. This configuration can also have additional third-party equipment synced as well as offline measurements.

B Experiment Data

B.1 Wild Type Strain Data Using Glucose

Table B.1: Wild type strain using glucose (with no GABA production) sugar and biomass experiment data

Sugars				**Biomass**					
Real Time	**time (days)**	**Concentration (mM)**	**C glucose ($g \cdot L^{-1}$)**	**Real Time**	**time (days)**	**Sample**	**OD diluted**	**Dilution**	**OD real**
27/06/19 13:00	0.000		20	27/06/19 13:00	0.00				1
27/06/19 14:55	0.080	n.a.		27/06/19 14:39	0.07	B1	0.227	10	2.27
27/06/19 16:42	0.154	n.a.		27/06/19 16:13	0.13	B2	0.165	20	3.3
27/06/19 18:42	0.238	92.0596	16.62228138	27/06/19 18:13	0.22	B3	0.164	40	6.56
27/06/19 20:42	0.321	63.7044	11.50246646	27/06/19 20:13	0.30	B4	0.138	80	11.04
27/06/19 22:42	0.404	36.4319	6.578143864	27/06/19 22:13	0.38	B5	0.154	100	15.4
28/06/19 0:42	0.488	2.6294	0.474764464	28/06/19 0:13	0.47	B6	0.212	100	21.2
28/06/19 2:42	0.571	2.2176	0.400409856	28/06/19 2:13	0.55	B7	0.212	100	21.2
28/06/19 4:42	0.654	1.1908	0.215010848	28/06/19 4:13	0.63	B8	0.209	100	20.9
28/06/19 6:42	0.738	2.2812	0.411893472	28/06/19 6:13	0.72	B9	0.208	100	20.8
28/06/19 8:42	0.821	2.2932	0.414060192	28/06/19 8:13	0.80	B10	0.208	100	20.8
28/06/19 10:42	0.904	1.1784	0.212771904	28/06/19 10:13	0.88	B11	0.205	100	20.5
28/06/19 12:42	0.988	19.026	3.43533456	28/06/19 12:13	0.97	B12	0.226	100	22.6
28/06/19 14:42	1.071	61.9318	11.18240581	28/06/19 14:13	1.05	B13	0.164	200	32.8
28/06/19 16:42	1.154	4.4986	0.812267216	28/06/19 16:13	1.13	B14	0.217	200	43.4
28/06/19 18:42	1.238	0.967	0.17460152	28/06/19 18:13	1.22	B15	0.201	200	40.2
28/06/19 20:42	1.321	n.a.		28/06/19 20:13	1.30	B16	0.189	200	37.8
28/06/19 22:42	1.404	0.9008	0.162648448	28/06/19 22:13	1.38	B17	0.183	200	36.6
29/06/19 0:42	1.488	1.7024	0.307385344	29/06/19 0:13	1.47	B18	n.a.	200	
29/06/19 2:42	1.571	n.a.		29/06/19 2:13	1.55	B19	0.177	200	35.4
29/06/19 4:42	1.654	n.a.		29/06/19 4:13	1.63	B20	0.177	200	35.4
29/06/19 6:42	1.738	n.a.		29/06/19 6:13	1.72	B21	0.176	200	35.2
29/06/19 8:42	1.821	n.a.		29/06/19 8:13	1.80	B22	0.18	200	36
29/06/19 10:42	1.904	n.a.		29/06/19 10:13	1.88	B23	0.169	200	33.8
29/06/19 12:42	1.988	n.a.		29/06/19 12:13	1.97	B24	0.168	200	33.6
29/06/19 14:42	2.071	n.a.		29/06/19 14:13	2.05	B25	0.183	200	36.6
29/06/19 16:42	2.154	n.a.		29/06/19 16:13	2.13	B26	0.168	200	33.6
29/06/19 18:42	2.238	n.a.		29/06/19 18:13	2.22	B27	0.173	200	34.6
29/06/19 20:42	2.321	n.a.		29/06/19 20:13	2.30	B28	0.17	200	34
29/06/19 22:42	2.404	n.a.		29/06/19 22:13	2.38	B29	0.154	200	30.8
30/06/19 0:42	2.488	n.a.		30/06/19 0:13	2.47	B30	0.164	200	32.8
30/06/19 2:42	2.571	n.a.		30/06/19 2:13	2.55	B31	0.169	200	33.8
30/06/19 4:42	2.654	n.a.		30/06/19 4:13	2.63	B32	0.159	200	31.8
30/06/19 6:42	2.738	n.a.		30/06/19 6:13	2.72	B33	0.161	200	32.2
30/06/19 8:42	2.821	n.a.		30/06/19 8:13	2.80	B34	0.161	200	32.2
30/06/19 10:42	2.904	n.a.		30/06/19 10:13	2.88	B35	0.157	200	31.4
30/06/19 12:42	2.988	n.a.		30/06/19 12:13	2.97	B36	0.157	200	31.4

B.2 GMO Strain Data Using Glucose

Table B.2: GMO strain using glucose (with GABA production) sugar and biomass experiment data

Sugars				Biomass						GABA			
Real Time	**time (days)**	**Concentration (mM)**	**C glucose ($g \cdot L^{-1}$)**	**Real Time**	**time (days)**	**Sample**	**OD diluted**	**Dilution**	**OD real**	**Real Time**	**time (days)**	**Concentration (mM)**	**C GABA ($g \cdot L^{-1}$)**
10/22/19 14:30	0.000		40.2	10/22/19 14:30	0.00				1	10/22/19 14:30	0.000		0
10/22/19 16:10	0.069	252.2133	45.53963345	10/22/19 15:40	0.05	B1	0.203	10	2.03	10/22/19 16:10	0.069	0.0555	0.00572316
10/22/19 18:10	0.153	250.042	45.14758352	10/22/19 17:40	0.13	B2	0.221	10	2.21	10/22/19 18:10	0.153	0.0537	0.005537544
10/22/19 20:10	0.236	245.619	44.34896664	10/22/19 19:40	0.22	B3	0.119	20	2.38	10/22/19 20:10	0.236	0.0932	0.009610784
10/22/19 22:10	0.319	244.8233	44.20529505	10/22/19 21:40	0.30	B4	0.125	20	2.5	10/22/19 22:10	0.319	0.1584	0.016334208
10/23/19 0:10	0.403	242.135	43.7198956	10/22/19 23:40	0.38	B5	0.124	20	2.48	10/23/19 0:10	0.403	0.2138	0.022047056
10/23/19 2:10	0.486	233.2524	42.11605334	10/23/19 1:40	0.47	B6	0.125	20	2.5	10/23/19 2:10	0.486	0.2741	0.028265192
10/23/19 4:10	0.569	231.8741	41.8671875	10/23/19 3:40	0.55	B7	0.132	20	2.64	10/23/19 4:10	0.569	0.3688	0.038030656
10/23/19 6:10	0.653	232.0904	41.90624262	10/23/19 5:40	0.63	B8	0.13	20	2.6	10/23/19 6:10	0.653	0.2988	0.030812256
10/23/19 8:10	0.736	225.6759	40.7480405	10/23/19 7:40	0.72	B9	0.14	20	2.8	10/23/19 8:10	0.736	0.289	0.02980168
10/23/19 10:10	0.819	224.3556	40.50964714	10/23/19 9:40	0.80	B10	0.15	20	3	10/23/19 10:10	0.819	0.3409	0.035153608
10/23/19 12:10	0.903	227.4536	41.06902202	10/23/19 11:40	0.88	B11	0.165	20	3.3	10/23/19 12:10	0.903	0.4516	0.046568992
10/23/19 14:10	0.986	231.7255	41.84035628	10/23/19 13:40	0.97	B12	0.189	20	3.78	10/23/19 14:10	0.986	0.3383	0.034885496
10/23/19 16:10	1.069	224.6022	40.55417323	10/23/19 15:40	1.05	B13	0.226	20	4.52	10/23/19 16:10	1.069	0.1935	0.01995372
10/23/19 18:10	1.153	218.1775	39.3941294	10/23/19 17:40	1.13	B14	0.138	40	5.52	10/23/19 18:10	1.153	0.1259	0.012982808
10/23/19 20:10	1.236	214.698	38.76587088	10/23/19 19:40	1.22	B15	0.175	40	7	10/23/19 20:10	1.236	0.1167	0.012034104
10/23/19 22:10	1.319	201.1098	36.31238549	10/23/19 21:40	1.30	B16	0.219	40	8.76	10/23/19 22:10	1.319	0.1818	0.018747216
10/24/19 0:10	1.403	185.5253	33.49844817	10/23/19 23:40	1.38	B17	0.222	50	11.1	10/24/19 0:10	1.403	0.2704	0.027883648
10/24/19 2:10	1.486	162.9542	29.42301035	10/24/19 1:40	1.47	B18	0.143	100	14.3	10/24/19 2:10	1.486	0.0698	0.007197776
10/24/19 4:10	1.569	120.6785	21.78970996	10/24/19 3:40	1.55	B19	0.196	100	19.6	10/24/19 4:10	1.569	0.1768	0.018231616
10/24/19 6:10	1.653	59.6386	10.76834562	10/24/19 5:40	1.63	B20	0.023	1000	23	10/24/19 6:10	1.653	0.3737	0.038535944
10/24/19 8:10	1.736	7.13	1.2873928	10/24/19 7:40	1.72	B21	0.037	1000	37	10/24/19 8:10	1.736	0.0217	0.002237704
10/24/19 10:10	1.819	7.2059	1.301097304	10/24/19 9:40	1.80	B22	0.04	1000	40	10/24/19 10:10	1.819	0.0204	0.002103648
10/24/19 12:10	1.903	8.8023	1.589343288	10/24/19 11:40	1.88	B23	0.036	1000	36	10/24/19 12:10	1.903	0.018	0.00185616
10/24/19 14:10	1.986	6.8411	1.235229016	10/24/19 13:40	1.97	B24	0.034	1000	34	10/24/19 14:10	1.986	0.0112	0.001154944
10/24/19 16:10	2.069	0	0	10/24/19 15:40	2.05	B25	0.033	1000	33	10/24/19 16:10	2.069	0.016	0.00164992
10/24/19 18:10	2.153	0	0	10/24/19 17:40	2.13	B26	0.072	500	36	10/24/19 18:10	2.153	0.0117	0.001206504
10/24/19 20:10	2.236	92.6994	16.73780366	10/24/19 19:40	2.22	B27	0.063	500	31.5	10/24/19 20:10	2.236	0.327	0.03372024
10/24/19 22:10	2.319	289.6961	52.30752782	10/24/19 21:40	2.30	B28	0.059	500	29.5	10/24/19 22:10	2.319	0.7142	0.073648304
10/25/19 0:10	2.403	287.0516	51.8300369	10/24/19 23:40	2.38	B29	0.05	500	25	10/25/19 0:10	2.403	0.808	0.08332096
10/25/19 2:10	2.486	281.4058	50.81063125	10/25/19 1:40	2.47	B30	0.049	500	24.5	10/25/19 2:10	2.486	0.7016	0.072348992
10/25/19 4:10	2.569	264.234	47.71009104	10/25/19 3:40	2.55	B31	0.048	500	24	10/25/19 4:10	2.569	0.7444	0.076762528
10/25/19 6:10	2.653	253.8206	45.82984754	10/25/19 5:40	2.63	B32	0.048	500	24	10/25/19 6:10	2.653	0.9042	0.093241104
10/25/19 8:10	2.736	244.149	44.08354344	10/25/19 7:40	2.72	B33	0.047	500	23.5	10/25/19 8:10	2.736	0.8992	0.092725504
10/25/19 10:10	2.819	236.74	42.7457744	10/25/19 9:40	2.80	B34	0.046	500	23	10/25/19 10:10	2.819	0.761	0.07847432
10/25/19 12:10	2.903	226.7913	40.94943713	10/25/19 11:40	2.88	B35	0.046	500	23	10/25/19 12:10	2.903	0.9272	0.095612864
10/25/19 14:10	2.986	222.3868	40.15416061	10/25/19 13:40	2.97	B36	0.047	500	23.5	10/25/19 14:10	2.986	0.8046	0.082970352
10/25/19 16:10	3.069	126.513	22.84318728	10/25/19 15:40	3.05	B37	0.047	500	23.5	10/25/19 16:10	3.069	0.6239	0.064336568
10/25/19 18:10	3.153	118.4162	21.38122907	10/25/19 17:40	3.13	B38	0.045	500	22.5	10/25/19 18:10	3.153	0.7685	0.07924772
10/25/19 20:10	3.236	109.9353	19.84991777	10/25/19 19:40	3.22	B39	0.046	500	23	10/25/19 20:10	3.236	0.7224	0.074493888
10/25/19 22:10	3.319	102.3113	18.47332833	10/25/19 21:40	3.30	B40	0.047	500	23.5	10/25/19 22:10	3.319	0.6114	0.063047568
10/26/19 0:10	3.403	89.1343	16.09408921	10/25/19 23:40	3.38	B41	0.046	500	23	10/26/19 0:10	3.403	0.701	0.07228712
10/26/19 2:10	3.486	87.4167	15.78395935	10/26/19 1:40	3.47	B42	0.0455	500	22.75	10/26/19 2:10	3.486	0.666	0.06867792
10/26/19 4:10	3.569	78.4602	14.16677371	10/26/19 3:40	3.55	B43	0.045	500	22.5	10/26/19 4:10	3.569	0.5496	0.056674752
10/26/19 6:10	3.653	69.2319	12.50051186	10/26/19 5:40	3.63	B44	0.042	500	21	10/26/19 6:10	3.653	0.6023	0.062109176
10/26/19 8:10	3.736	69.2204	12.49843542	10/26/19 7:40	3.72	B45	0.041	500	20.5	10/26/19 8:10	3.736	0.5376	0.055437312
10/26/19 10:10	3.819	47.9286	8.653988016	10/26/19 9:40	3.80	B46	0.04	500	20	10/26/19 10:10	3.819	0.3766	0.038834992
10/26/19 12:10	3.903	54.9792	9.927044352	10/26/19 11:40	3.88	B47	0.037	500	18.5	10/26/19 12:10	3.903	0.5879	0.060624248
10/26/19 14:10	3.986	49.3834	8.916666704	10/26/19 13:40	3.97	B48	0.036	500	18	10/26/19 14:10	3.986	0.476	0.04908512
10/26/19 16:10	4.069	42.0424	7.591175744	10/26/19 15:40	4.05	B49	0.036	500	18	10/26/19 16:10	4.069	0.5214	0.053766768
10/26/19 18:10	4.153	37.108	6.70022048	10/26/19 17:40	4.13	B50	0.036	500	18	10/26/19 18:10	4.153	0.5315	0.05480828
10/26/19 20:10	4.236	32.8353	5.928741768	10/26/19 19:40	4.22	B51	0.04	500	20	10/26/19 20:10	4.236	0.5137	0.052972744
10/26/19 22:10	4.319	26.881	4.85363336	10/26/19 21:40	4.30	B52	0.039	500	19.5	10/26/19 22:10	4.319	0.4287	0.044207544
10/27/19 0:10	4.403	22.8283	4.121877848	10/26/19 23:40	4.38	B53	0.036	500	18	10/27/19 0:10	4.403	0.4396	0.045331552
10/27/19 2:10	4.486	17.657	3.18814792	10/27/19 1:40	4.47	B54	0.037	500	18.5	10/27/19 2:10	4.486	0.3848	0.039680576
10/27/19 4:10	4.569	13.5377	2.444367112	10/27/19 3:40	4.55	B55	0.037	500	18.5	10/27/19 4:10	4.569	0.3971	0.040948952
10/27/19 6:10	4.653	9.372	1.69220832	10/27/19 5:40	4.63	B56	0.039	500	19.5	10/27/19 6:10	4.653	0.3556	0.036669472
10/27/19 8:10	4.736	0	0	10/27/19 7:40	4.72	B57	0.038	500	19	10/27/19 8:10	4.736	0.32	0.0329984
10/27/19 10:10	4.819	0	0	10/27/19 9:40	4.80	B58	0.039	500	19.5	10/27/19 10:10	4.819	0.3059	0.031544408
10/27/19 12:10	4.903	0	0	10/27/19 11:40	4.88	B59	0.036	500	18	10/27/19 12:10	4.903	0.2566	0.026460592
10/27/19 14:10	4.986	0	0	10/27/19 13:40	4.97	B60	0.04	500	20	10/27/19 14:10	4.986	0.1719	0.017726328

B.3 GMO Strain Data Using Synthetic SSL

Table B.3: GMO strain using synthetic SSL (with GABA production) sugar, biomass, and GABA experiment data

Sugars								Biomass						GABA			
Real Time	time (days)	Concentration (mM)	C glucose ($g \cdot L^{-1}$)	Xylose (mM)	Xylose ($g \cdot L^{-1}$)	Mannose (mM)	Mannose ($g \cdot L^{-1}$)	Real Time	time (days)	Sample	OD diluted	Dilution	OD real	Real Time	time (days)	Concentration (mM)	C GABA ($g \cdot L^{-1}$)
10/22/19 14:30	0.000		7.2		9		22	10/22/19 14:30	0.00				1	10/22/19 14:30	0.000		0
10/22/19 15:10	0.028	49.3533	8.911231848	67.8446	10.1855098	133.0271	23.96563023	10/22/19 14:40	0.01	A1	0.179	10	1.79	10/22/19 15:10	0.028	0.0593	0.006115016
10/22/19 17:10	0.111	48.4042	8.739862352	68.7386	10.31972602	135.2908	24.37344936	10/22/19 16:40	0.09	A2	0.201	10	2.01	10/22/19 17:10	0.111	0.0771	0.007950552
10/22/19 19:10	0.194	45.2872	8.177056832	68.0841	10.22146593	134.3606	24.20586825	10/22/19 18:40	0.17	A3	0.114	20	2.28	10/22/19 19:10	0.194	0.1185	0.01221972
10/22/19 21:10	0.278	44.07	7.9572792	69.8737	10.49013858	137.8339	24.83160409	10/22/19 20:40	0.26	A4	0.117	20	2.34	10/22/19 21:10	0.278	0.1662	0.017138544
10/22/19 23:10	0.361	41.567	7.50533752	68.4511	10.27656364	136.4413	24.58071884	10/22/19 22:40	0.34	A5	0.118	20	2.36	10/22/19 23:10	0.361	0.2325	0.0239754
10/23/19 1:10	0.444	37.645	6.7971812	70.1513	10.53181467	132.897	23.94219193	10/23/19 0:40	0.42	A6	0.116	20	2.32	10/23/19 1:10	0.444	0.2446	0.025223152
10/23/19 3:10	0.528	35.2914	6.372215184	68.4455	10.27572292	131.2688	23.64886193	10/23/19 2:40	0.51	A7	0.114	20	2.28	10/23/19 3:10	0.528	0.3183	0.032823096
10/23/19 5:10	0.611	30.6196	5.528674976	62.607	9.39918891	126.9497	22.87075015	10/23/19 4:40	0.59	A8	0.115	20	2.3	10/23/19 5:10	0.611	0.0447	0.004609464
10/23/19 7:10	0.694	28.6656	5.175860736	62.2229	9.341523977	126.1689	22.73008435	10/23/19 6:40	0.67	A9	0.125	20	2.5	10/23/19 7:10	0.694	0.0465	0.00479508
10/23/19 9:10	0.778	26.6858	4.818388048	62.0336	9.313104368	126.5172	22.79283268	10/23/19 8:40	0.76	A10	0.13	20	2.6	10/23/19 9:10	0.778	0.2043	0.021067416
10/23/19 11:10	0.861	28.4698	5.140507088	64.6483	9.705649279	133.3967	24.03221589	10/23/19 10:40	0.84	A11	0.137	20	2.74	10/23/19 11:10	0.861	0.1942	0.020025904
10/23/19 13:10	0.944	27.0536	4.884798016	68.7991	10.32880888	136.8141	24.647881	10/23/19 12:40	0.92	A12	0.155	20	3.1	10/23/19 13:10	0.944	0.0831	0.008569272
10/23/19 15:10	1.028	23.7717	4.292218152	67.1348	10.07894752	135.8283	24.47028321	10/23/19 14:40	1.01	A13	0.184	20	3.68	10/23/19 15:10	1.028	0.0822	0.008476464
10/23/19 17:10	1.111	19.7211	3.560841816	65.6359	9.853917667	134.501	24.23116216	10/23/19 16:40	1.09	A14	0.114	40	4.56	10/23/19 17:10	1.111	0.1203	0.012405336
10/23/19 19:10	1.194	13.2763	2.397168728	63.5308	9.537879004	133.7093	24.08853265	10/23/19 18:40	1.17	A15	0.145	40	5.8	10/23/19 19:10	1.194	0.1762	0.018169744
10/23/19 21:10	1.278	0	0	58.7233	8.816129029	131.5998	23.70849357	10/23/19 20:40	1.26	A16	0.202	40	8.08	10/23/19 21:10	1.278	0.282	0.02907984
10/23/19 23:10	1.361	0	0	52.5618	7.891103034	124.8511	22.49267477	10/23/19 22:40	1.34	A17	0.21	50	10.5	10/23/19 23:10	1.361	0.3251	0.033524312
10/24/19 1:10	1.444	0	0	42.2014	6.335696182	113.5243	20.45208379	10/24/19 0:40	1.42	A18	0.152	100	15.2	10/24/19 1:10	1.444	0.0619	0.006383128
10/24/19 3:10	1.528	0	0	31.1927	4.682960051	97.18	17.50756008	10/24/19 2:40	1.51	A19	0.214	100	21.4	10/24/19 3:10	1.528	0.0908	0.009363296
10/24/19 5:10	1.611	0	0	17.4262	2.616195406	66.1315	11.91398651	10/24/19 4:40	1.59	A20	0.029	1000	29	10/24/19 5:10	1.611	0.2619	0.027007128
10/24/19 7:10	1.694	0	0	9.2766	1.392695958	23.0099	4.145371544	10/24/19 6:40	1.67	A21	0.039	1000	39	10/24/19 7:10	1.694	0.5524	0.056963488
10/24/19 9:10	1.778	0	0	9.9821	1.498612673	0	0	10/24/19 8:40	1.76	A22	0.037	1000	37	10/24/19 9:10	1.778	0.0479	0.004939448
10/24/19 11:10	1.861	0	0	10.64255	1.597766032	0	0	10/24/19 10:40	1.84	A23	0.037	1000	37	10/24/19 11:10	1.861	0.0461	0.004753832
10/24/19 13:10	1.944	0	0	11.303	1.69691939	0	0	10/24/19 12:40	1.92	A24	0.035	1000	35	10/24/19 13:10	1.944	0.0443	0.004568216
10/24/19 15:10	2.028	0	0	11.1062	1.667373806	0	0	10/24/19 14:40	2.01	A25	0.033	1000	33	10/24/19 15:10	2.028	0.0147	0.001515864
10/24/19 17:10	2.111	0	0	10.0135	1.503326755	0	0	10/24/19 16:40	2.09	A26	0.07	500	35	10/24/19 17:10	2.111	0.018	0.00185616
10/24/19 19:10	2.194	0	0	0	0	0	0	10/24/19 18:40	2.17	A27	0.072	500	36	10/24/19 19:10	2.194	0.1675	0.0172726
10/24/19 21:10	2.278	42.3684	7.650038304	63.7217	9.566538821	133.6839	24.08395669	10/24/19 20:40	2.26	A28	0.072	500	36	10/24/19 21:10	2.278	0.5346	0.055127952
10/24/19 23:10	2.361	54.1782	9.782415792	82.7893	12.42915761	182.2908	32.84078136	10/24/19 22:40	2.34	A29	0.067	500	33.5	10/24/19 23:10	2.361	0.7689	0.079288968
10/25/19 1:10	2.444	48.4143	8.741686008	78.9549	11.85349914	181.855	32.76226938	10/25/19 0:40	2.42	A30	0.061	500	30.5	10/25/19 1:10	2.444	1.1011	0.113545432
10/25/19 3:10	2.528	42.8732	7.741184992	75.5313	11.33951407	181.0178	32.61144278	10/25/19 2:40	2.51	A31	0.058	500	29	10/25/19 3:10	2.528	1.2013	0.123878056
10/25/19 5:10	2.611	38.2242	6.901761552	73.1716	10.98525231	181.9687	32.78275312	10/25/19 4:40	2.59	A32	0.056	500	28	10/25/19 5:10	2.611	1.1113	0.114597256
10/25/19 7:10	2.694	33.5657	6.060622792	70.4592	10.5780397	180.8565	32.58238361	10/25/19 6:40	2.67	A33	0.055	500	27.5	10/25/19 7:10	2.694	1.4731	0.151906072
10/25/19 9:10	2.778	28.8496	5.209083776	67.9055	10.19465272	179.454	32.32971482	10/25/19 8:40	2.76	A34	0.053	500	26.5	10/25/19 9:10	2.778	1.453	0.14983336
10/25/19 11:10	2.861	23.3325	4.2129162	62.986	9.45608818	171.8434	30.95861957	10/25/19 10:40	2.84	A35	0.049	500	24.5	10/25/19 11:10	2.861	1.4128	0.145687936
10/25/19 13:10	2.944	19.5508	3.530092448	62.1464	9.330039032	175.2029	31.56385365	10/25/19 12:40	2.92	A36	0.052	500	26	10/25/19 13:10	2.944	1.4024	0.144615488
10/25/19 15:10	3.028	7.1078	1.283384368	23.21	3.4845173	128.4127	23.13431838	10/25/19 14:40	3.01	A37	0.04	500	20	10/25/19 15:10	3.028	1.8828	0.194154336
10/25/19 17:10	3.111	7.4212	1.339971872	20.5341	3.082784433	123.189	22.19323748	10/25/19 16:40	3.09	A38	0.027	500	13.5	10/25/19 17:10	3.111	1.9698	0.203125776
10/25/19 19:10	3.194	7.7124	1.392550944	18.5772	2.788995036	119.9205	21.6043976	10/25/19 18:40	3.17	A39	0.036	500	18	10/25/19 19:10	3.194	2.1099	0.217572888
10/25/19 21:10	3.278	8.2795	1.49494652	17.7985	2.672088805	116.0448	20.90616699	10/25/19 20:40	3.26	A40	0.029	500	14.5	10/25/19 21:10	3.278	2.2126	0.228163312
10/25/19 23:10	3.361	8.3647	1.510330232	16.5159	2.479532067	111.2747	20.04680485	10/25/19 22:40	3.34	A41	0.029	500	14.5	10/25/19 23:10	3.361	2.0353	0.209880136
10/26/19 1:10	3.444	7.691	1.38868696	12.8682	1.931902866	106.8163	19.24359734	10/26/19 0:40	3.42	A42	0.025	500	12.5	10/26/19 1:10	3.444	2.5349	0.261398888
10/26/19 3:10	3.528	8.1426	1.470227856	12.7271	1.910719523	103.5933	18.66295455	10/26/19 2:40	3.51	A43	0.026	500	13	10/26/19 3:10	3.528	2.1987	0.226729944
10/26/19 5:10	3.611	8.0579	1.454934424	11.91855	1.789331912	94.59335	17.04155956	10/26/19 4:40	3.59	A44	0.026	500	13	10/26/19 5:10	3.611	0.6284	0.064800608
10/26/19 7:10	3.695	7.9732	1.439640992	11.11	1.6679443	85.5934	15.42016457	10/26/19 6:40	3.67	A45	0.026	500	13	10/26/19 7:10	3.695	1.8206	0.187740272
10/26/19 9:10	3.778	9.0381	1.631919336	12.5384	1.882389992	92.2077	16.6117704	10/26/19 8:40	3.76	A46	0.026	500	13	10/26/19 9:10	3.778	2.7367	0.282208504
10/26/19 11:10	3.861	8.7405	1.57818468	14.933	2.24189129	87.5411	15.77105441	10/26/19 10:40	3.84	A47	0.023	500	11.5	10/26/19 11:10	3.861	2.7904	0.287746048
10/26/19 13:10	3.945	9.0815	1.63975564	14.2331	2.136815303	80.8757	14.57024261	10/26/19 12:40	3.92	A48	0.02	500	10	10/26/19 13:10	3.945	2.7474	0.283311888
10/26/19 15:10	4.028	9.1426	1.650787856	13.0355	1.957019615	78.2407	14.09553155	10/26/19 14:40	4.01	A49	0.025	500	12.5	10/26/19 15:10	4.028	2.2733	0.234422696
10/26/19 17:10	4.111	9.303875	1.67990767	14.0653	2.111623489	77.1744	13.90343121	10/26/19 16:40	4.09	A50	0.024	500	12	10/26/19 17:10	4.111	2.7584	0.284446208
10/26/19 19:10	4.195	9.46515	1.709027484	12.2062	1.832516806	70.77565	12.750658	10/26/19 18:40	4.17	A51	0.017	500	8.5	10/26/19 19:10	4.195	2.3557	0.242919784
10/26/19 21:10	4.278	9.76788	1.763688413	9.9373	1.491886849	64.3769	11.5978848	10/26/19 20:40	4.26	A52	0.022	500	11	10/26/19 21:10	4.278	2.3087	0.238073144
10/26/19 23:10	4.361	10.07061	1.818349342	13.0145	1.953866885	65.8183	11.85756165	10/26/19 22:40	4.34	A53	0.019	500	9.5	10/26/19 23:10	4.361	2.4649	0.254180488
10/27/19 1:10	4.445	10.37334	1.87301027	12.9251	1.940445263	62.9123	11.33402832	10/27/19 0:40	4.42	A54	0.022	500	11	10/27/19 1:10	4.445	2.3913	0.246590856
10/27/19 3:10	4.528	10.1426	1.831347856	9.3938	1.410291194	56.1832	10.12174058	10/27/19 2:40	4.51	A55	0.018	500	9	10/27/19 3:10	4.528	2.0872	0.215232064
10/27/19 5:10	4.611	10.409335	1.879509528	12.6551	1.899910163	58.1797	10.48142203	10/27/19 4:40	4.59	A56	0.023	500	11.5	10/27/19 5:10	4.611	2.3531	0.242651672
10/27/19 7:10	4.695	10.67607	1.927671199	14.0053	2.102615689	53.76035	9.685249615	10/27/19 6:40	4.67	A57	0.024	500	12	10/27/19 7:10	4.695	2.2024	0.227111488
10/27/19 9:10	4.778	8.6953	1.570023368	10.2794	1.543246322	49.341	8.889077196	10/27/19 8:40	4.76	A58	0.025	500	12.5	10/27/19 9:10	4.778	1.8419	0.189936728
10/27/19 11:10	4.861	7.9382	1.433321392	10.6637	1.600941281	49.8014	8.972021018	10/27/19 10:40	4.84	A59	0.022	500	11	10/27/19 11:10	4.861	1.7372	0.179140064
10/27/19 13:10	4.945	7.2396	1.307182176	11.6498	1.748984474	47.0463	8.475673223	10/27/19 12:40	4.92	A60	0.019	500	9.5	10/27/19 13:10	4.945	1.2754	0.131519248

B.4 GMO Strain Data Using SSL

Table B.4: GMO strain using SSL (with GABA production) biomass data

Sugars								Biomass						GABA			
Real Time	time (days)	Concentration (mM)	C glucose ($g \cdot L^{-1}$)	Xylose (mM)	Xylose ($g \cdot L^{-1}$)	Mannose (mM)	Mannose ($g \cdot L^{-1}$)	Real Time	time (days)	Sample	OD diluted	Dilution	OD real	Real Time	time (days)	Concentration (mM)	C GABA ($g \cdot L^{-1}$)
2/25/20 12:40	0.000		7.2		9		22	2/25/20 12:40	0.00		0.125	10	1.25	2/25/20 12:40	0.000		
2/25/20 13:03	0.016							2/25/20 13:03	0.02	B1	0.126	10	1.26	2/25/20 13:03	0.016		
2/25/20 14:58	0.096							2/25/20 14:58	0.10	B2	0.187	10	1.87	2/25/20 14:58	0.096		
2/25/20 16:58	0.179							2/25/20 16:58	0.18	B3	0.02	100	2	2/25/20 16:58	0.179		
2/25/20 18:58	0.263							2/25/20 18:58	0.26	B4	0.025	100	2.5	2/25/20 18:58	0.263		
2/25/20 20:58	0.346							2/25/20 20:58	0.35	B5	0.049	100	4.9	2/25/20 20:58	0.346		
2/25/20 22:58	0.429							2/25/20 22:58	0.43	B6	0.064	100	6.4	2/25/20 22:58	0.429		
2/26/20 0:58	0.513							2/26/20 0:58	0.51	B7	0.083	100	8.3	2/26/20 0:58	0.513		
2/26/20 2:58	0.596							2/26/20 2:58	0.60	B8	0.109	100	10.9	2/26/20 2:58	0.596		
2/26/20 4:58	0.679							2/26/20 4:58	0.68	B9	0.1	100	10	2/26/20 4:58	0.679		
2/26/20 6:58	0.763							2/26/20 6:58	0.76	B10	0.06	100	6	2/26/20 6:58	0.763		
2/26/20 8:58	0.846							2/26/20 8:58	0.85	B11	0.076	100	7.6	2/26/20 8:58	0.846		
2/26/20 10:58	0.929							2/26/20 10:58	0.93	B12	0.077	100	7.7	2/26/20 10:58	0.929		
2/26/20 12:58	1.013							2/26/20 12:58	1.01	B13	0.086	100	8.6	2/26/20 12:58	1.013		
2/26/20 14:58	1.096							2/26/20 14:58	1.10	B14	0.091	100	9.1	2/26/20 14:58	1.096		
2/26/20 16:58	1.179							2/26/20 16:58	1.18	B15	0.105	100	10.5	2/26/20 16:58	1.179		
2/26/20 18:58	1.263							2/26/20 18:58	1.26	B16	0.101	100	10.1	2/26/20 18:58	1.263		
2/26/20 20:58	1.346							2/26/20 20:58	1.35	B17	0.121	100	12.1	2/26/20 20:58	1.346		
2/26/20 22:58	1.429							2/26/20 22:58	1.43	B18	0.124	100	12.4	2/26/20 22:58	1.429		
2/27/20 0:58	1.513							2/27/20 0:58	1.51	B19	0.136	100	13.6	2/27/20 0:58	1.513		
2/27/20 2:58	1.596							2/27/20 2:58	1.60	B20	0.175	100	17.5	2/27/20 2:58	1.596		
2/27/20 4:58	1.679							2/27/20 4:58	1.68	B21	0.196	100	19.6	2/27/20 4:58	1.679		
2/27/20 6:58	1.763							2/27/20 6:58	1.76	B22	0.207	100	20.7	2/27/20 6:58	1.763		
2/27/20 8:58	1.846							2/27/20 8:58	1.85	B23	0.044	500	22	2/27/20 8:58	1.846		
2/27/20 10:58	1.929							2/27/20 10:58	1.93	B24	0.0525	500	26.25	2/27/20 10:58	1.929		
2/27/20 12:58	2.013							2/27/20 12:58	2.01	B25	0.061	500	30.5	2/27/20 12:58	2.013		
2/27/20 14:58	2.096							2/27/20 14:58	2.10	B26	0.099	500	49.5	2/27/20 14:58	2.096		
2/27/20 16:58	2.179							2/27/20 16:58	2.18	B27	0.106	500	53	2/27/20 16:58	2.179		
2/27/20 18:58	2.263							2/27/20 18:58	2.26	B28	0.084	500	42	2/27/20 18:58	2.263		
2/27/20 20:58	2.346							2/27/20 20:58	2.35	B29	0.103	500	51.5	2/27/20 20:58	2.346		
2/27/20 22:58	2.429							2/27/20 22:58	2.43	B30	0.08	500	40	2/27/20 22:58	2.429		
2/28/20 0:58	2.513							2/28/20 0:58	2.51	B31	0.101	500	50.5	2/28/20 0:58	2.513		
2/28/20 2:58	2.596							2/28/20 2:58	2.60	B32	0.093	500	46.5	2/28/20 2:58	2.596		
2/28/20 4:58	2.679							2/28/20 4:58	2.68	B33	0.093	500	46	2/28/20 4:58	2.679		
2/28/20 6:58	2.763							2/28/20 6:58	2.76	B34	0.092	500	37	2/28/20 6:58	2.763		
2/28/20 8:58	2.846							2/28/20 8:58	2.85	B35	0.074	500	49	2/28/20 8:58	2.846		
2/28/20 10:58	2.929							2/28/20 10:58	2.93	B36	0.098	500	49	2/28/20 10:58	2.929		
2/28/20 12:58	3.013							2/28/20 12:58	3.01	B37	0.103	500	51.5	2/28/20 12:58	3.013		
2/28/20 14:55	3.094							2/28/20 14:55	3.09	B38	0.119	500	59.5	2/28/20 14:55	3.094		
2/28/20 17:58	3.221							2/28/20 17:58	3.22	B39	0.138	500	69	2/28/20 17:58	3.221		
2/28/20 20:58	3.346							2/28/20 20:58	3.35	B40	0.165	500	82.5	2/28/20 20:58	3.346		
2/28/20 23:58	3.471							2/28/20 23:58	3.47	B41	0.192	500	96	2/28/20 23:58	3.471		
2/29/20 2:58	3.596							2/29/20 2:58	3.60	B42	0.179	500	89.5	2/29/20 2:58	3.596		
2/29/20 5:58	3.721							2/29/20 5:58	3.72	B43	0.169	500	84.5	2/29/20 5:58	3.721		
2/29/20 8:58	3.846							2/29/20 8:58	3.85	B44	0.164	500	82	2/29/20 8:58	3.846		
2/29/20 11:58	3.971							2/29/20 11:58	3.97	B45	0.158	500	79	2/29/20 11:58	3.971		
2/29/20 14:58	4.096							2/29/20 14:58	4.10	B46	0.155	500	77.5	2/29/20 14:58	4.096		
2/29/20 17:58	4.221							2/29/20 17:58	4.22	B47	0.151	500	75.5	2/29/20 17:58	4.221		
2/29/20 20:58	4.346							2/29/20 20:58	4.35	B48	0.149	500	74.5	2/29/20 20:58	4.346		
2/29/20 23:58	4.471							2/29/20 23:58	4.47	B49	0.15	500	75	2/29/20 23:58	4.471		
3/1/20 2:58	4.596							3/1/20 2:58	4.60	B50	0.151	500	75.5	3/1/20 2:58	4.596		

B.5 Cell Dry Weight Experiment Data

Table B.5: Wild type strain using glucose (with no GABA production) cell dry weight experiment biomass data

Time (hr)	**CDW** ($g \cdot L^{-1}$)	**Std** ($g \cdot L^{-1}$)	**OD600** ($g \cdot L^{-1}$)
0	1.211111	0.4565031	1.09
2.9166667	2.333333	0.3138766	1.7
5.8333333	4.111111	1.1864461	7.6
8.8333333	6.111111	0.7622255	13.3
10.833333	10.41667	0.15	20.1
11.333333	7.466667	0.6480741	22.4
11.833333	9.65	0.05	21.5
13.166667	9.488889	1.2413652	21.2
21.5	8.522222	0.7804715	20.8
22.833333	11.82222	1.5329307	23.4
26.5	21.55	0.8833333	55.6
29.5	19	1.596524	22.3
46.333333	17.58333	0.1166667	19.3

Table B.6: Wild type strain using glucose (with no GABA production) cell dry weight experiment sugar data

Sugars			
Real Time	time (days)	Concentration (mM)	C glucose ($g \cdot L^{-1}$)
18/04/20 13:10	0		
18/04/20 13:39	0.020139	145.6949	26.22508
18/04/20 16:31	0.139583	106.8665	19.23597
18/04/20 19:32	0.265278	89.9962	16.19932
18/04/20 22:32	0.390278	26.7797	4.820346
19/04/20 1:32	0.515278	n.a	
19/04/20 4:32	0.640278	n.a	
19/04/20 7:32	0.765278	n.a	
19/04/20 10:32	0.890278	n.a	
19/04/20 13:32	1.015278	98.6901	17.76422
19/04/20 16:32	1.140278	n.a	
19/04/20 19:32	1.265278	n.a	
19/04/20 22:32	1.390278	n.a	
20/04/20 1:32	1.515278	n.a	
20/04/20 4:32	1.640278	n.a	
20/04/20 7:32	1.765278	n.a	
20/04/20 10:32	1.890278	n.a	

C Additional Media Composition

C.1 CGXII

Table C.7: Composition of CGXII used in the broth and feed medium for each experiment

Component	Concentration (g/L)
$(NH_4)_2SO_4$	10.00
CH_4N_2	5.00
KH_2PO_4	0.26
K_2HPO_4	0.53
Ca-stock 1000X	1.00
Mg-stock 1000X	1.00

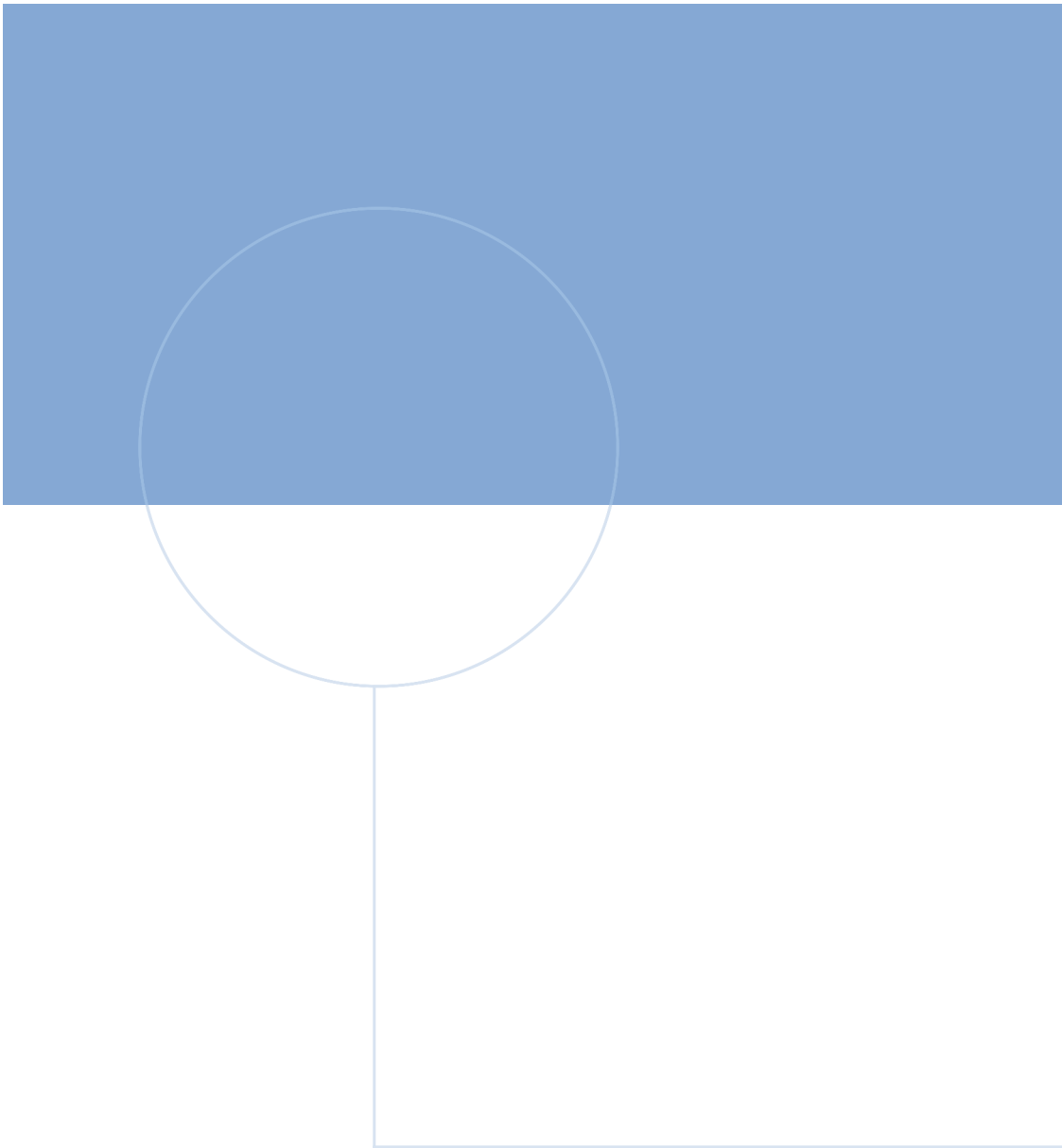

NTNU

Kunnskap for en bedre verden